JAERI-M
91-174

EVALUATION REPORT ON CCTF CORE-II REFLOOD TEST C2-5 (RUN 63)

—EFFECT OF DECAY HEAT LEVEL ON PWR REFLOOD PHENOMENA—

October 1991

Tadashi IGUCHI, Takashi SUDOH,* Kazuharu OKABE,** Jun SUGIMOTO
Hajime AKIMOTO, Tsutomu OKUBO and Yoshio MURAO

日本原子力研究所
Japan Atomic Energy Research Institute

JAERI-Mレポートは，日本原子力研究所が不定期に公刊している研究報告書です。
入手の問合わせは，日本原子力研究所技術情報部情報資料課（〒319-11茨城県那珂郡東海村）あて，お申しこしください。なお，このほかに財団法人原子力弘済会資料センター（〒319-11 茨城県那珂郡東海村日本原子力研究所内）で複写による実費頒布をおこなっております。

JAERI-M reports are issued irregularly.
Inquiries about availability of the reports should be addressed to Information Division Department of Technical Information, Japan Atomic Energy Research Institute, Tokai-mura, Naka-gun, Ibaraki-ken 319-11, Japan.

編集兼発行　日本原子力研究所
印　　刷　いばらき印刷㈱

JAERI-M 91-174

Evaluation Report on CCTF Core-II Reflood Test C2-5 (Run 63)
- Effect of Decay Heat Level on PWR Reflood Phenomena -

Tadashi IGUCHI, Takashi SUDOH*, Kazuharu OKABE**, Jun SUGIMOTO+
Hajime AKIMOTO, Tsutomu OKUBO and Yoshio MURAO

Department of Reactor Engineering
Tokai Research Establishment
Japan Atomic Energy Research Institute
Tokai-mura, Naka-gun, Ibaraki-ken

(Received October 1, 1991)

The following items on decay heat effect on PWR reflood phenomena were revealed by investigation on results of CCTF tests in the range of 1.06 kW/m to 1.4 kW/m of initial average linear power (Peak linear power: 2.04 kW/m to 2.69 kW/m; Total power: 7.1 MW to 9.4 MW). These power levels simulate most probable case to very conservative case for PWR LOCA analyses.

(1) The overall flow characteristics in the low power test (1.06 kW/m of initial average linear power) were qualitatively similar to that of the base case test (1.4 kW/m of initial average linear power). Any qualitatively different phenomena were not recognized during reflood phase. This indicates that it is reasonable to utilize the physical reflood model developed from the result of the base case test under the low power condition at least up to 1.06 kW/m of the initial average linear power for a prediction of PWR reflood phenomena.

(2) On the other hand, the following quantitative influence of the power on PWR reflood phenomena was observed. This result was consistent

---

+ Department of Fuel Safety Research

* NKK Corporation

** Mitsubishi Atomic Power Industries, Inc.

to that previously observed in FLECHT-SET tests performed in the scope of the initial average linear power from 1.88 kW/m to 2.35 kW/m.

(i) The steam generation rates in the core were nearly identical in the above power range during the early period regardless the different power level, since the steam generation rate was mainly contributed to the release of the energy stored initially in the core rather than the supplied power. On the other hand, the steam generation rates were higher with the higher power during the later period, since the stored energy became higher with the higher power.

(ii) The core flooding mass flow rates were nearly identical in the above power range during the whole reflood period. The pressures in the upper plenum and the subcoolings at the core inlet were also nearly identical regardless the differnt power level. These indicate that the core boundary condition important for core cooling is little influenced by decay heat level. The insensitiveness of the core flooding mass flow rate against the decay heat level was also analytically confirmed.

(iii) The heat transfer coefficients were nearly identical in the above power range until the turnaround time. It was lower with the higher power during the later period. This characteristic leads to the higher turnaround temperature and the later quenching with the higher power. This indicates that it is conservative to assume the higher decay heat for reactor safety evaluation, which is consistent to current reactor safety evaluation treatment.

(3) Observed special phenomenon induced by the low power condition is a short-term (a few seconds) differential pressure oscillation around the cold legs, which was caused by (1) the complete steam condensation at cold leg ECC ports and (2) the formation of the water plug in the cold legs. However, this oscillation had no adverse effect on the core cooling. The oscillation was observed when the power level reached the value corresponding to the decay heat at about 730 s after scram.

Keywords: Reactor Safety, LOCA, Steam Binding, Reflood, ECCS, CCTF, PWR, Two-phase Flow, Core Cooling, Decay Heat

大型再冠水円筒第二次炉心試験C2－5(Run 63)の評価
－PWR 再冠水現象に及ぼす崩壊熱の影響－

日本原子力研究所東海研究所原子炉工学部
井口　正・須藤　高史*・岡部　一治**・杉本　純+
秋本　肇・大久保　努・村尾　良夫

(1991年10月1日受理)

崩壊熱がPWR 再冠水現象に及ぼす影響を調べるための試験を，円筒炉心試験装置を用いて実施した。試験では，初期平均炉心線出力を1.06kW/m～1.4kW/m の範囲で変えた（最高炉心線出力：2.04 kW/m～2.69kW/m；炉心出力：7.1MW～9.4MW)。この炉心出力はPWRのLOCA時において実現すると考えられる値および安全評価で厳しい仮定をしたときの値に相当する。

(1) 低炉心出力試験（1.06kW/m）での再冠水現象は基準試験（1.4kW/m)での再冠水現象と定性的に殆ど等しかった。このことは，PWR の再冠水現象予測を行うに際し，基準試験結果を基礎にして開発した再冠水物理モデルを少なくとも平均炉心線出力が1.06kW/mの条件まで拡張して使用することに問題はないことを示す。

(2) 一方，定量的には次のような炉心出力の影響が見られた。この結果は，従来初期平均炉心線出力が1.88kW/m～2.35kW/mの範囲で実施されたFLECHT-SET試験の結果と等しい。

（ｉ）再冠水初期の炉心内での蒸気発生量は，炉心出力の違いに拘らずほぼ等しかった。
これは，蒸気発生が炉心出力よりもむしろ炉心温度に影響されるためである。また，再冠水中期以降の炉心内での蒸気発生量は，炉心出力が大きいほど多かった。これは，炉心出力が大きいほど炉心温度が高くなるためである。

（ii）炉心冠水流量は，再冠水全期間で炉心出力の違いに拘らずほぼ等しかった。上部プレナム内圧力および炉心入口水温もほぼ等しかった。これらは，炉心冷却に対して重要な影響因子である炉心境界条件が炉心出力の違いに拘らずほぼ等しいことを示す。
炉心冠水流量が炉心出力の違いに拘らずほぼ等しいことは，解析的にも確かめた。

（iii）熱伝達率は，再冠水初期の炉心温度が最高値に達するまでは，炉心出力の違いに拘らずほぼ

東海研究所：〒319-11　茨城県那珂郡東海村白方字白根2-4
＋　燃料安全工学部
＊　日本鋼管
＊＊　三菱原子力工業

等しかった。また，再冠水中期以降は炉心出力が大きいほど小さかった。この特性により，炉心出力が大きいほど炉心最高温度は高く，炉心全体がクエンチする時間は遅い。これは，事故時安全評価において高崩壊熱を仮定する現行の安全評価手法が妥当であることを示す。

(3) 低炉心出力条件によりもたらされた特殊な挙動として，コールドレグ周辺で短周期（数秒）の差圧振動が見られた。これは，(1)コールドレグの非常用冷却水注入口での蒸気の完全凝縮と(2)コールドレグに水プラグが形成されることによる。この差圧振動により炉心冷却が悪影響されるということはなかった。なお，この振動が見られた炉心出力レベルは，PWR スクラム後730sにおける崩壊熱に相当する。

Contents

目　　次

Table List

Figure List

1. Introduction

CCTF program

A reflood test program[1] using large scale test facilities has been conducted at Japan Atomic Energy Research Institute (JAERI). The facilities are the Cylindrical Core Test Facility (CCTF)[2] and the Slab Core Test Facility (SCTF)[3]. This report describes the evaluated result of the CCTF test C2-5 (Run 63), which is a low power test for investigating the low decay heat effect on reflood behavior in the primary coolant system of a PWR.

The CCTF is an experimental facility designed to model a full-height core section, four primary loops and their components of pressurized water reactors (PWRs). This facility is used to provide information of the refill-reflood behaviors in pressure vessel (core, downcomer, upper and lower plena) and in primary loops (including steam generators and pumps) at a hypothetical loss-of-coolant accident (LOCA) of a PWR. The central part of the test facility is a non-nuclear core which consists of 1,824 electrically heated rods and 224 non-heated rods arranged in a cylindrical array. The core is housed in a pressure vessel which includes a downcomer, lower plenum and upper plenum in addition to the core. The core design is based on 8 x 8 rod assemblies which model typical 15 x 15 fuel assemblies of a PWR. Volumetric scaling ratio to a 1,100 MWe four-loop PWR is 1/21 based on core flow area scaling.

The objectives of the test program using the CCTF are:

a. Demonstration of capability of emergency core cooling system (ECCS) during refill and reflood periods
b. Verification of reflood analysis codes
c. Collection of information on the reflood phenomena to improve the thermo-hydrodynamic models in the analysis codes, such as (1) in-core thermal hydraulics including multi-dimensional effect, (2) upper plenum thermal hydraulics, (3) loop thermal hydraulics including those in hot legs, SGs, cross over legs, primary pumps and cold legs, (4) downcomer thermal hydraulics, and (5)lower plenum thermal hydraulics.

As the first series of the CCTF tests, twenty-seven CCTF Core-I tests were conducted. The CCTF Core-I test series was initiated in March 1979 and completed in April 1981. Subsequently as the second series of the CCTF tests, the CCTF Core-II test series was initiated in March 1982 and completed in 1985. The CCTF tests presented a lot of information[4],[5],[6] on the system thermo-hydrodynamic behavior as well as the core behavior during the refill and reflood phases of a LOCA in a PWR. Through the evaluation of the test results, the phenomenological understanding on the reflood phenomena was obtained. Based on the understanding, it became possible to

predict the reflood phenomena in PWRs[7],[8]. The phenomenological understanding was obtained mainly based on the experimental result of the test which was performed under the relatively high decay heat (In CCTF scale, the decay heat at the reflood initiation was 9.4 MW) test. To verify that the phenomenological understanding is applicable to wide boundary conditions, it is necessary to obtain the date for the verification and to evaluate them.

Test discussed in this report

The test discussed in this report is a low power test C2-5 (Run 63). The objective of the test is to study the effect of the low decay heat on the PWR reflood phenomena.

The decay heat during PWR reflood phase depends on reflood initiation time after pipe rupture followed by scram, transient of decay heat of fission product, and so on. According to the licensing calculation which assumes the severe situation for the reactor safety evaluation, the reflood initiation time is 30s-40s after scram. On the other hand the transient of the decay heat was evaluated in the licensing calculation based on the previous ANS standard with 20% margin. However, in 1981 it was approved to use the decay heat envelope predicted with the new ANS standard presented in 1978 with proper margin. This change of decay heat evaluation method in the licensing calculation led to the reduction of the decay heat during the reflood phase. Resultantly, the supposed decay heat at the reflood initiation changed from 9.35 MW to 7.99 MW in CCTF tests (Reflood initiation time was supposed to be 30 s after scram.; Extra margin of 7% was added for CCTF tests). The decay heat based on the previous evaluation method is nearly the same as the experimental condition of the CCTF base case test. The decay heat based on the newly revised evaluation meathod is much lower than the experimental condition of the CCTF base case test. The decay heat at the reflood initiation is 7.1 MW if the reflood initiation is 40s after scram and no margin is taken into account.

Based on the above background, the low power test C2-5 (Run 63) was conducted at the low initial power supplied to the core (simulating the decay heat; 7.1 MW at the reflood initiation) as a counterpart test of the base case test C2-4[9] (Run 62; initial power 9.4 MW). Other initial and boundary conditions were set to be identical between the low power test and the base case test. The ECC flow conditions were same as those of the Evaluation Model test[10] in CCTF Core-I. For the evaluation of the decay heat effect, another CCTF test, C2-SH2 (Run 54; initial power 7.9 MW)[11], was performed. Above three CCTF tests have been evaluated in this report.

2. Test facility

CCTF was designed to be a full-height, 1/21 scale model of the primary coolant system of a 1,100 MWe four-loop PWR in order to study the overall primary system response as well as the in-core behavior during the refill and reflood phases of a large cold leg break LOCA. Figure 2.1 depicts the major components in the facility. They included a pressure vessel, four primary piping loops (three intact and one broken), two steam generators, four pump simulators, and two tanks attached to the ends of the broken loop to simulate containment. Vertical dimensions and locations of system components were as close as practicable to the corresponding dimensions and locations in the reference reactor.

The schematic diagram of the CCTF is shown in Fig.2.2 and Fig.2.3. The scaled dimensions of the components are given in Tables 2.1 and 2.2.

2.1 Pressure vessel and internals

Figures 2.4 and 2.5 show the CCTF pressure vessel. The full-height pressure vessel housed a downcomer, lower plenum, core, and upper plenum. Pressure vessel flow area was scaled at a ratio of 1/21.4 as compared to a 1,100 MWe PWR, except that the downcomer annulus was somewhat larger to avoid excessive hot wall effects which would lead to an unrealistically low effective downcomer driving head. To simulate the effective downcomer driving head more realistically, the baffle area of PWR was included in the downcomer. Resultantly, the gap size of the downcomer was 61.5 mm, which was larger than the scaled gap. The design pressure of the pressure vessel and the entire primary system was 0.6 MPa. The pressure vessel wall was constructed of carbon steel which was cladded with stainless steel lining. The wall was 90 mm thick and simulated the stored energy as reasonably as possible during a test. Electrical resistance heaters on the wall of the pressure vessel were used to preheat the wall before a test, to accurately simulate the release of latent heat which would occur during a LOCA in PWR. The CCTF-II pressure vessel was the same as that used in CCTF-I, except for the addition of an upper ring containing an upper plenum emergency core coolant (ECC) injection header and additional instrumentation nozzles.

The design of upper plenum internals was based on that of the new Westinghouse 17 x 17 type fuel assemblies instead of the old type simulated in CCTF-I. The internals consisted of ten control rod guide tubes, ten support columns and twelve open holes as shown in Fig.2.5. The radius of each internals was scaled down by factor of 8/15 from that of an reference reactor. They are illustrated in Fig.2.6. Flow resistance baffles were inserted into the guide tubes. The baffles consisted of kinds of baffle

plates and a shaft, simulating real ones. The baffle plates are shown in Fig.2.7.

The end box and the upper core support plate (UCSP) were installed between the core and the upper plenum, as in PWRs. The structure for one heater rod bundle is shownin Fig.2.8. The tie plate was a 10 mm thick perforated plate with round flow holes. Plugging devices were installed on the tie plate as shown in Figs.2.8 and 2.9 to simulate the flow resistance more correctly. The UCSP was a 60 mm thick perforated plate. The geometry of the perforation was analogous to that of an reference reactor.

2.2 Heater rod assembly

The heater rod assembly simulating the fuel assembly consisted of thirty−two 8 x 8 array rod bundles. Each bundle consisted of fifty−seven electrically heated rods and seven non−heated rods as shown in Fig.2.10. The core was usually subdivided into three regions to achieve a desired radial power distribution. This is shown in Fig.2.5. The high, medium and low power regions were named as A, B and C regions, respectively. The local peaking factor of heated rods in a bundle was unity, that is, all heated rods in a bundle had the same power density.

A heater rod consisted of a nichrome heating element, magnesium oxide (MgO) and boron nitride (BN) insulators, and inconel−600 sheath. BN was used for only central part of the heated region and MgO for the other part as shown in Fig.2.11. The heated length and the outer diameter of the heater rods were 3.66 m and 10.7 mm, respectively, which are identical to the corresponding dimensions of reference PWR fuel rods. The sheath wall thickness was 1.0 mm and was thicker than the reference fuel cladding, because of the requirements for thermocouple installation to measure the clad temperature. The heating element was a helical coil with a varying pitch to generate a 17 steps chopped cosine axial power profile as shown in Fig.2.12. The axial peaking factor was 1.40.

Non−heated rods were either stainless steel pipes or solid bars of 13.8 mm O.D. All the pipes were utilized for installation of instruments such as steam superheat probes and thermocouples. All the bars were used for carrying the assembly loads.

The heater rods and non−heated rods were held in radial position by grid spacers which were located at six elevations along the axial length as shown in Fig.2.12. A grid spacer was a lattice structure composed of stainless steel plates of 0.4 mm and 0.8 mm thick and 40 mm high. The top and the bottom edges of the stainless steel plates were sharpened. The rod pitch was 14.3 mm, which was the same as that of the reference PWR.

The heater rods penetrated through the bottom plate of the pressure vessel to facilitate lead out of the power cables. The outer diameter of the rods in the lower

plenum was reduced to 8.6 mm. Three phase electric current was used for heating the heater rods and the electrical neutral point was at the top of the rods, where they were inter−connected to each other.

2.3 Primary loops

The primary loop arrangement is shown in Figs.2.13 and 2.14. Primary loop consisted of three intact loops and a broken loop. Each loop consisted of hot leg and cold leg pipings (including cross over legs), a steam generator simulator and a pump simulator. Each intact loop connected the upper plenum to the upper portion of the downcomer, as a reference PWR. A broken loop simulated 200% cold leg break about 2 m from the pressure vessel wall, and consisted of two parts. One of them connected the upper plenum to a containment tank simulator (Containment tank 2) through a steam generator simulator. This part was called a broken loop SG side in CCTF. The other connected the upper portion of the downcomer to a containment tank simulator (Containment tank 1). This part was called a broken loop PV side in CCTF.

The inner diameter of the hot leg and cold leg pipings (0.155 m) was scaled down in proportion to the core flow area scaling. The length of each piping section was almost the same as the corresponding sections of the reference PWR.

The steam generator simulators were of U−tube and shell type heat exchangers as shown in Fig.2.15. The tube length was about 5 m shorter than the reference PWR. The vertical height of the steam generator simulators was also about 5 m lower than the reference PWR. During a test, the steam generator secondary sides contained high pressure saturated water at 540 K and 5.3 MPa. These conditions corresponded to those in the secondary side of the steam generators in a PWR during the reflood portion of a LOCA. The primary coolant passed through the tube side and the secondary coolant was stagnant in the shell side during the tests. The steam generator simulators of two loops were housed in a single shell assembly which had two sets of separated inlet and outlet headers for two loops. The wall thickness of the U−tube was 2.9 mm instead of 1.27 mm of the reference PWR, because of a higher pressure difference between the primary and secondary sides in the steam generator simulator.

The pump simulator consisted of the casing and vane simulators and an orifice plate as shown in Fig.2.16. The each loop flow resistance was simulated with the orifice plate. Each orifice plate had one hole with diameter and thickness of 95 mm and 10 mm, respectively.

The 200% cold leg break was simulated with two fast−open break valves (Blowdown valves) located at the two ends of the cold leg break, as shown in Figs.2.1, 2.2 and 2.13.

Two interconnected tanks (Containment tank 1 and containment tank 2), one

attached to each of the two ends of the cold leg break, simulated the PWR containment (Figs.2.1 and 2.2). On the Containment tank 2 connected to the hot leg side of the break, a pressure regulation system maintained the pressure at a preselected value by venting steam, as needed, to the atmosphere.

2.4 ECC injection system

ECC water could be injected into each cold leg and lower plenum, as shown in Figs.2.2 and 2.13. The ECC water stored two water supply tanks (Fig.2.3): the "Acc" tank, capable of providing water at a high flow rate for a short duration, and the "LPCI" tank, capable of providing water at a lower flow rate for a longer duration. Each tank could supply water to either the lower plenum or to the four cold legs through the feeding lines and the ECC nozzles (ECC ports).

The ECC water in the Acc tank was supplied to the primary loop with the pressurization by nitrogen, as in the reference PWR. The water flow rate was adjusted with the pressure in the Acc tank and the flow resistance of the feeding lines. The ECC water in the LPCI tank was supplid to the primary loop with the LPCI pumps, as in the reference PWR. The water flow rate was adjusted with the control valves located in the feeding lines.

The cold leg feeding lines were connected to the top of the cold leg pipings with 45 degree (Fig.2.14), as in the reference PWR. To simulate the linear velocity of the ECC water, the flow area of the exit of the feeding lines was adjusted by inserting a throtling devices.

2.5 Instrumentation

The instrumentation is divided into two groups. One of them is JAERI−supplied instruments measuring the temperatures, absolute pressures, differential pressures, water levels and flow rates. Thermocouples measured the temperatures of the rod surface, fluid and structure. The absolute pressures were measured in the upper and lower plena, steam generator plena and containment tanks. The differential pressure measurements were carried out at many locations covering the whole system almost completely. In the ECC water supply tanks and the containment tank 1, the liquid levels were measured. The flow meters measured the ECC water flow rate. Furthermore, flow rates in the downcomer, cross over leg pipings and vent line from the containment tank 2 to the atmosphere were measured with the drag disk flow meter, pitot tubes and ventulli tube, respectively. The total number of the JAERI−supplied instruments were 1316 channels and the signals from these instruments were recorded on magnetic tapes.

The other group of the instrumentation is the USNRC−supplied instruments.

They are the advanced instrumentation for the two-phase flow measurement. The names and quantities of those are tabulated in Table 2.3. The total number was 536 channels.

3. Test procedure and test conditions

3.1 Test procedure

The test procedure of the present low power test, C2-5 (Run 63), was as follows (Fig.3.1). The test procedure in the counterpart tests C2-4 (Run 62) and C2-SH2 (Run 54) was the same.:

i) Set-up of facility; Blowdown valves were set open. Pressure regulation valves on the containment tank-2 were controlled to keep pressure in the tank at a specified value (0.2 MPa) upto the end of the test.

ii) Setting of initial conditions; The primary system was preheated with external heaters to its specified temperature (Downcomer wall: 470 K, Core internals: 394 K, Primary loop pipings: 392 K) (During the test, the external heaters were turned off.). The pressure vessel and primary loops was pressurized to a specified pressure (0.2 MPa) with saturated steam. Temperature of water for ECC injection was set to a specified values (Water in Acc tank: 308 K; Water in LPCI tank: 308 K). ECC feeding lines was heated by circulating water in LPCI tank through circulation lines (During the test, this lines were closed.). The water in the secondary side of steam generator simulators was heated and pressurized (540 K and 5.2 MPa). The water level in lower plenum was set to a specified level (0.86 m in depth) with a suturated water. Core, upper plenum, loops and downcomer had no water for pretest conditioning phase.

iii) Supply of electric power to the heated rods in the core; Electric power was supplied to heat the heated rods after initial conditions had stabilized. Since steam around the heated rods was stagnant, the temperature of the heated rods increased adiabatically and reached a specified clad temperature (995 K) for initiation of ECC water injection. Figure 3.2 shows the initial set-up for C2-5 (Run 63).

iv) ECC water injection into lower plenum; When the temperature of the heated rods reached a specified clad temperature, ECC water injection into lower plenum was initiated (Note 1) for simulation of ECC water injection from Acc and LPCI tanks and accordingly the water level in lower plenum rose. ECC water injection rate was 0.106 m^3/s.

v) Initiation of decaying of electric power; When the water level in lower plenum reached the bottom of the core (This is called the reflood

initiation or BOCREC.), the decay of electric power was initiated to simulate the decay of heat of nuclear fuels at a LOCA.

vi) Termination of ECC water injection into lower plenum and starting of ECC water injection into cold legs; Few seconds after the reflood initiation, ECC water injection was switched from lower plenum to intact cold legs. ECC water injection rate was reduced to 0.091 m^3/s for simulation of ECC water injection from Acc and LPCI tanks. At a specified time (26.5 s) after initiation of ECC water injection to lower plenum, injection from Acc tank was terminated. As the result, ECC water injection rate decreased (0.011 m^3/s) for simulation of ECC water injection only from LPCI tank. The ECC water injection rate was maintained constantly until the end of the test.

vii) Termination of test: Clad temperature of heated rods was monitored during the test. When all thermocouples on the clad of heated rods indicated quenching of the heated rods, it was judged that the test was terminated. Several tens seconds after the termination of the test, electric power supplied to the heated rods was turned off. Then ECC water injection was stopped.

(Note 1)

In PWR, ECC water was injected only to cold legs. Therefore, ECC water injection into lower plenum in the tests was not real simulation to PWR case. However, since the violent condensation at ECC ports in cold legs may atypically affect the reflood behavior in CCTF tests, ECC water was injected first into lower plenum. After sufficient steam flow was established through intact cold legs, ECC water was injected into intact cold legs. Atypicality of this ECC injection method was investigated through the result of other CCTF tests called refill simulation tests.
The conclusion of the tests is that the atypical ECC injection procedure has no major influence on the test result and it is considered that the present ECC injection procedure is valid for simulation of PWR reflood behavior.

3.2 Test condition

Table 3.1 lists the initial test conditions of the present low power test C2-5 (Run 64). The test conditions were selected to simulate the reflood behavior under evaluation model (EM) condition of PWR 200% cold-leg break LOCA. Therefore, the test conditions were the same as those in the CCTF base case test C2-4 (Run 62), simulating EM conditions, except for the power supplied to heater rods in the core. In C2-4 (Run 63) the power at the reflood initiation was set at 7.1 MW, while in

C2-3 (Run 62) it was set at 9.4 MW. In other counterpart test C2-SH2 (Run 54) it was set at 7.9 MW. In summary,

- C2-4 9.4 MW : ANS x 1.2 + Act. x 1.1, decay at 30 s after scram
- C2-SH2 7.9 MW : ANS x 1.0 + Act. x 1.1, decay at 30 s after scram
- C2-5 7.1 MW : ANS x 1.0 + Act. x 1.1, decay at 40 s after scram

Figure 3.3 shows the comparison of the power. Figures 3.4 and 3.5 show the comparison of the injected ECC flow rates and the pressure in Containment tank 2. It is shown that the injected ECC flow rates are identical among three tests, as adjusted in the experiments. The pressure of C2-5 is slightly lower than those of other tests.

Basic phylosophy to determine the test conditions is summarized in the following.

(1) Pressure

Typical reactor safety evaluation result indicated that the pressure in the containment tank was 0.2-0.26 MPa during the reflood phase. This pressure depends on steam discharge rate from the primary system to the containment, condensation characteristics in the containment, and volume of the containment. Accordingly, the pressure depends on the type of containment. For the most probable case, the pressure is considered to be higher than the pressure indicated in the reactor safety evaluation (eg. 0.4 MPa). In addition, CCTF had small containment simulators (Containment tank 1 and containment tank 2) comparing with the containment of reference PWRs and the pressure in the CCTF containment simulators was controlled by discharging the excessive steam from the containment tank 2 to the atmosphere. Therefore, the pressure was not simulated exactly and then it was necessary to study the pressure effect on the reflood behavior in scope of the pressure of 0.2-0.4 MPa.

Based on discussion mentioned above, the pressure in the present tests was set at 0.2 MPa to simulate severe pressure condition.

(2) Power profile

Axial peaking factor for each heated rods was 1.4.

Radial power profile was convex, which meant that the power density was high in the central zone of the core and low in the peripheral zone of the core. The power ratios for the central, intermediate and peripheral zones were set at 1.37, 1.20, and 0.76, respectively. Radial power profile of the reference PWR was somewhat different profile. The power ratio was the highest in the intermediate zone of the core, which was between the central and the peripheral zones. It was the lowest in the peripheral

zone of the core. Averaged power ratio of each zone for the beginning life was 1.09, 1.13 and 0.9 in the reference PWR. Therefore, the radial power profile of the present test is steeper than PWR case.

(3) Total power to heated rods and power decay

The decay heat during PWR reflood phase depends on reflood initiation time after pipe rupture followed by scram, transient of decay heat of fission product, and so on. According to the licensing calculation which assumes the severe situation for the reactor safety evaluation, the reflood initiation time is 30s~40s after scram. On the other hand the transient of the decay heat was evaluated in the licensing calculation based on the previous ANS standard (Old ANS standard) with 20% margin. However, in 1981 it was approved to use the decay heat envelope predicted with the new ANS standard presented in 1978 with proper margin. This change of decay heat evaluation method in the licensing calculation led to the reduction of the decay heat during the reflood phase. Resultantly, the supposed decay heat at the reflood initiation changed from 9.35 MW to 7.99 MW in CCTF tests (Reflood initiation time was supposed to be 30 s after scram.; Extra margin of 7% was added for CCTF tests). The decay heat based on the previous evaluation method is nearly the same as the experimental condition of the CCTF base case test. The decay heat based on the newly revised evaluation method is much lower than the experimental condition of the CCTF base case test. The decay heat at the reflood initiation is 7.1 MW if the reflood initiation is 40s after scram and no margin is taken into account. Based on the above background, the total power for the present tests was determined as follows.

Total power of 9.35 MW for base case test C2-4 was determined to simulate the EM condition with the following equation.

P_{CCTF} = 1.02 x P_{0PWR} x F_S x F_M x (Old ANS x 1.2 + Act. x 1.1)
P_{0PWR} = steady state power of reference PWR = 3411 MW
F_S = CCTF scaling factor = 1/21.2
F_M = CCTF experimental margin = 1.07
Old ANS x 1.2 + Act. x 1.1 = 0.0532 (Assuming 30 seconds after scram)

Factor 1.02 in the above equation is to account for the instrument error required for the licensing calculation. CCTF scale factor can be obtained in two ways as follows.

F_S = 1824/39372 = 1/21.59 based on number of heated rods

F_S = 0.26/5.5 = 1/21.2 based on core flow area

Since the difference between the two scaling factors above was less than 2%, F_S=1/21.2 was used. CCTF experimental margin was taken to account for the instrument error in the experiment and the contribution of the delayed neutron fission which is neglected in the licensing calculation. This margin also gives the margin for the highest power density of heated rods as shown in (4) below.

As the result,

P_{CCTF} = 9.35 MW (Base case test C2-4)

Total power of 7.1 MW for the present low power test C2-5 was determined with the following equation.

P_{CCTF} = 1.02 x P_{0PWR} x F_S x (New ANS + proper allowance + Act.)

New ANS + proper allowance + Act. = 0.043 (Assuming 40 seconds after scram)

As the result,

P_{CCTF} = 7.1 MW (Present low power test C2-5)

Above value (7.1 MW) corresponds to the value under (Old ANS + Act. x 1.1) assuming 40 seconds after scram. For a counterpart test C2-SH2, another total power was selected.

P_{CCTF} = 7.9 MW (test C2-SH2)

(4) Highest power density of heated rods

In reference PWR, the highest power density can be obtained as follows:

q_{PWR} = 1.02 x P_{0PWR} x 0.95 x F_r x F_a x (Old ANS x 1.2 + Act. x 1.1)/(NL)

F_r = Radial peaking factor for hot rod = 1.552

F_a = Axial peaking factor = 1.495

N = Number of fuel rods = 39372 for 15 x 15 bundle array and
50952 for 17 x 17 bundle array

L = Heated length of fuel rods = 3.66 m

Factor 0.95 in the above equation was introduced to account for gamma heating. Resultantly,

q_{PWR} = 2.83 kW/m for 15 x 15 bundle array and
2.19 kW/m for 17 x 17 bundle array

On the other hand, in CCTF it can be obtained as follows:

q_{CCTF} = $P_{CCTF} \times F_r \times F_a \times F_t /(NL)$
F_r = Radial peaking factor for hot rod = 1.37 as shown in (2) above
F_a = Axial peaking factor = 1.4 as shown in (2) above
F_t = Power decay factor defined as follows

$$= \frac{\text{(Old ANS x 1.2 + Act.x 1.1) at time = t seconds after scram}}{\text{(Old ANS x 1.2 + Act.x 1.1) at time = 30 seconds after scram}}$$

N = Number of fuel rods = 1824
L = Heated length of fuel rods = 3.66 m

Resultantly,

q_{CCTF} = 2.69 kW/m for base case test C2－4
q_{CCTF} = 2.04 kW/m for present low power test C2－5
q_{CCTF} = 2.27 kW/m for test C2－SH2

2.69 kW/m is 5% less and 23% more for 15 x 15 and 17 x 17 bundle arrays of reference PWRs, respectively.

(5) Initial clad temperature

The highest initial clad temperature (1073 K; = Temperature at midplane of the heated rods in the highest power zone) at the reflood initiation was determined to simulate the clad temperature (1140 K) calculated in the representative reactor safety evaluation.

(6) Mode of ECC injection

In the licensing calculation followings were assumed for single failure of ECC injection system.

(1) ECC water injected into the broken loop is not effective.

(2) One LPCI pump out of two is not working.

Resultantly, three Acc systems out of four, two HCPI pumps and one LPCI pump out of two work. In CCTF tests the above injection mode was simulated as EM condition.

3.3 Chronology of events

The sequence of events that occurred during the low power test C2-5 (Run64) is listed in Table 3.2.

The data recording was initiated at the same time when the power supply to the heater rods in the core was initiated. This time was defined as 0 s. The Acc injection into the lower plenum was initiated at 118 s, the power decay was initiated at 126 s which was the bottom of core recovery time and the ECC injection location was changed from lower plenum to cold legs at 131 s. The ECC injection mode was changed from Acc injection to LPCI at 143 s. All the heater rods were quenched by 562 s. The power was turned off at 1160 s. LPCI was terminated at 1160 s and the data recording was ended at 1190 s.

4. Results and discussion

In the following figures, the low power test C2-5 (Run 63) is sometimes designated "Low power", while the base case test C2-4 (Run 62) "High power".

4.1 Overall flow characteristics in low power test

The overall flow characteristics in low power test, C2-5, was similar to that of CCTF base case test, C2-4, and a counterpart test C2-SH2. Any qualitatively different phenomena were not recognized during reflood phase (until whole core quenching). This indicates that it is reasonable to utilize the physical reflood model developed from the result of the base case test under the low decay heat condition at least up to 7.1 MW of total power in CCTF scale (1.06 kW/m average; 2.04 kW/m at peak). The following characteristics were commonly observed in C2-5, C2-4 and C2-SH2 tests.

(1) The differential pressure in the downcomer indicated the maximum value at the end of Acc injection period. Then, it slightly decreased and kept nearly constant value due to the voiding in the downcomer and the entrainment phenomena at the top downcomer.

(2) The overflow of the water from the downcomer to the containment tank 1 initiated approximately at the end of Acc injection period and continued through the rest of the whole transient.

(3) Flooding mass flow rate into the core was high (52 kg/m^2s) in Acc injection period. It experienced a stepwise decrease at the end of Acc injection period and was low (18 kg/m^2s) in LPCI injection period. Flooding mass flow rate was almost constant in LPCI injection period.

(4) The mass flow rate through each intact loop was identical with each other. No parallel oscillation occurred among the intact loops.

(5) Mass flow rate through the broken loop was nearly 150% of that through each intact loop. This is due to an additional differential pressure at the broken cold leg nozzle from the downcomer to the break. The additional differential pressure increased the steam flow through the broken loop.

(6) The fluid temperature in the upstream side of the steam generator showed a saturation temperature. On the contrary, the fluid temperature in the downstream side of the steam generator showed a fair amount of superheat. This indicates that the flow can be regarded as almost single-phase vapor there, and that the flowing water droplets evaporate in the steam generator completely by the heat exchange with water in the steam generators secondary side.

(7) In Acc injection period, the fluid temperature at the cold leg ECC ports was subcooled, and the flowing steam from the upper plenum to the downcomer was completely condensed. Resultantly, water plug was formed in the cold leg and moved oscillatorily. In LPCI injection period, the fluid temperature at the cold leg ECC ports was at saturation. Flowing steam was not condensed completely and the steam flow remained at exit of cold leg to the downcomer. Almost thermal equilibrium was established in cold legs.

(8) The broken cold leg nozzle pressure difference indicated a fairly large value comparing with the broken hot leg pressure difference. This indicates the effect of the broken cold leg nozzle pressure loss on the suppression of the steam flow through the intact loops is not negligible in order to estimate the core flooding mass flow rate.

(9) The water accumulation in the upper plenum and the steam generator inlet plenum was recognized, and then the steam binding effect is considered to be reduced.

(10) The cooling of the heater rods began just after the reflood initiation at the entire elevation of the core due to the early water spreading from the bottom to the top of the core.

(11) Both bottom quenching and top quenching occurred.

(12) The maximum turnaround temperature (1113 K) was observed at the midplane (1.83 m elevation) and in the central high power zone, which was in the region of the bottom quenching.

(13) The bottom quench front propagation was roughly one-dimensional in each power zone. The bottom quench front advanced more slowly in the higher power zones.

(14) The top quench time was very scattering depending on the radial location.

(15) The water accumulations in the downcomer, core, and upper plenum were azimuthally nearly uniform.

(16) The void fraction rapidly decreased after reflood initiation. The void fraction became almost constant at about 20 s after reflood initiation.

4.2 Quantitative comparison of low power test result with counterpart tests results

Referred tests

In order to investigate the effect of decay heat level on PWR reflood behavior, the result of the low power test C2-5 (Run 63) is compared quantitatively with the result of the CCTF Core-II base case test C2-4 (Run 62). The result of a counterpart test C2-SH2 is also compared in some aspects.

Summary of comparison

Comparison indicated the following characteristics.

(1) The steam generation rates in the core were nearly identical between both tests during the early period regardless the different power, since the steam generation rate was mainly contributed to release of the energy stored initially in the core rather than the supplied power. (Note that the initial stored energy is the same among the tests.) However, the steam generation rate was higher with the higher power during the later period, since the stored energy became higher with the higher power.

The above trend of the steam gemeration rate influenced the overall thermal hydraulics in the whole primary system, as below.

(2) The core differential pressures and the upper plenum differential pressures were nearly identical between both tests during the early period regardless the different power. They were lower in the high power during the later period, due to the higher steam velocity resulting in the higher void fraction (hence, less water accumulation, or the lower static head), and the higher water entrainment from the upper plenum to the loops.

(3) The intact and broken loop differential pressures were nearly identical between both tests during the early period regardless the different power. They were higher in the high power during the later period, due to the higher steam velocity resulting in the larger loop flow resistance.

(4) The core flooding mass flow rates were nearly identical between both tests during the early period regardless the different power. They were nearly identical between both tests also during the later period regardless the different power. This is because the less water accumulation in both the core and the upper plenumn and the higher steam and water flow rate from the core to the loops with the higher power compensate each other. (Note that the core flooding mass flow rate is considered to be the sum of the water accumulation rate in the core and the steam and water mass flow rate from the core to the loops.)

(5) The heat transfer coefficients were nearly identical between both tests until the turnaround time. It was lower in the higher power test in the later period. This is due to the higher void fraction. The above heat transfer characteristics led the higher turnaround temperature and the later quenching with the higher power.

The above results of the quantitative comparison are consistent with the results of FLECHT-SET tests performed in the scope of the initial average linear power from 1.88 kW/m to 2.35 kW/m[12),(13)]. Detailed comparison is shown in the following

sections 4.2.1 and 4.2.2.

4.2.1 Comparison of system behavior

(1) Steam generation rate in core

Figure 4.1 shows the transients of the evaluated steam generation rate in the core. The evaluated steam generation rate was obtained by the heat balance calculation in the core with the following equation, using the measured clad temperature of the heater rods.[14]

$$m_{go} = [\int_0^{z_0} N(q' - (c_p\rho A)_H (dT/dt)_H)dz - m_F c_{p\ell}(T_{sat} - T_F)] / (h_{fg} + c_{pg}(T_g - T_{sat})) \quad (1)$$

The evaluated steam generation rates are nearly identical between the tests C2-5 and C2-4 (5% discrepancy at 40 s after reflood initiation) in the early period (upto 100 s) in spite of the different power. This suggests that the heat released from the core in the period is mainly due to the initially stored energy rather than the supplied power, as described later.

In the later period (after 100 s), it is higher with the higher power (15% discrepancy at 250 s). The steam flow rates averaged in the time range of 200 s ~ 300 s are 3.4 kg/s in C2-5, 3.6 kg/s in C2-SH2 and 3.8 kg/s in C2-4, respectively.

(2) Contribution of stored energy and supplied energy to steam generation

The first term in the square blankets of Eq.(1) can be approximated as follows:

$$\begin{aligned} &\int_0^{z_0} N(q' - (c_p\rho A)_H (dT/dt)_H)\ dz = \int_0^{z_q - \Delta z} Nq'dz \\ &+ \int_{z_q + \Delta z}^{z_0} N\pi Dh(T_H - T_{sat})\ dz + N(c_p\rho A)_H (T_q - T_{sat})\ u_q \end{aligned} \quad (2)$$

The first and second terms in the right hand side of Eq.(2) are heat releases in the regions below and above the quench front, respectively. The third term is heat release at quench front due to quench front advancement. The first term depends mainly on the linear supplied power q' and the quenching elevation z_q, the second term mainly on the clad temperature T_H and z_q, and the last term mainly on the quench temperature T_q and quench velocity u_q.

Figure 4.2 shows the contribution of each term estimated with Eq.(2) by using measured q', z_q, T_H, T_q and u_q.

In the early period, the heat release below the quench front (first and third terms) is negligible and the heat release above the quench front (second term) is dominant. Therefore, it can be said that the heat release from the heater rods mainly depends on the clad temperature T_H and hence the stored heat in the heater rods rather

than the supplied power. Since the initial clad temperature were set to be identical with each other among the tests, it is considered that the steam generation rates were almost identical among the tests in the early period in spite of the different power.

On the other hand, in the later period, the heat release below the quench front (first term) becomes not negligible, as noticed from the figure. However, since q' is higher but z_q is lower with the higher power, the heat release below the quench front is almost identical among the tests. Most discrepancy comes from the heat release above quench front (second term) even in the later period. Since T_H becomes higher and $z_o-(z_q+\Delta_z)$ is larger with the higher power, the steam generation rate is higher with the higher power in the later period.

(3) Water accumulation in core

In Fig.4.3 the core differential pressure is shown, which is defined as the differential pressure between the bottom and the top of the core. The core differential pressure increases after reflood initiation. The increasing rate of the core differential pressure becomes generally smaller with time. This trend of the core differential pressure is commonly observed between both tests.

The core differential pressure is nearly equal to each other between both tests during the early period. However, it is lower (−10% at 200 s) with the higher power during the later period. This indicates the less water accumulation with the higher power. This is due to the higher void fraction and the higher carryover rate from the upper plenum to hot legs, caused by the higher steam velocity with the higher power.

The FLECHT-SET tests[12),13)] show that the core differential pressure in high power test (initial peak linear power: 2.35 kW/m) is the same as that in low power test (initial peak linear power: 1.88 kW/m) in the initial period of the reflood (30 s after reflood initiation) and afterwards the core differential pressure in high power test is lower (roughly −20%) than in low power test. This trend is the same as in the present CCTF tests.

The reason why the core differential pressure is regarded as water accumulation is explained below. The core differential pressure can be written as follows, since frictional and accelerational pressure losses are usually negligible during the reflood phase[15)] because of low steam and water superficial velocities.

$$\Delta P_c = \int_0^{z_o} \rho_\ell (1-\alpha) g dz = \frac{g M_c}{S_c} \qquad (3)$$

Thus the core differential pressure is affected by the axial void fraction distribution and indicates the water accumulation M_c multiplied by (g/S_c). According

to Murao-Iguchi void fraction correlation which has been developed for the reflood phase[15], void fraction is dependent mainly on steam flow rate and is higher with the higher steam flow rate. The identical core differential pressures during the early period in the present tests are explained by the identical void fraction distribution caused by the identical steam generation rates in spite of the different power, as shown in (1). On the other hand, the lower core differential pressure with the higher power during the later period is explained by the higher void fraction caused by the higher steam generation rate with the higher power.

(4) Pressure balance in system

Figure 4.4 shows the differential pressure in various locations. The following pressure balance must be established during the entire transient[16].

$$\Delta P_D = \Delta P_L + \Delta P_C + \Delta P_U + \Delta P_I \tag{4}$$

The terms ΔP_D, ΔP_L, ΔP_C and ΔP_U are the static heads of the water accumulated in the downcomer, the lower plenum, the core and the upper plenum, respectively. Only the term ΔP_I is the pressure loss due to the flow resistance through intact loops.

The core and upper plenum differential pressures are almost the same during the early period and are lower with the higher power during the later period, indicating the less water accumulation in the core and the upper plenum with the higher power. The reason has already described above.

On the contrary, the intact loop differential pressure is larger with the higher power. The reason is explained below. The intact loop differential pressure can be approximated as follows.

$$\Delta P_I = K_I \frac{m_I^2}{2\rho_g S_I^2} \qquad (I = \textit{Intact or Broken}) \tag{5}$$

The larger intact loop differential pressure ΔP_I with the higher power is attributed to the larger fluid flow rate m_I resulted by the larger steam generation rate in the core with the higher power, as mentioned in (1).

The lower plenum differential pressures are almost identical between both tests. The values correspond to the differential pressure when the lower plenum is filled with water, and therefore indicates the situation (The lower plenum is filled with water).

Except for the period of 200 s ~ 350 s, the downcomer differential pressures are almost identical between both tests, indicating the insensitiveness of both differential pressures against the power. The lower ΔP_C and the lower ΔP_U in the higher power

Thus, the power little affects the core flooding rate during the entire transient of the reflood, and it is inferred that the insensitiveness of the core flooding rate against the power can be extrapolated to a PWR scale.

(6) Pressure and fluid temperature as core boundary condition

Figure 4.11 shows the pressure in the upper plenum and the fluid temperature at the core inlet. The differences of the pressure and the fluid temperature at a given time between both tests are within 20 kPa and 5 K. Thus, the boundary conditions around the core are nearly equal between both tests. (Note that the core flooding rate is nearly equal among the tests in spite of the different power.) It can be said that the power little affects the boundary conditions of the core.

4.2.2 Comparison of core cooling behavior

(1) Clad temperature

Figure 4.12 shows an example of the clad temperature transient of the maximum power rod (high power zone) at the elevations of 1.83 m and 2.44 m. The higher turnaround temperature, the longer turnaround time and the longer quench time with the higher power are observed at the elevations.

Figure 4.13 shows the effect of the power on the axial distribution of the turnaround and the quench times. The longer turnaround and quench times with the higher power are observed along the entire axial length, especially in the upper elevation of the core.

Figure 4.14 shows the effect of the power on the axial distribution of the turnaround and the quench temperatures, and the temperature rise. The temperature rise is defined as the difference between the turnaround and the initial clad temperatures. The effect of the power on the turnaround temperature and the temperature rise is very small in the lower half of the core (up to the 1.5 m elevation). This is because of the immediate turnaround occurrence in the lower core just after reflood initiation, as shown in Fig.4.13. The turnaround temperature and the temperature rise are higher with the higher power in the upper core.

Until the turnaround occurrence the heat transfer coefficient is the same between both tests, as shown in Fig.4.15, and hence the higher turnaround temperature and temperature rise with the higher power can be attributed to direct result of the higher power.

Figure 4.16 shows the effect of the power on the turnaround temperature and the temperature rise in the medium power region. The 20% increased power (9.4 MW vs 7.9 MW) results in the 40% increased temperature rise and the 10% decreased

power (7.1 MW vs 7.9 MW) results in the 30% decreased temperature rise.

(2) Heat transfer coefficient

Figure 4.15 shows the heat transfer coefficient of the maximum power rod. The heat transfer coefficient was defined as follows.

$$h = \frac{q'-(C_p\rho A)_H(dT/dt)_H}{\pi D(T_H-T_{sat})}$$

During the early period (until 80 s at the 1.83 m elevation and 200 s at the 2.44 m elevation), the heat transfer coefficients are nearly identical between both tests independently of the different power. In this period, turnaround was experienced. After the period, the heat transfer coefficient is lower with the higher power. These indicate that it is conservative to assume the higher power in reactor safety evaluation.

The FLECHT-SET results also showed the insensitiveness of the heat transfer coefficient against the power during the early period until turnaround was experienced.

The insensitiveness of heat transfer coefficient against the power during the early period is explained by using Murao-Sugimoto heat transfer coefficient correlation[17] as follows. According to the correlation which has been assessed for the reflood phase, heat transfer coefficient is dependent mainly on void fraction and distance from quench front and it is lower with the higher void fraction and the larger distance. The above insensitiveness can be attributed to the identical heat releases, as shown in section 4.2.1(1), leading to the identical void fraction and the identical quench front elevation. The lower heat transfer coefficient with the higher power during the later period is considered to be due to the higher heat release with the higher power, as shown in section 4.2.1(1), leading to the higher void fraction and the lower quench front elevation (i.e. larger distance from quench front).

(3) Sectional differential pressure in core

Figure 4.17 shows the sectional differential pressure in the lower core (0 m~1.83 m). Generally, the sectional core differential pressure is smaller with the power. Only during the period when it shows the increasing (ex. 30 s~90 s in the section of 0.61 m~1.22 m elevation and 100 s~200 s in the section of 1.22 m~1.83 m elevation), the smaller differential pressure with the higher power is observed. This is mainly due to the slower quench front propagation with the higher power, which is shown before. Figure 4.18 shows the sectional differential pressure in the upper core. The smaller sectional differential pressure with the higher power is also observed in the upper core. It is caused by the higher steam velocity.

are compensated with the larger ΔP_I, as noticed from Eq.(4). This leads to the insensitiveness of the downcomer differential pressure against the power.

In Figs. 4.5 and 4.6, the broken loop differential pressure ΔP_B and the broken cold leg differential pressure ΔP_{BCL} are shown. They are larger with the higher power, due to the higher steam flow rate.

(5) Core flooding rate

Figure 4.7 shows the core flooding mass flux and its time integration. The core flooding mass fluxes are nearly the same during the whole transient between both tests, independent of the different power. Figure 4.8 shows the effect of major parameters on the core flooding mass. The major test conditions referred in the figure are shown in Table 4.1. The core flooding mass is affected by the pressure, the initial clad temperature and the ECC injection rate. By comparing Fig.4.7 with Fig.4.8, it can be said that the power effect on the core flooding mass is very small in comparison with other parameter effect.

The FLECHT-SET data[12] also showed the core flooding rate was nearly the same even under the different power, as shown in Fig.4.9. Thus, the insensitiveness of the core flooding rate against the power is commonly observed. The reason is considered as follows.

The core flooding rate can be written as[16]

$$m_F = dM_C/dt + dM_U/dt + m_L \qquad (6)$$

The water accumulation rate in the core dM_C/dt was estimated from measured ΔP_C by using Eq.(3). Similarly dM_U/dt was estimated from measured ΔP_U. The total loop mass flow rate m_L was estimated from the measured differential pressure across the pump simulator by using the given flow resistance coefficient. The contribution of each term is shown in Fig.4.10.

During the early period (upto 100 s), M_C, M_U and $\int m_L dt$ are nearly the same between both tests, resulting in the same $\int m_F dt$. For this period, the initially stored heat of rods is a dominant factor for steam generation, as mentioned before. This leads to the identical steam generation rates causing the identical, M_C, M_U and m_L in spite of the different power.

On the other hand, during the later period, M_C and M_U are lower and $\int m_L dt$ is higher with the higher power. For this period, the steam generation rate is higher with the higher power. This leads to the lower dM_C/dt and dM_U/dt and the higher m_L with the higher power. The insensitiveness of the core flooding rate against the power is caused by the compensation of lower dM_C/dt and dM_U/dt and the higher m_L with the higher power during the later period.

4.3 Special phenomena under low power condition

Under the low power condition of test C2-SH2 (Run 54), significant pressure oscillation was observed. This oscillation is observed after about 700 s after reflood initiation in the test, as shown in Fig. 4.19.

The oscillation begins when the broken cold leg nozzle pressure difference becomes zero, as noticed from Fig.4.19. This suggests that the complete steam condensation at ECC ports and the formation of the stagnant subcooled water plug at the ECC ports are the causes of this type of the oscillation. The measured subcooled fluid temperature at ECC port, shown in Fig.4.20, supports the formation of the subcooled water plug at ECC ports in the cold legs. Data indicated that the period of the pressure oscillation is a few seconds. The above situation was realized when the power supply was decreased to about 1.7 MW. This value corresponds the estimated power decay at 730 s after scram in PWR.

Although the significant pressure oscillation occurred under the low power condition, the oscillation indicated no adverse effect on the core cooling. During the oscillation, the whole core was kept to be cooled down.

4.4 Discussion on insensitiveness of decay heat to core flooding rate

The insensitiveness of the core flooding mass flow rate against the decay heat has been explained experimentally and qualitatively in section 4.2.1 (5). In this section, quantitative explanation on this subject is performed by using reflood analysis code REFLA[7],[8].

The REFLA code predicts the transient of static head in core ΔP_{cj} at a given linear power density q'_j. From this, we can predict the water accumulation rate dM_{cj}/dt as follows, neglectiong the frictional and accelerational pressure losses.

$$dM_{cj}/dt = \frac{S_c}{g}\left[\frac{d\Delta P_{cj}}{dt}\right] \tag{7}$$

On the other hand, from equations (4) and (5), the intact loop mass flow rate can be approximated as follows:

$$m_{lj} = \sqrt{\frac{2\rho_g S_I^2(\Delta P_D - \Delta P_L - \Delta P_{cj})}{K_I}} \tag{8}$$

According to CCTF tests, the broken loop mass flow rate can be assumed to be

1.5 times of the intact loop mass flow rate. Finally, the core flooding mass flow rate m_{Fj} at a given linear power density can be obtained from predicted ΔP_{cj} with Eqs. (7),(8), and (9).

$$m_{Fj} = dM_{cj}/dt + 3m_{Ij} + m_{Bj} = dM_{cj}/dt + 4.5m_{Ij} \quad (9)$$

Figure 4.21 shows the predicted linear density effect on the core flooding mass flow rate. It can be noticed from Fig. 4.21 (1) that the integration of the core flooding mass flow rate is little affected by the linear power density in the investigated range. In addition, it can be noticed from Fig. 4.21 (2) that the core flooding mass flow rate is less in dependent on linear power density with the higher linear power density.

Thus, the insensitiveness of the core flooding mass flow rate against the linear power density was analytically confirmed in the range referring the very conservative case and the most probable case. Therefore, the insensitiveness is considered to be extrapolated to a PWR scale.

5. Conclusions

The following items on decay heat level effect on PWR reflood phenomena were revealed by investigation on results of CCTF tests in the range of 1.06 kW/m to 1.4 kW/m of initial average linear power (Peak linear power: 2.04 kW/m to 2.69 kW/m; Total power: 7.1 MW to 9.4 MW). These power levels simulate most probable case to very conservative case for PWR LOCA analyses.

(1) The overall flow characteristics in the low power test (1.06 kW/m of initial average linear power) were qualitatively similar to that of the base case test (1.4 kW/m of initial average linear power). Any qualitatively different phenomena were not recognized during reflood phase. This indicates that it is reasonable to utilize the physical reflood model developed from the result of the base case test under the low power condition at least up to 1.06 kW/m of the initial average linear power for a prediction of PWR reflood phenomena.

(2) On the other hand, the following quantitative influence of the power on PWR reflood phenomena was observed. This result was consistent to that previously observed in FLECHT-SET tests performed in the scope of the initial average linear power from 1.88 kW/m to 2.35 kW/m.

(i) The steam generation rates in the core were nearly identical in the above power range during the early period (approximately until 100 s after reflood initiation) regardless the different power level, since the steam generation rate was mainly contributed to the release of the energy stored initially in the core rather than the supplied power. On the other hand, the steam generation rates were higher with the higher power during the later period, (approximately later than 100 s after reflood initiation) since the stored energy became higher with the higher power.

(ii) The core flooding mass flow rates were nearly identical in the above power range during the whole reflood period. The pressures in the upper plenum and the subcoolings at the core inlet were also nearly identical regardless the different power level. These indicates that the core boundary condition important for core cooling is little influenced by decay heat level. The insensitiveness of the core flooding mass flow rate against the decay heat was analytically confirmed.

(iii) The heat transfer coefficients were nearly identical in the above power range until the turnaround time. It was lower with the higher power during the later period. This characteristic leads to the higher turnaround temperature and the later quenching with the higher power. This indicates that it is conservative to assume the higher decay heat for

reactor safety evaluation, which is consistent to current reactor safety evaluation treatment.

(3) The little influence of the decay heat level on core flooding mass flow rate and heat transfer coefficient during the early period in the above power range is considered to be due to the fact that the steam generation rate in the core is contributed mostly by the release of the initial stored energy rather than the power supplied to the core.

(4) The identical core flooding mass flow rate during the later period is the result of the compensation between the decrease in water accumulation rate in the core and the increase of mass flow rate from core with the increase in the power.

(5) The lower heat transfer coefficient with the higher power during the later period is considered to be due to the higher void fraction and the lower quench front elevation, resulted by the higher steam generation with the higher power.

(6) Observed special phenomenon induced by the low power condition is a short-term (few seconds) differential pressure oscillation around the cold legs, which was caused by (1) the complete steam condensation at cold leg ECC ports and (2) the formation of the water plug in the cold legs. However, this oscillation had no adverse effect on the core cooling. The oscillation was observed when the power level reached the value corresponding to the decay heat at about 730 s after scram.

Nomenclature

A	:	Area	(m^2)
c_p	:	Specific heat	(J/kg/K)
D	:	Diameter of heater rods	(m)
g	:	Acceleration of gravity	(m^2/s)
h	:	Heat transfer coefficient	(W/m^2K)
h_{fg}	:	Latent heat of evaporation	(J/kg)
K	:	Flow resistance	
m	:	Mass flow rate	(kg/s)
M	:	Accumulated mass	(kg)
N	:	Number of heater rods	
q'	:	Linear power	(W/m)
S	:	Flow area	(m^2)
t	:	Time	(s)
T	:	Temperature	(K)
u	:	Velocity	(m/s)
u_q	:	Quench velocity	(m/s)
Z	:	Elevation	(m)
α	:	Void fraction	
ΔP	:	Differential pressure	(Pa)
ρ	:	Density	(kg/m^3)

(Subscript)

a	:	Acceleration
B	:	Broken loop
c	:	Core
D	:	Downcomer
f	:	Friction
F	:	At core inlet
g	:	Gas phase
H	:	Heater rod
I	:	Intact loop
ℓ	:	Liquid phase
L	:	Lower plenum
o	:	At core outlet
q	:	At quench front
sat	:	Saturation

U : Upper plenum
Δ : Differentiation

Acknowledgement

The authors are much indebted to Drs. Y. Kaneko and T. Hiraoka for their guidance and encouragements for this program. The authors wish to express their appreciation to the members of their analysis group for valuable discussions. They also would like to express their thanks to the 2D/3D project members of the USA and FRG for valuable discussions.

References

(1) Hirano, K. and Murao, Y.: "Large Scale Reflood Test", Nihon−Genshiryoku−Gakkai Shi (J. At. Energy Soc. Jpn.)[in Japanese], 2(10), 681, (1980)
(2) Iguchi, T., et al.: "Analysis report on CCTF reflood tests" [in Japanese], to be published as a JAERI−M report
(3) Adachi, H. et al.: "Design of Slab Core Test Facility (SCTF) in Large Scale Reflood Test Program, Part I: Core−I", JAERI−M 83−080, (1983)
(4) Murao, Y., et al.: "Analysis Report on CCTF Core−I Reflood Tests", to be published as a JAERI−M report.
(5) Murao, Y., et al.: "Evaluation Report on CCTF Core−I Reflood Test C1−5 (Run 014) − Over−all System Thermo−hydrodynamic Behaviors observed in the Base Case Test", JAERI−M 83−027, February (1983).
(6) Iguchi, T., et al.: "Assessment of current safety evaluation analysis on reflood behavior during PWR−LOCA by using CCTF data", J. Nucl. Sci. Technol., 24(11), PP. 887~896, November (1987).
(7) Okubo, T., and Murao, Y.: "Assessment of core thermal−hydrodynamic models of REFLA−1D code with CCTF data for reflood phase of PWR−LOCA", J. Nucl. Sci. Techol., 22(12), PP. 983~994, December (1985).
(8) Okubo, T., et al.: "Developmental assessment of REFLA−1DS code with data from CCTF tests for reflood phase of LOCA in PWRs with cold−leg−injection type ECCS", Fourth international topical meeting on nuclear reactor thermal−hydaulics (NURETH−4), Vol. 1
(9) Okubo, T., et al.: "Evaluation Report on CCTF Core−II Reflood Test C2−4

U : Upper plenum
Δ : Differentiation

Acknowledgement

The authors are much indebted to Drs. Y. Kaneko and T. Hiraoka for their guidance and encouragements for this program. The authors wish to express their appreciation to the members of their analysis group for valuable discussions. They also would like to express their thanks to the 2D/3D project members of the USA and FRG for valuable discussions.

References

(1) Hirano, K. and Murao, Y.: "Large Scale Reflood Test", Nihon−Genshiryoku−Gakkai Shi (J. At. Energy Soc. Jpn.)[in Japanese], 2(10), 681, (1980)
(2) Iguchi, T., et al.: "Analysis report on CCTF reflood tests" [in Japanese], to be published as a JAERI−M report
(3) Adachi, H. et al.: "Design of Slab Core Test Facility (SCTF) in Large Scale Reflood Test Program, Part I: Core−I", JAERI−M 83−080, (1983)
(4) Murao, Y., et al.: "Analysis Report on CCTF Core−I Reflood Tests", to be published as a JAERI−M report.
(5) Murao, Y., et al.: "Evaluation Report on CCTF Core−I Reflood Test C1−5 (Run 014) − Over−all System Thermo−hydrodynamic Behaviors observed in the Base Case Test", JAERI−M 83−027, February (1983).
(6) Iguchi, T., et al.: "Assessment of current safety evaluation analysis on reflood behavior during PWR−LOCA by using CCTF data", J. Nucl. Sci. Technol., 24(11), PP. 887−896, November (1987).
(7) Okubo, T., and Murao, Y.: "Assessment of core thermal−hydrodynamic models of REFLA−1D code with CCTF data for reflood phase of PWR−LOCA", J. Nucl. Sci. Techol., 22(12), PP. 983−994, December (1985).
(8) Okubo, T., et al.: "Developmental assessment of REFLA−1DS code with data from CCTF tests for reflood phase of LOCA in PWRs with cold−leg−injection type ECCS", Fourth international topical meeting on nuclear reactor thermal−hydaulics (NURETH−4), Vol. 1
(9) Okubo, T., et al.: "Evaluation Report on CCTF Core−II Reflood Test C2−4

U : Upper plenum
Δ : Differentiation

Acknowledgement

The authors are much indebted to Drs. Y. Kaneko and T. Hiraoka for their guidance and encouragements for this program. The authors wish to express their appreciation to the members of their analysis group for valuable discussions. They also would like to express their thanks to the 2D/3D project members of the USA and FRG for valuable discussions.

References

(1) Hirano, K. and Murao, Y.: "Large Scale Reflood Test", Nihon−Genshiryoku−Gakkai Shi (J. At. Energy Soc. Jpn.)[in Japanese], 2(10), 681, (1980)
(2) Iguchi, T., et al.: "Analysis report on CCTF reflood tests" [in Japanese], to be published as a JAERI−M report
(3) Adachi, H. et al.: "Design of Slab Core Test Facility (SCTF) in Large Scale Reflood Test Program, Part I: Core−I", JAERI−M 83−080, (1983)
(4) Murao, Y., et al.: "Analysis Report on CCTF Core−I Reflood Tests", to be published as a JAERI−M report.
(5) Murao, Y., et al.: "Evaluation Report on CCTF Core−I Reflood Test C1−5 (Run 014) − Over−all System Thermo−hydrodynamic Behaviors observed in the Base Case Test", JAERI−M 83−027, February (1983).
(6) Iguchi, T., et al.: "Assessment of current safety evaluation analysis on reflood behavior during PWR−LOCA by using CCTF data", J. Nucl. Sci. Technol., 24(11), PP. 887−896, November (1987).
(7) Okubo, T., and Murao, Y.: "Assessment of core thermal−hydrodynamic models of REFLA−1D code with CCTF data for reflood phase of PWR−LOCA", J. Nucl. Sci. Techol., 22(12), PP. 983−994, December (1985).
(8) Okubo, T., et al.: "Developmental assessment of REFLA−1DS code with data from CCTF tests for reflood phase of LOCA in PWRs with cold−leg−injection type ECCS", Fourth international topical meeting on nuclear reactor thermal−hydaulics (NURETH−4), Vol. 1
(9) Okubo, T., et al.: "Evaluation Report on CCTF Core−II Reflood Test C2−4

(Run 62) - Investigation of Reproducibility -", JAERI-M 85-026, March (1985).

(10) Murao, Y., et al.: "Evaluation Report on CCTF Core-I Reflood Test C1-19 (Run 38) - Experimental Assessment of the Evaluation Model for the Safety Analysis on the Reflood Phase of a PWR-LOCA", JAERI-M 83-029, February (1983).

(11) Iguchi, T., et al.: "Evaluation of CCTF Core-II Second Shakedown Test C2-SH2 (Run 054) - Effect of Core Supplied Power on Reflood Phenomena", JAERI-M 85-025, March (1985).

(12) Waring, J. P., et al.: "PWR FLECHT-SET Phase B1 Evaluation Report", WCAP-8583, August (1975).

(13) Cermak, J. O., et al.: "PWR full length emergency cooling heat transfer (FLECHT) group I test report", WCAP-7435, January (1970).

(14) Akimoto, H., et al., "Core radial power profile effect on system and core cooling behavior during reflood phase of PWR-LOCA with CCTF data", J. Nucl. Sci. Technol., 22(7), PP. 538~550, July (1985).

(15) Murao, Y. and Iguchi, T.: "Experimental modeling of core hydrodynamics during reflood phase of LOCA", J. Nucl. Sci. Technol., 19(8), PP. 613~627, August (1982).

(16) Murao, Y., et al.: "Experimental study of system behavior during reflood phase of PWR-LOCA using CCTF", J. Nucl. Sci. Technol., 19(9), PP. 705~719, September (1982)

(17) Murao, Y. and Sugimoto, J.: "Correlation of heat transfer coefficient for saturated film boiling during reflood phase prior to quenching", J. Nucl. Sci. Technol., 18(4), PP. 275~284, April (1981).
(1981)

Table 2.1 Scaled dimensions of CCTF components

(Scaling of components)

Component		PWR	CCTF	Ratio
Pressure vessel				
Vessel inside diameter	(mm)	4394 (173″)	1084	
Vessel thickness	(mm)	216 (8 1/2″)	90	
Core barrel outside diameter	(mm)	3874	961	
Core barrel inside diameter	(mm)	3760	929	
Thermal shield outside diameter	(mm)	4170		
Thermal shield inside diameter	(mm)	4030		
Downcomer length	(mm)	4849	4849	1/1
Downcomer gap	(mm)	114.3	61.5	
Downcomer flow area	(m^2)	4.23	0.197	1/21.44
Lower plenum volume	(m^3)	29.6	1.38	1/21.44
Upper plenum volume	(m^3)	43.6	2.76	1/15.8
Fuel (heater rod) assembly				
Number of bundles	(--)	193	32	
Rod array per bundle	(--)	15x15	8x8	
Rod heated length	(mm)	3660	3660	1/1
Rod pitch	(mm)	14.3	14.3	1/1
Fuel rod outside diameter	(mm)	10.72	10.7	1/1
Thimble tude diameter	(mm)	13.87	13.8	1/1
Instrument tude diameter	(mm)	13.87	13.8	1/1
Number of heater rods	(--)	39372	1824	1/21.58
Number of non-heated rods	(--)	4053	244	1/18.09
Core flow area	(m^2)	5.29	0.25	1/21.2
Core fluid volume	(m^3)	17.95	0.915	1/19.6
Primary loop				
Hot leg inside diameter	(mm)	736.6 (29″)	155.2	1/4.75
Hot leg flow area	(m^2)	0.426	0.019	1/22.54
Hot leg length	(mm)	3940	3940	1/1
Pump suction inside diameter	(mm)	787.4 (31″)	155.2	1/5.07
Pump suction flow area	(m^2)	0.487	0.019	1/25.77
Pump suction length	(mm)	9750	7950	1/1
Cold leg inside diameter	(mm)	698.5 (27.5″)	155.2	1/4.50
Cold leg flow area	(m^2)	0.383	0.019	1/20.26
Cold leg length	(mm)	5600	5600	1/1

Table 2.1 (Cont.)

Component		PWR	CCTF	Ratio
Steam generator simulator				
Number of tubes/loop	(--)	3388	158	1/21.44
Tube length (average)	(m)	20.5	15.2	1/1.35
Tube outside diameter	(mm)	22.225 (0.875″)	25.4	
Tube inside diameter	(mm)	19.7 (0.05″)	19.6	1/1
Tube wall thickness	(mm)	1.27	2.9	
Heat transfer area/loop	(m^2)	4784 (51500 ft^2)	192	1/24.92
Tube flow area/loop	(m^2)	1.03	0.048	1/21.44
Inlet plenum volume/loop	(m^3)	4.25	0.198	1/21.44
Outlet plenum volume/loop	(m^3)	4.25	0.198	1/21.44
Primary side volume/loop	(m^3)	30.50 (1077 ft^3)	1.2	1/25.4
Secondary side volume/loop	(m^3)	157.33 (5556 ft^3)	2.5	1/62.9
Others				
Containment tank 1	(m^3)		30	
Containment tank 2	(m^3)		50	
Storage tank	(m^3)		25	
Acc. tank	(m^3)		5	
Saturated water tank	(m^3)		3.5	

Table 2.2 Elevations of CCTF components

(Elevation of components)

Component		PWR	CCTF	Discrepancy
Bottom of heated region in core	(mm)	0	0	0
Top of heated region in core	(mm)	3660	3660	0
Top of downcomer	(mm)	4849	4849	0
Bottom of downcomer	(mm)	0	0	0
Centerline of cold leg	(mm)	5198	4927	-271
Bottom of cold leg (inside)	(mm)	4849	4849	0
Centerline of loop seal lower end	(mm)	2056	2047	-9
Bottom of loop seal lower end	(mm)	1662	1959	+297
Center of hot leg	(mm)	5198	4927	-271
Bottom of hot leg (inside)	(mm)	4830	4849	+19
Bottom of upper core plate	(mm)	3957	3957	0
Top of lower core plate	(mm)	-108	-50	+58
Bottom of tube sheet of steam generator	(mm)	7308	7307	-1
Lower end of steam generator plenum	(mm)	5713	5712	-1
Top of tubes of steam generator (avg)	(mm)	17952.7	14820	-3132.7

(Number of upper plenum internals)

Component	PWR (New type)	CCTF-II	
	Quantity	Desired quantity	Selected quantity
Control rod guide tubes	57	9.45	10
Support columns without mixers	50	8.29	10
Orifice plates	16	2.65	--
Open holes	70	11.61	12
Total	193	32	32

Table 2.3 Instruments provided by USNRC

Instrument	Number of sets	Number of sensors
DC FDG	18	162
DC VOP	1	1
DC drag disk	4	4
Core velocimeter	4	4
Core impedance probe	12	24
Core LLD	6	96
LP LLD	3	15
End box turbine meter	8	8
UP turbine meter	4	4
UP FDG	11	110
UP film probe	2	4
UP prong probe	2	4
UP VOP	1	1
VV turbine meter	2	2
VV string probe	2	2
HL film probe	2	4
HL VOP	1	1
Reference probe	1	1
Spool piece	8	89
Total	92	536

Note:

DC : Downcomer, FDG: Fluid distribution grid,
VOP: Video optical probe, LLD: Liquid level detector,
LP : Lower plenum, UP : Upper plenum,
VV : Vent valve HL : Hot leg

Table 3.1 Summary of measured test conditions for test C2-5 (Run 63)

		Measured	
Power			
Total (MW)	:	7.1	(Initial)
Linear (kW/m)	:	1.06	(Initial, Average)
Radial Power Distribution	:	1.37:1.20:0.76	
Decay Type: ANSx1.0 + Actinidex1.1		(40 sec after Scram)	
Pressure (MPa)			
System	:	0.20	
Steam Generator Secondary	:	5.2	
Temperature (K)			
Downcomer Wall	:	470	(Initial)
Primary Piping Wall	:	392	(Initial)
Steam Generator Secondary	:	540	(Initial)
Peak Clad at ECC Initiation	:	995	
Peak Clad at BOCREC	:	1075	
Lower Plenum Filled Liquid	:	390	(Initial)
ECC Liquid	:	308	
Water Level (m)			
Lower Plenum	:	0.86	(Initial)
Steam Generator Secondary	:	7.2	(Initial)
Injection Rate (m^3/s)			
Accumulator : into lower plenum		0.106	
into cold leg		0.091	
LPCI :		0.011	
ECC Injection Duration Time (s)			
Accumulator (After BOCREC)	:	17.0	

Table 3.2 Chronology of events for test C2-5 (Run 63)

Event	Time after test initiation (s)	Time after reflood initiation (s)
Test Initiated (Heater Rods Power on) (Data Recording Initiated)	0	-126.0
Accumulator Injection Initiated	118.0	-8.0
Power Decay Initiated (Bottom of Core Recovery)	126.0	0.0
Accumulator Injection Switched from Lower Plemum to Cold Leg	131.0	5.0
Accumulator Injection Ended and LPCI Injection Initiated	143.0	17.0
All Heater Rod Quenched	562.0	436.0
Power Turned off	1160.0	1034.0
LPCI Injection Ended	1160.0	1034.0
Test Ended (Data Recording Ended)	1190.0	1064.0

Table 4.1 Major test conditions referred in Fig. 4.8

	High pressure test	High ECC injection rate test	Low initial clad temperature test
Initial average linear power (kW/m)	1.4	1.2	1.4
Radial power profile	1.37 : 1.20 : 0.76	1.37 : 1.20 : 0.76	1.50 : 1.14 : 0.77
Pressure (MPa)	0.42	0.2	0.2
Initial peak clad temperature (K)	1073	1073	873
ECC injection rate (m^3/s) x Duration (s)			
Early period	0.089 x (0～17s)	0.092 x (0～17s)	0.085 x (0～17s)
Later period	0.011 x (17s onward)	0.025 x (17s onward)	0.011 x (17s onward)

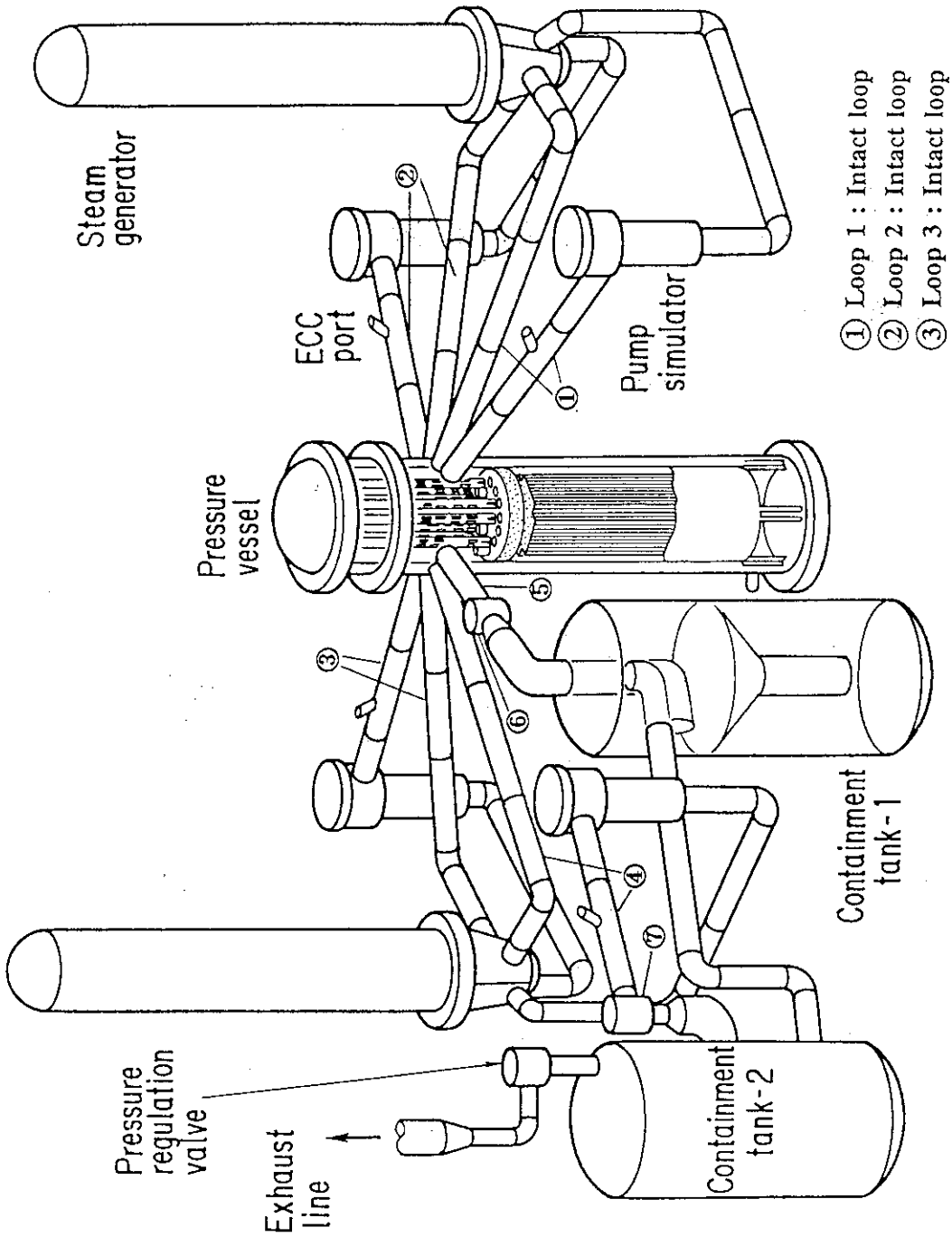

Fig. 2.1 Bird's-eye view of CCTF

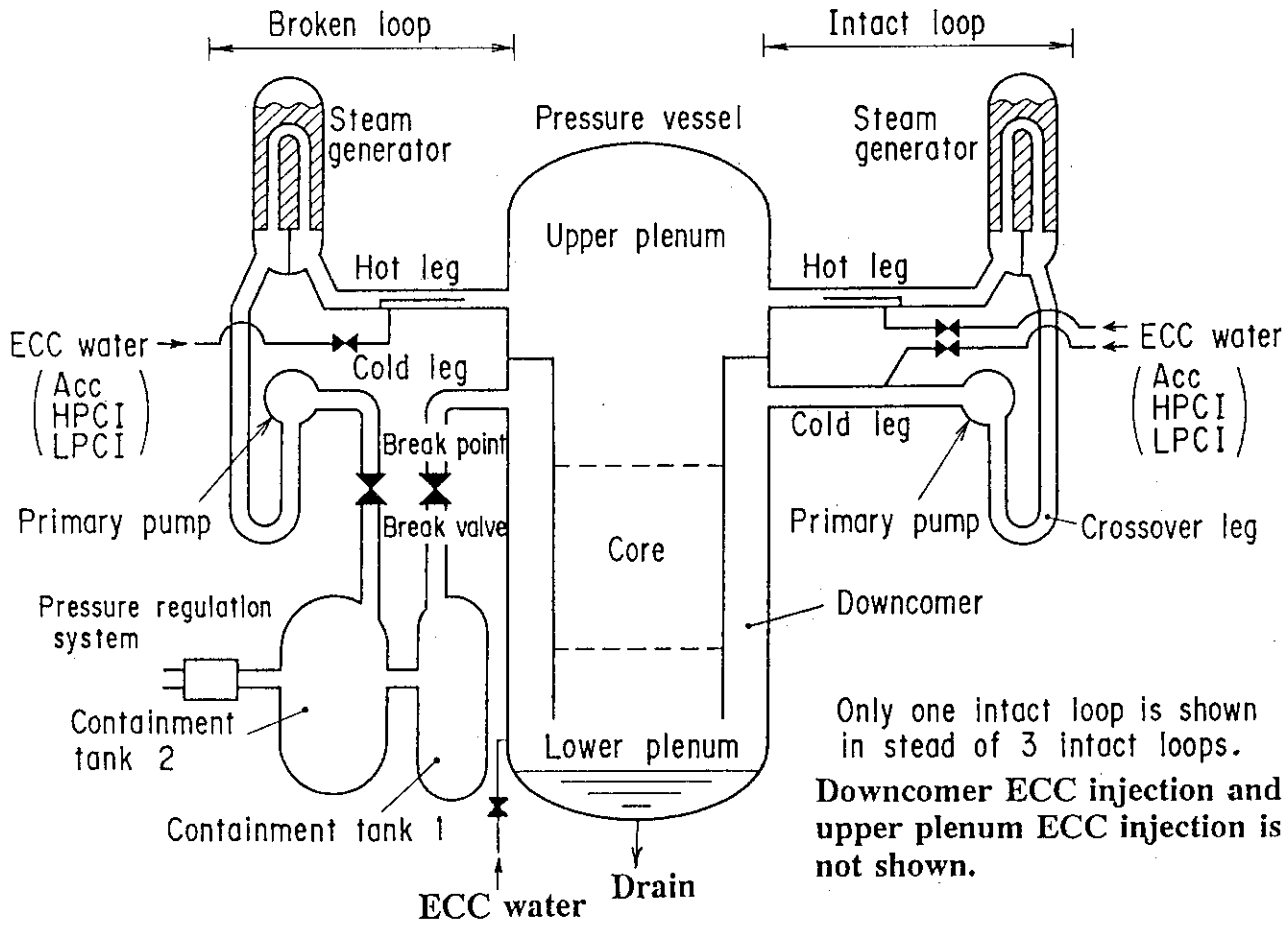

Fig. 2.2 Schematic diagram of CCTF main parts

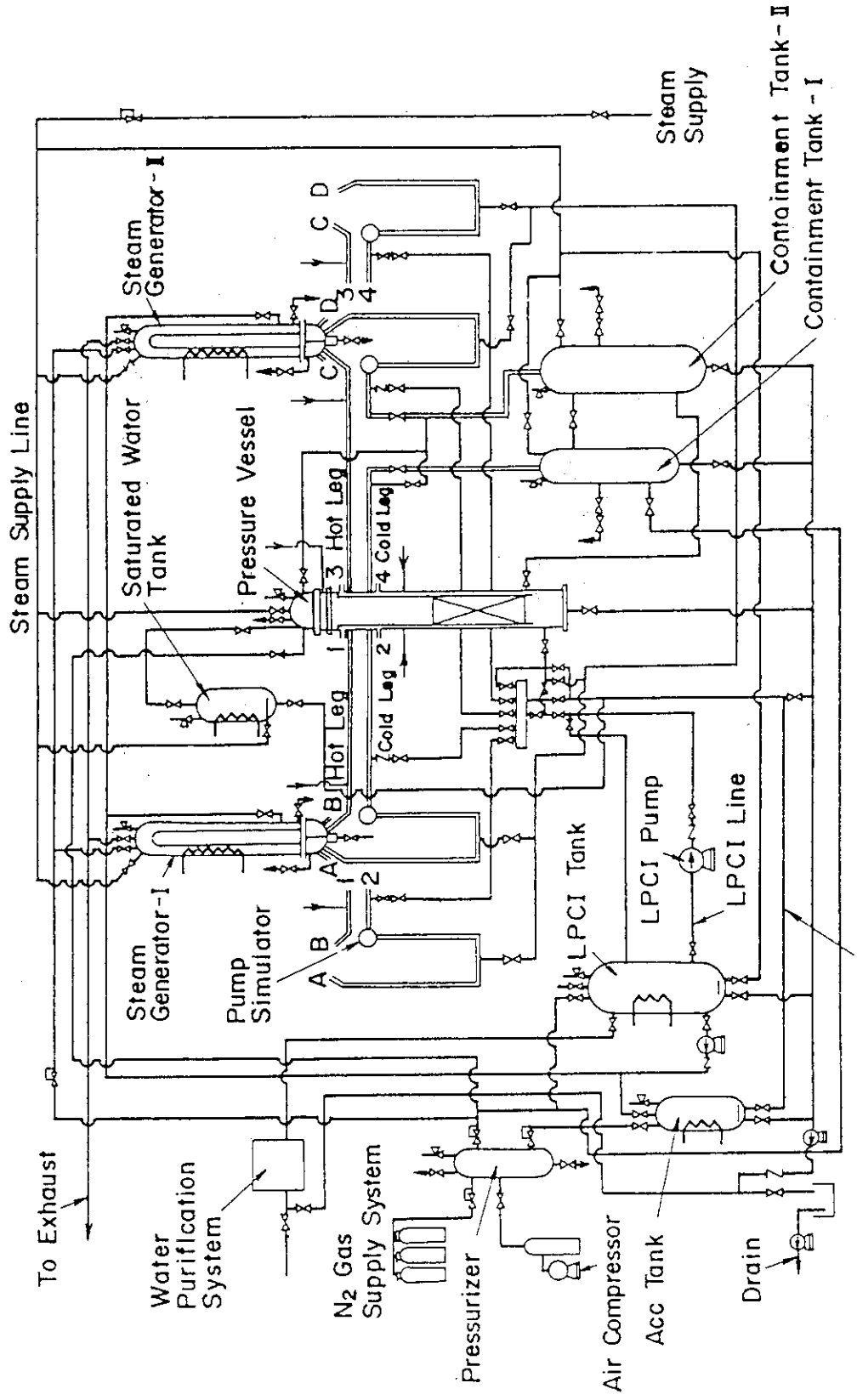

Fig. 2.3 Flow diagram of CCTF

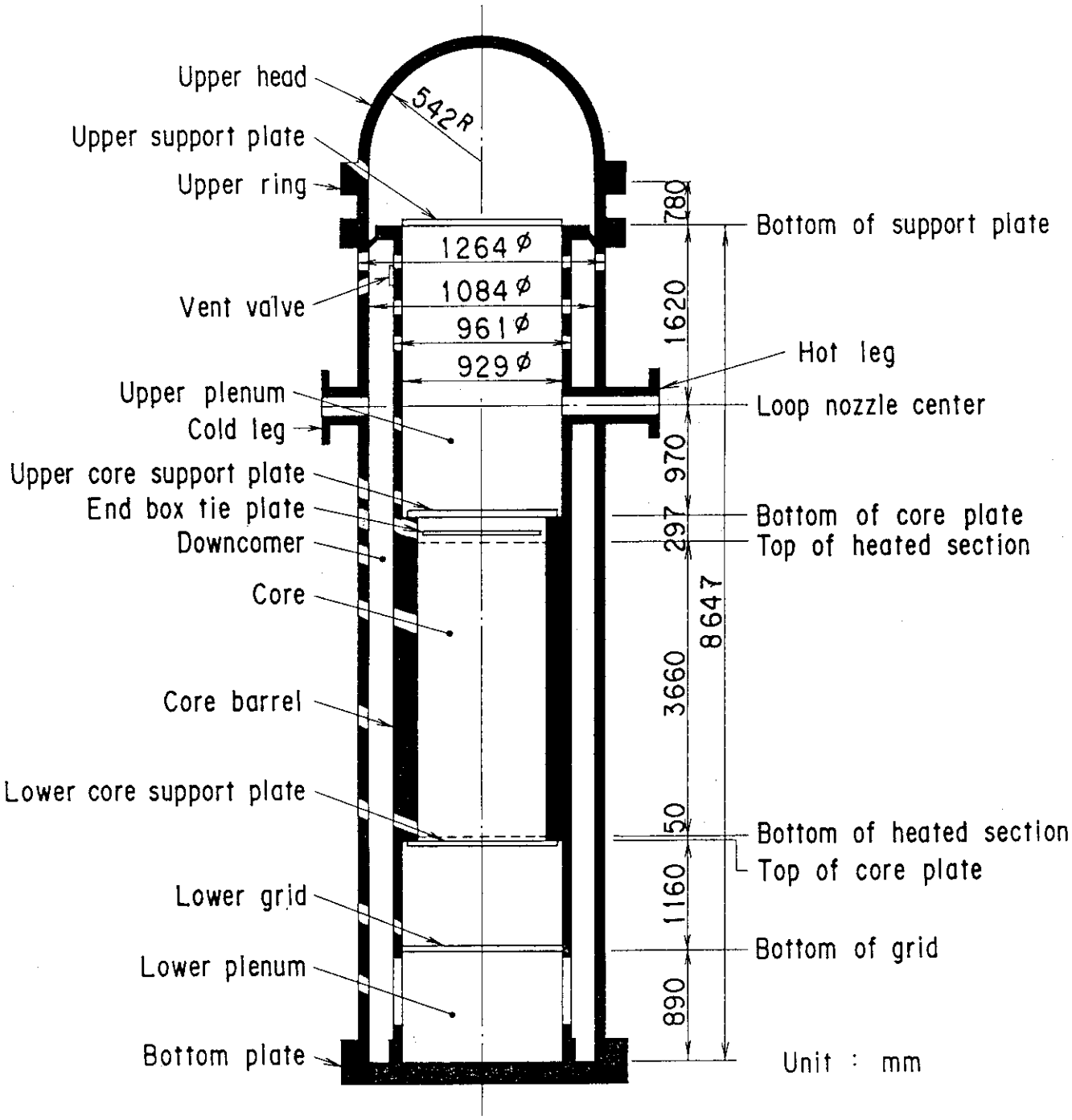

Fig. 2.4 CCTF Core-II pressure vessel

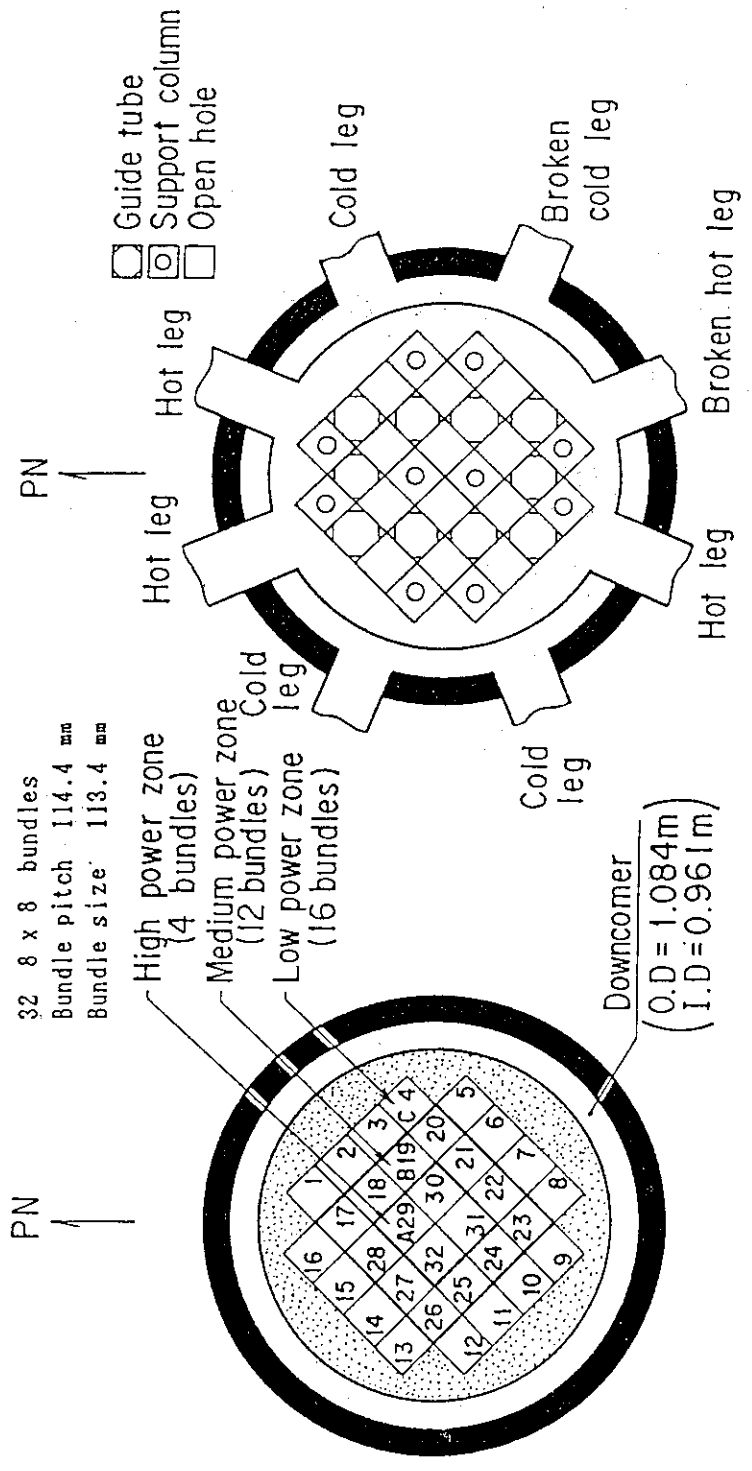

Fig. 2.5 Cross section of CCTF Core-II pressure vessel

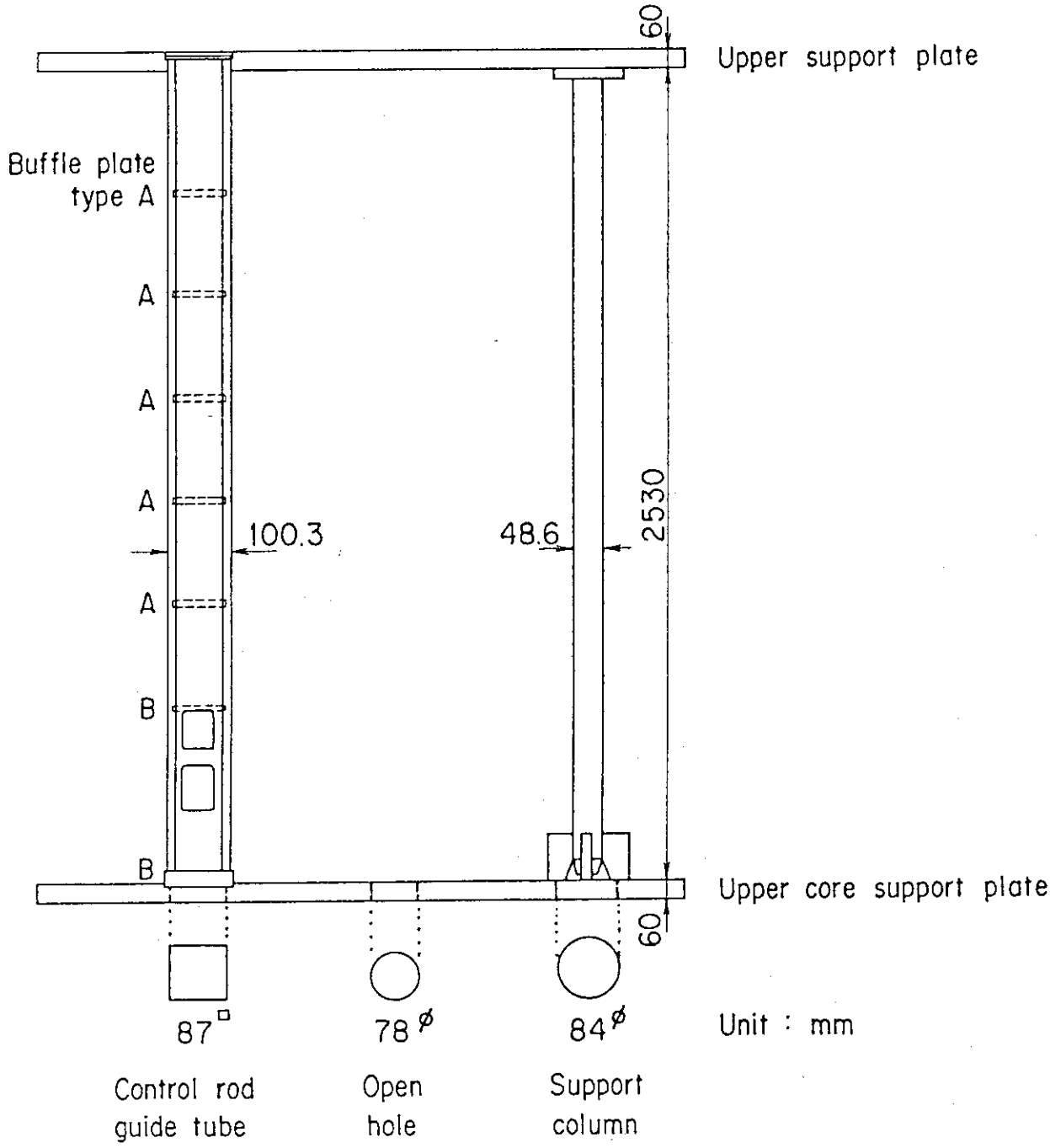

Fig. 2.6 Upper plenum internals

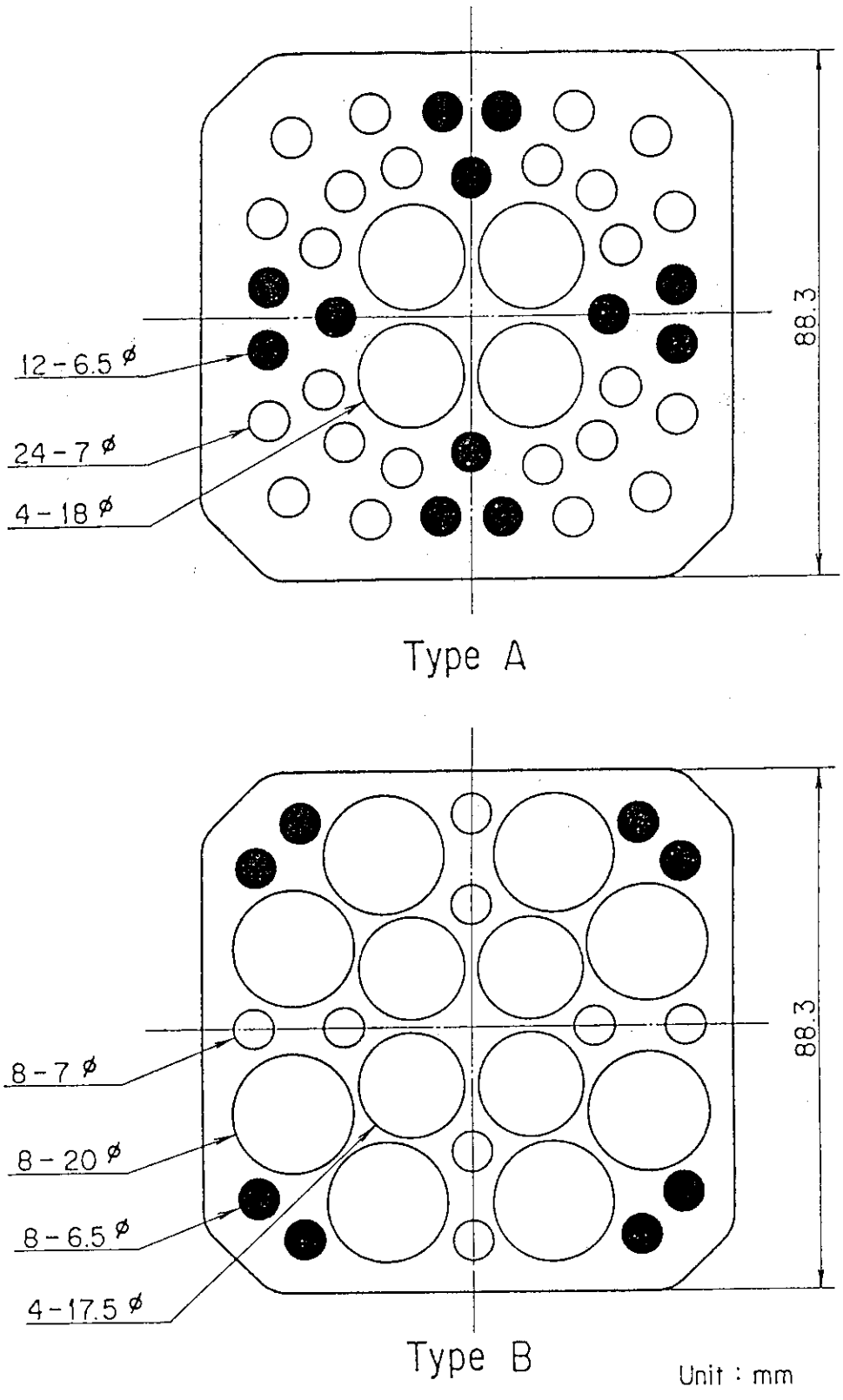

Fig. 2.7 Buffle plates in control rod guide tube

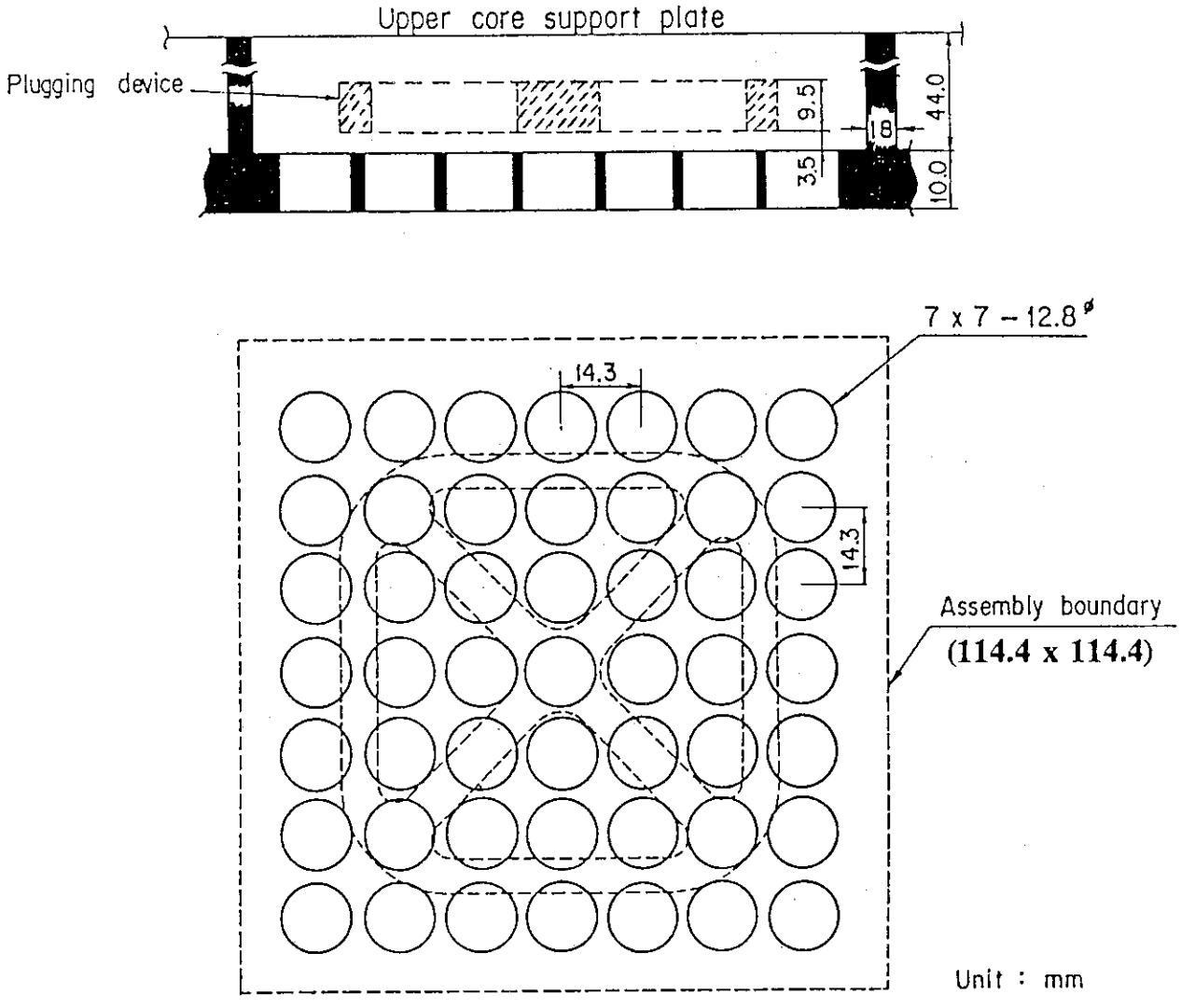

Fig. 2.8 Dimensions of holes of end box tie plate

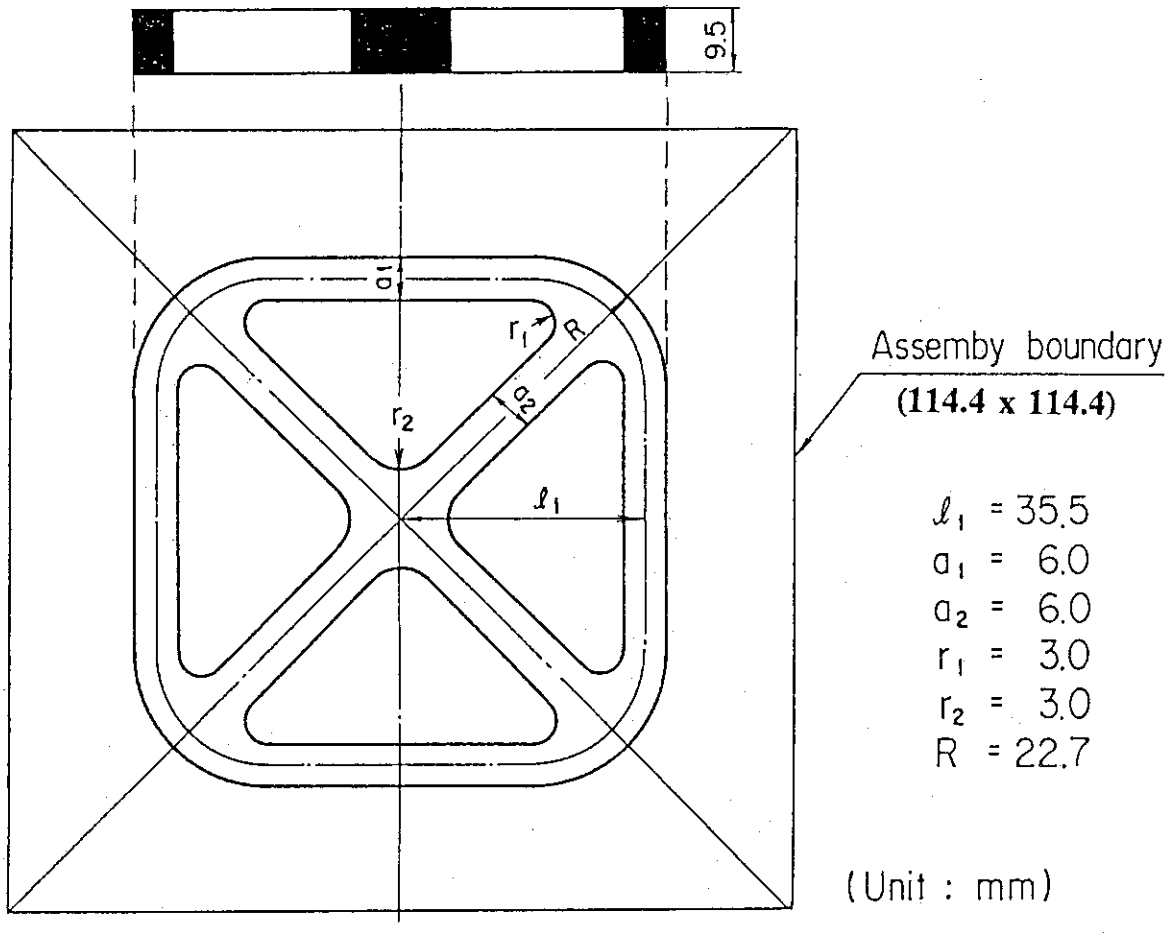

Fig. 2.9 Dimensions of plugging device

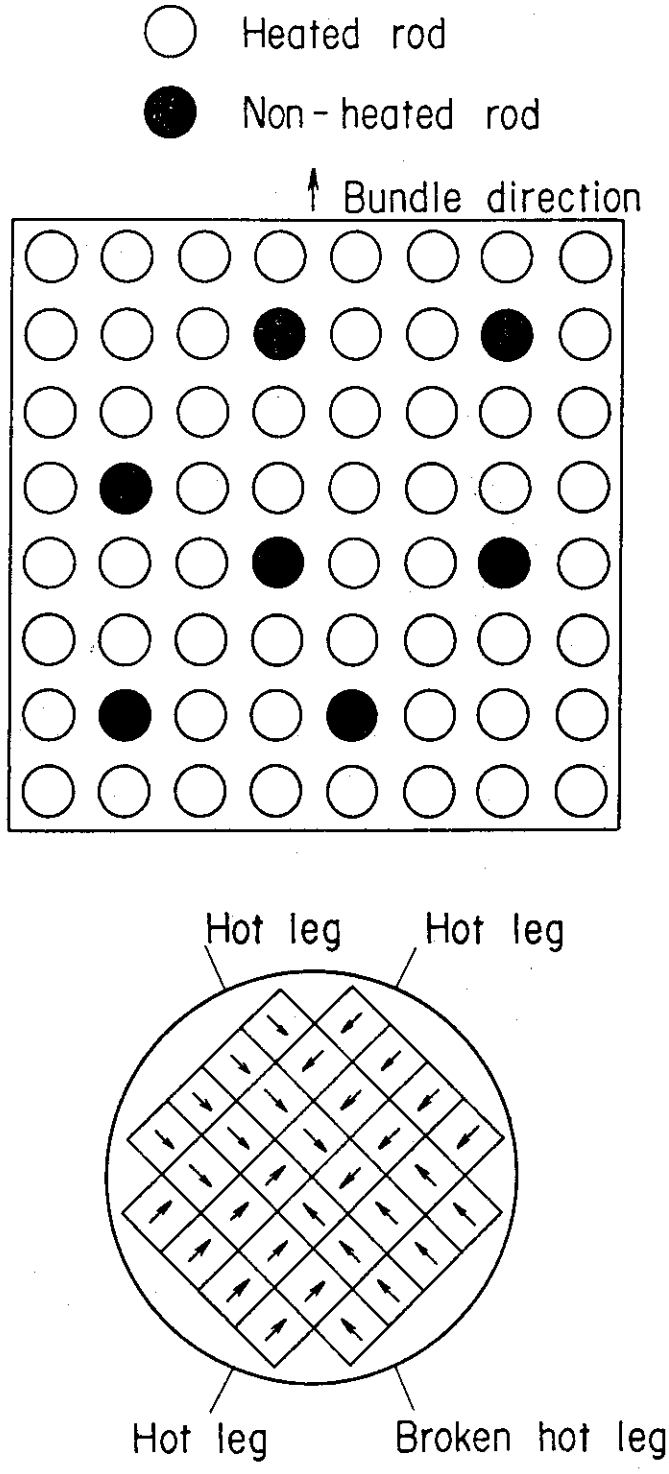

Fig. 2.10 Arrangement of non-heated rods

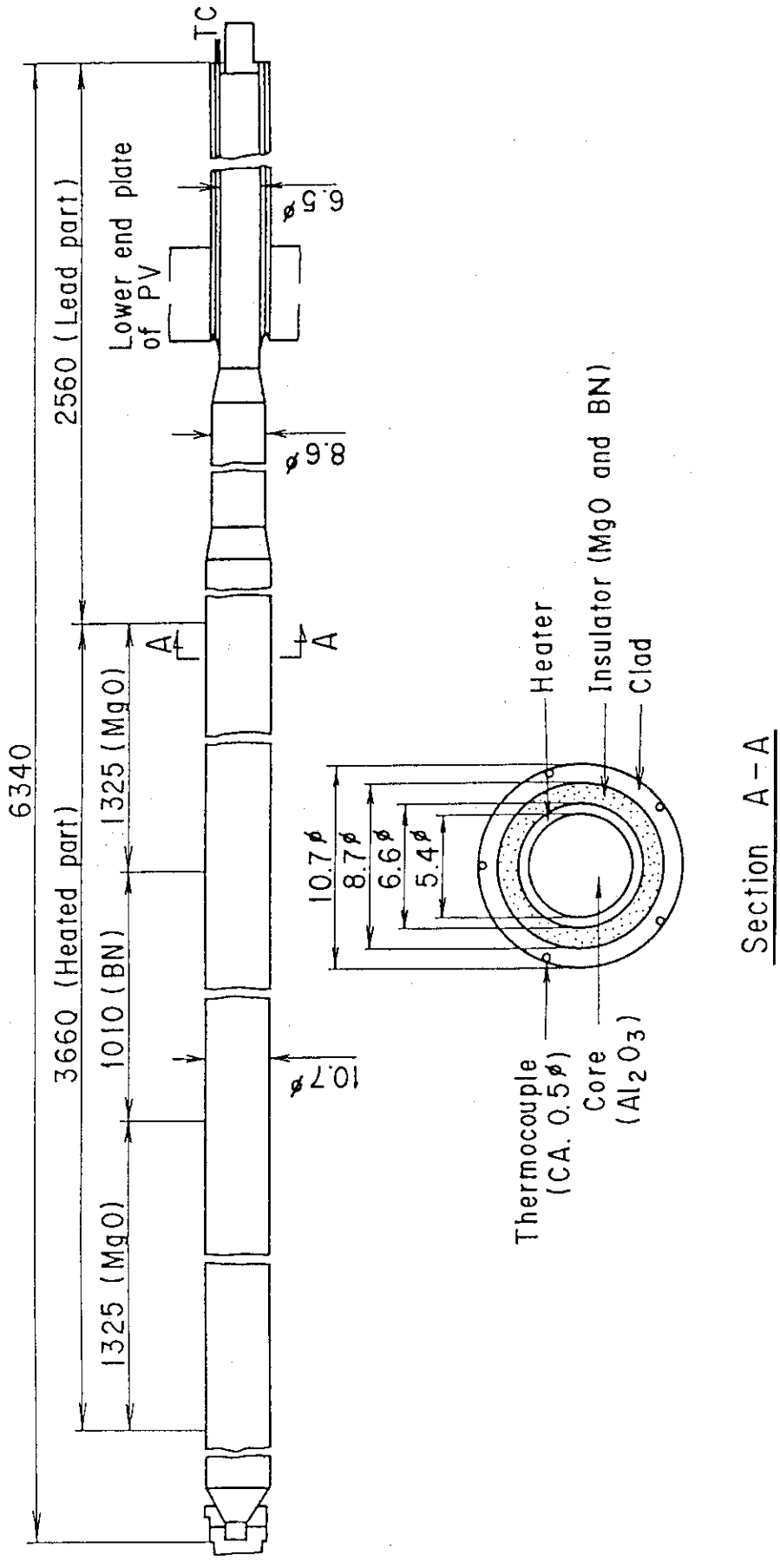

Fig. 2.11 Heater rod

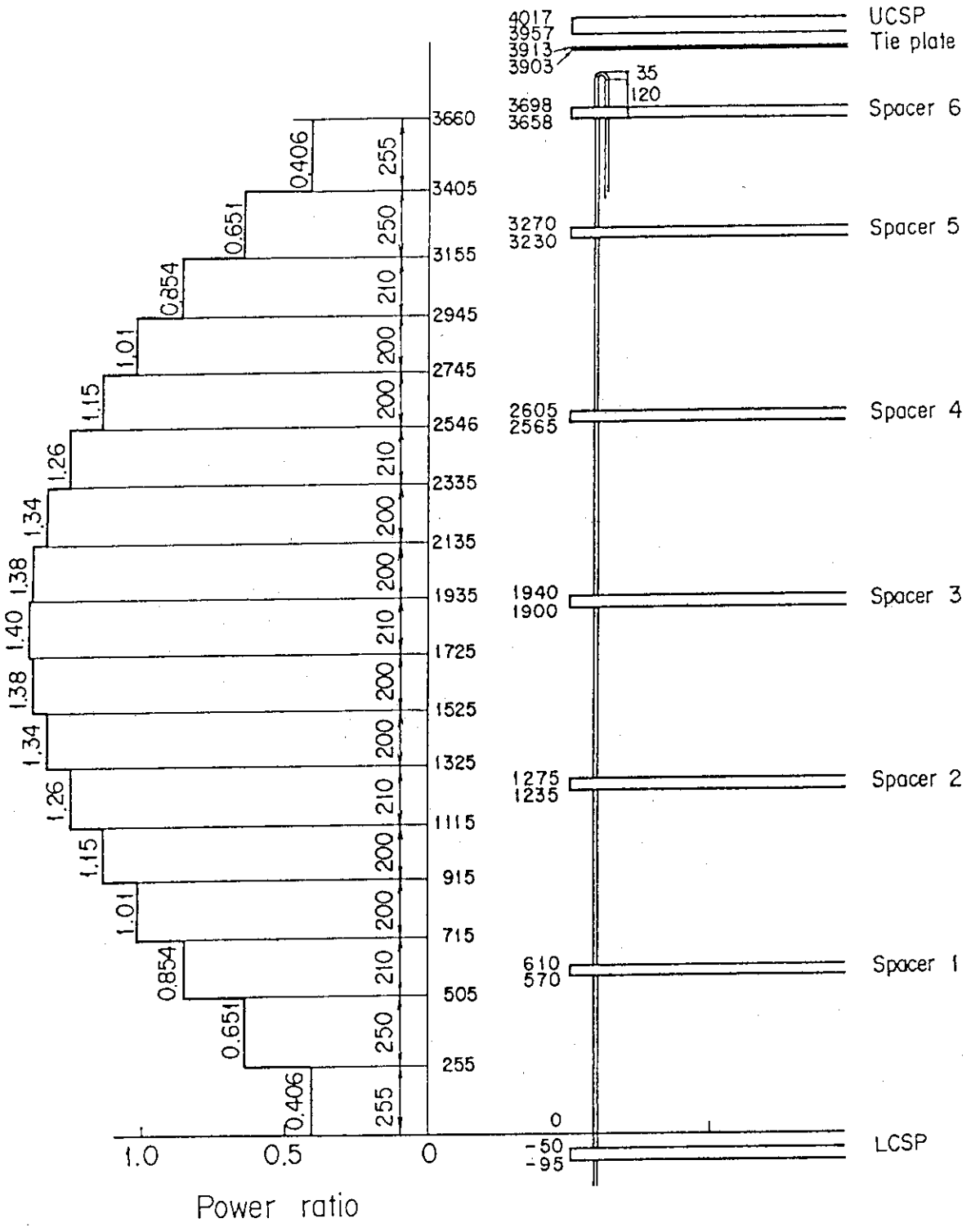

Fig. 2.12 Axial power profile of CCTF Core-II heater rod

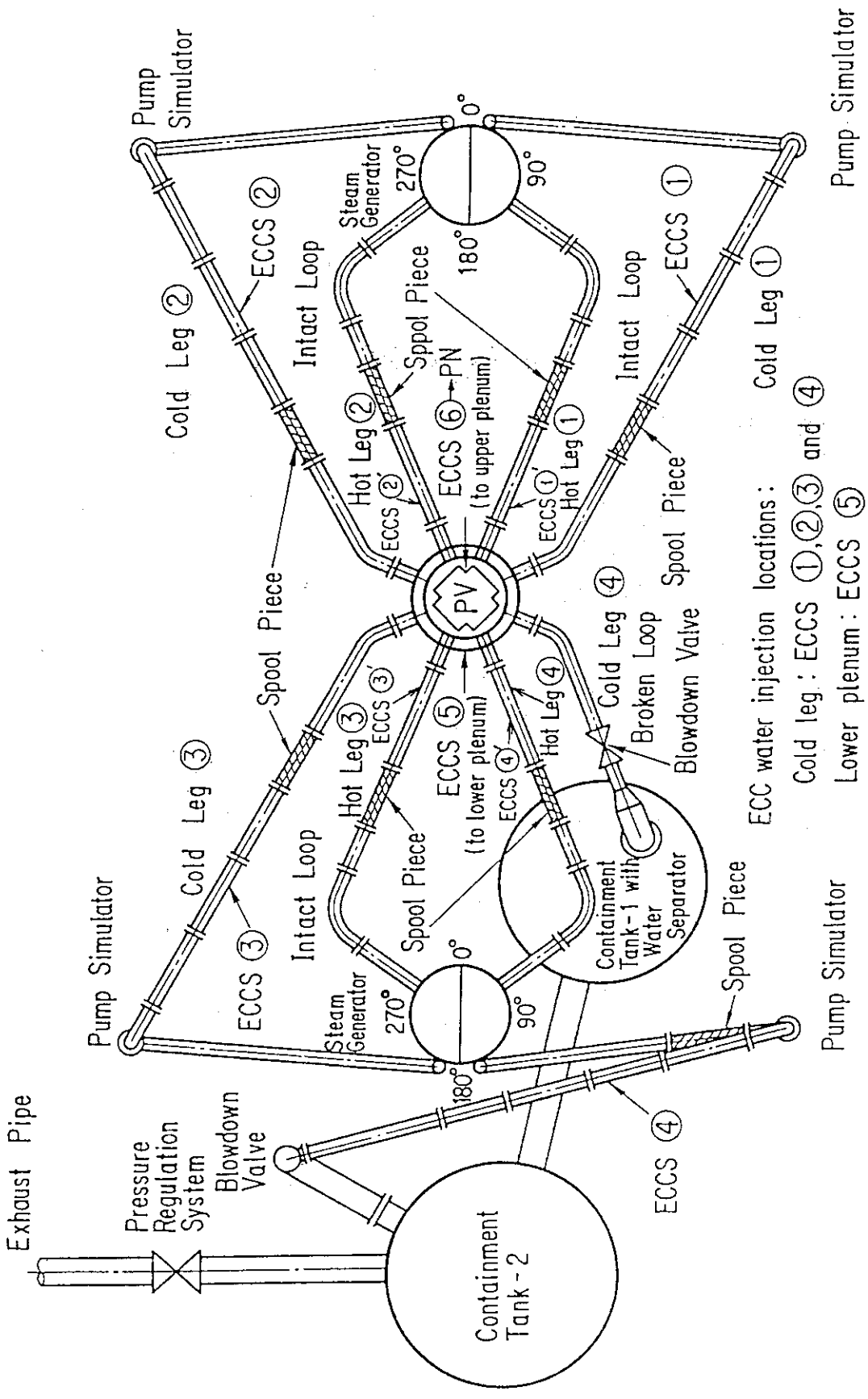

Fig. 2.13 Top view of primary loop pipings

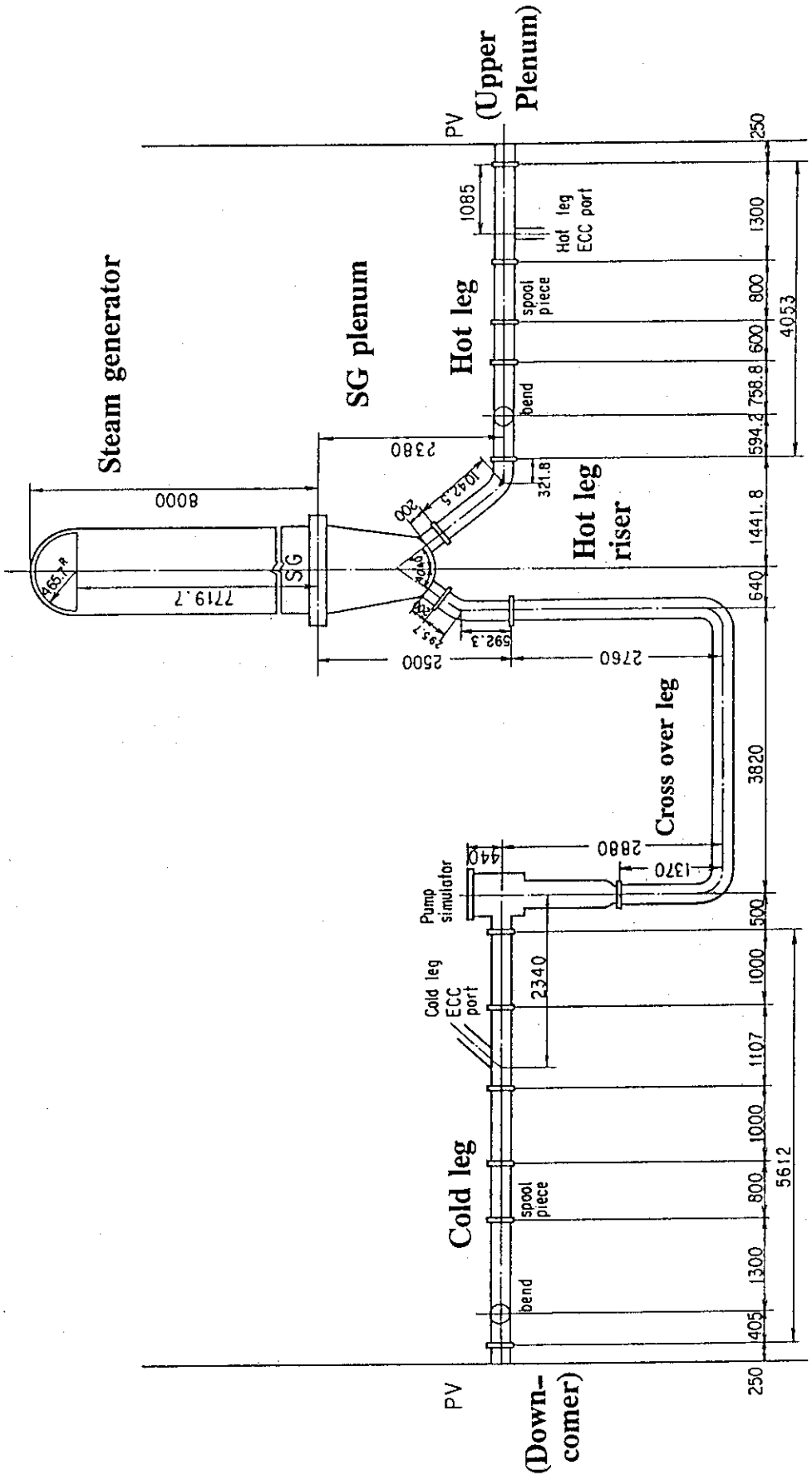

Fig. 2.14 Dimensions of intact loop

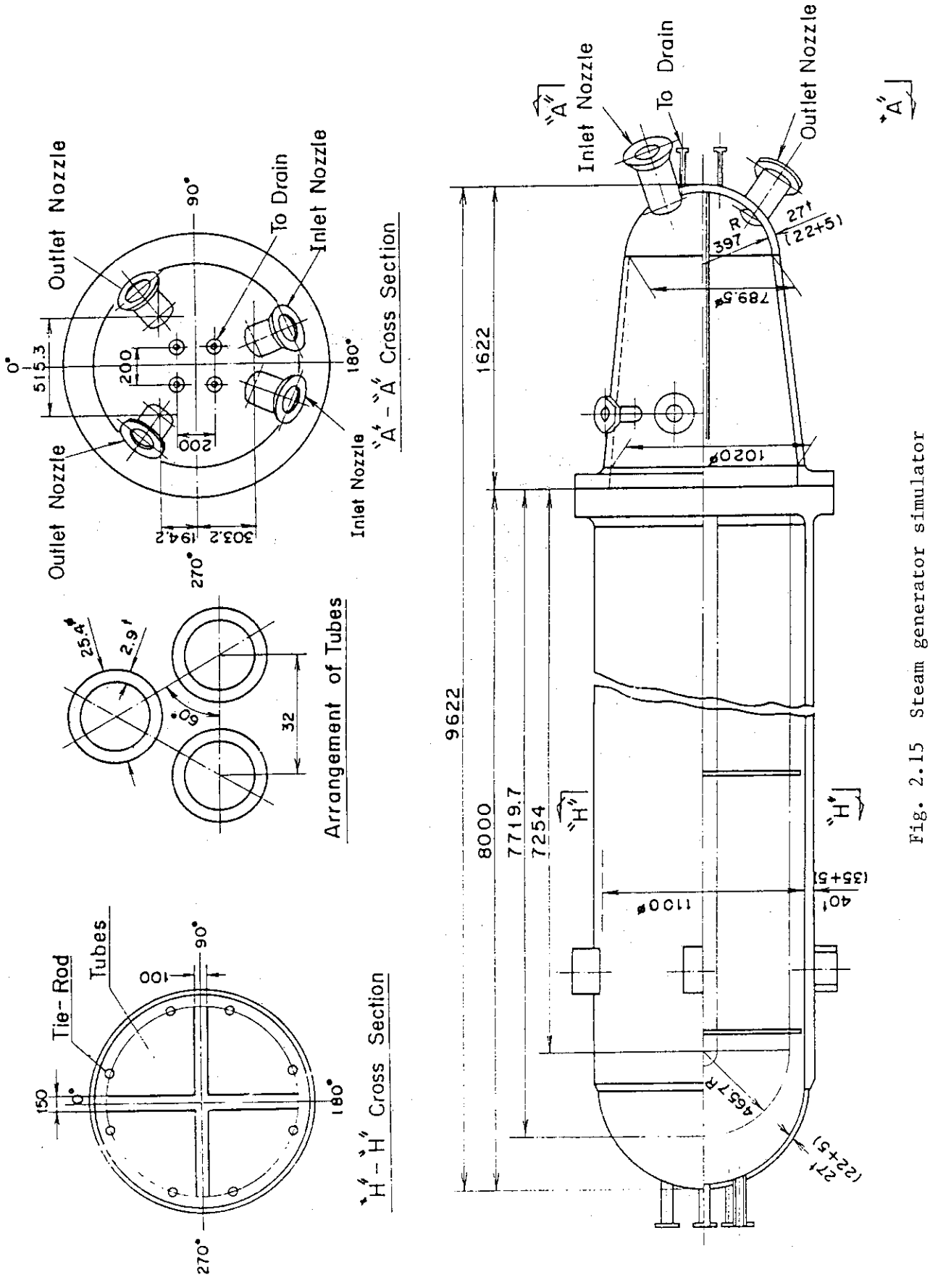

Fig. 2.15 Steam generator simulator

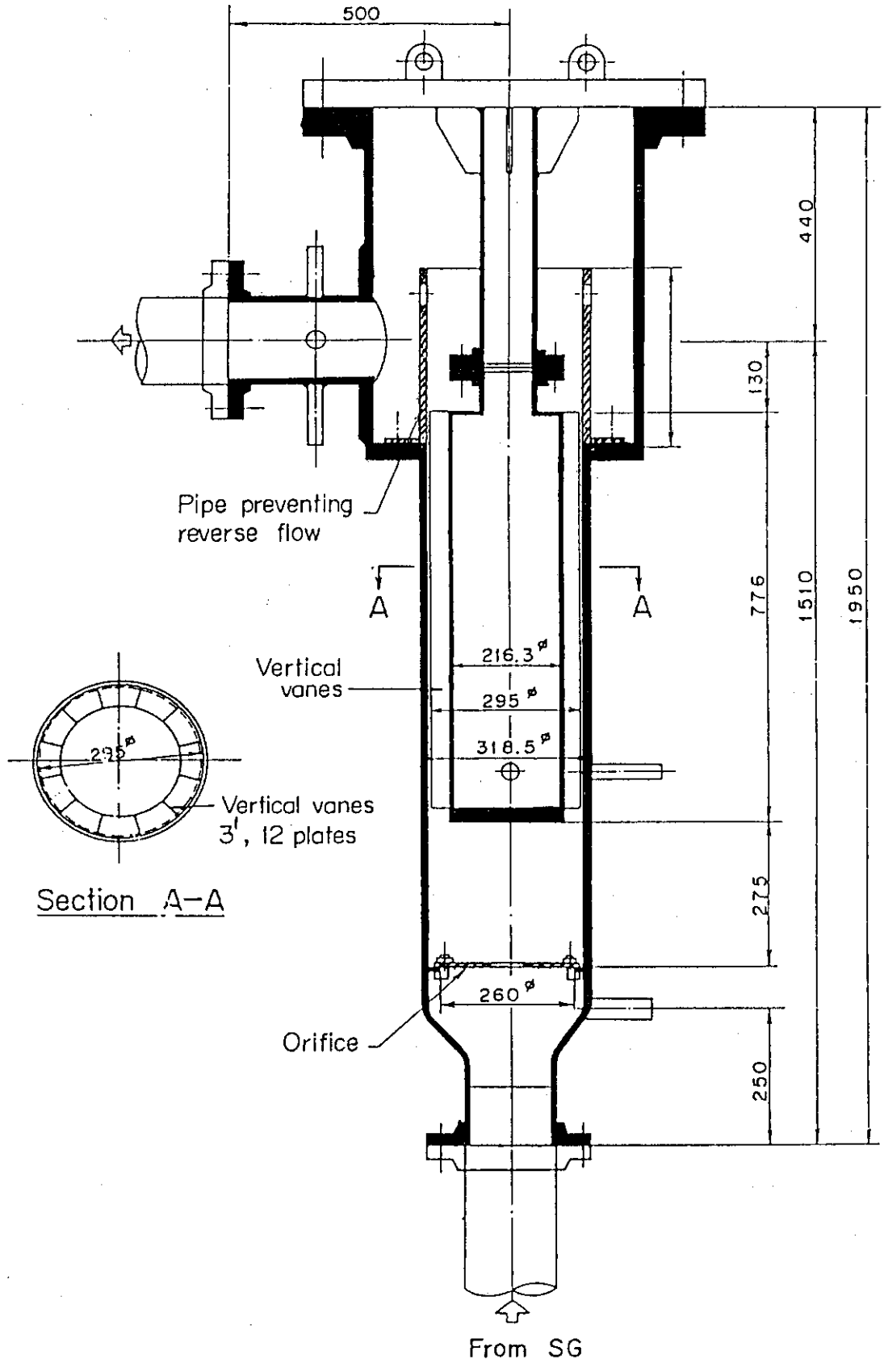

Fig. 2.16 Pump simulator

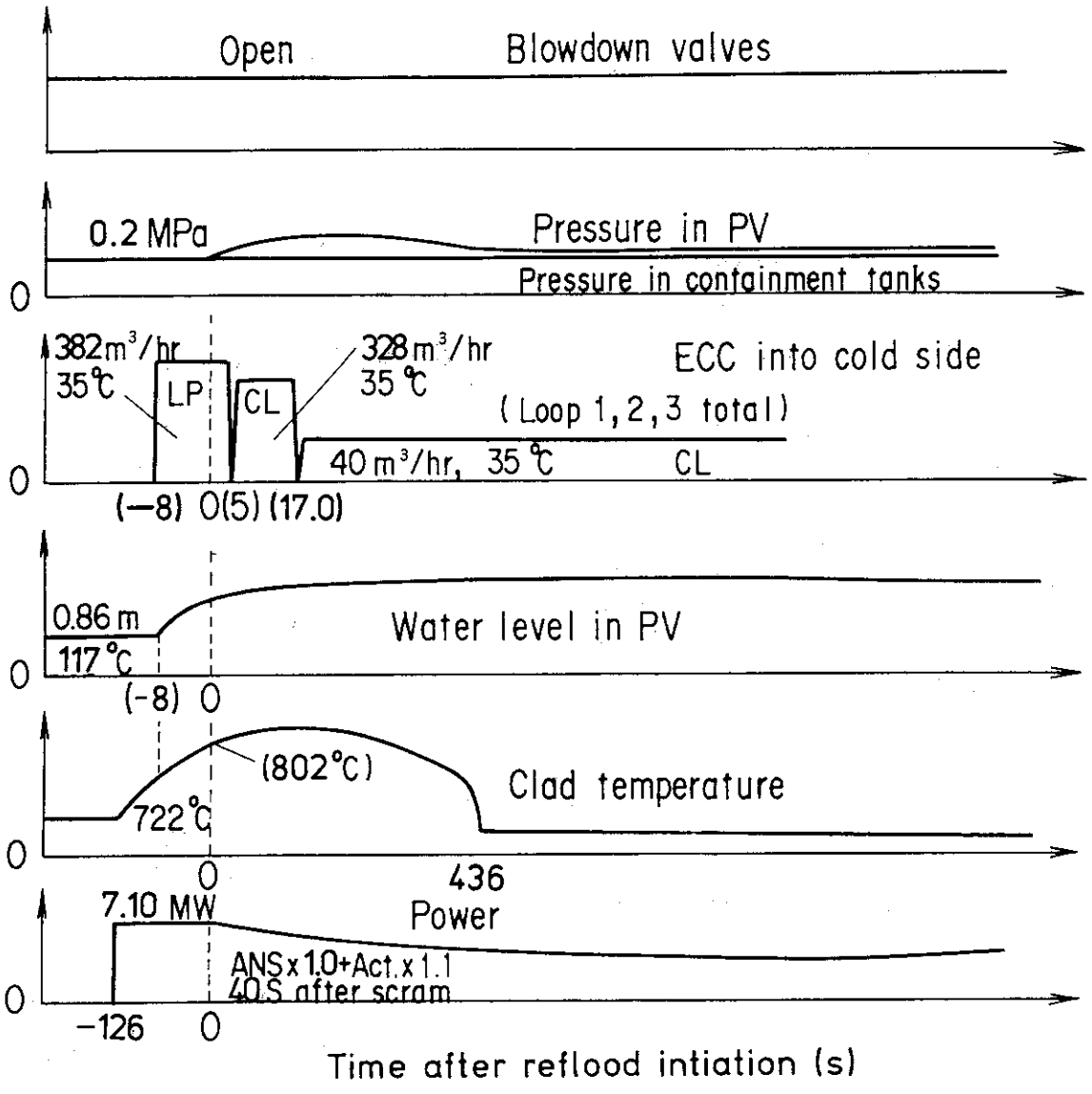

Note : ( ) means predicted value.

Fig. 3.1 Test sequence of test C2-5 (Run 63)

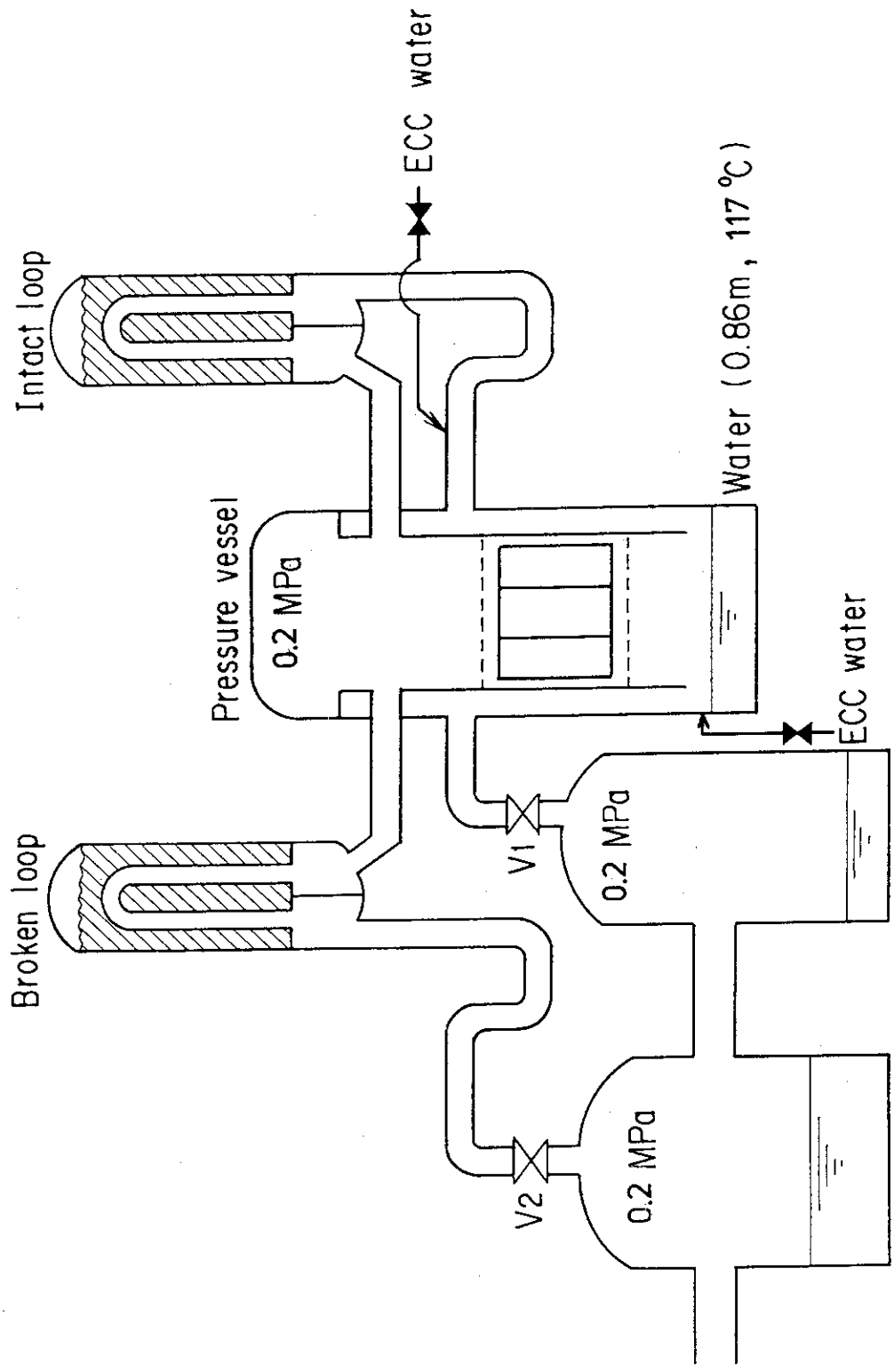

Fig. 3.2 Initial set-up of test C2-5 (Run 63)

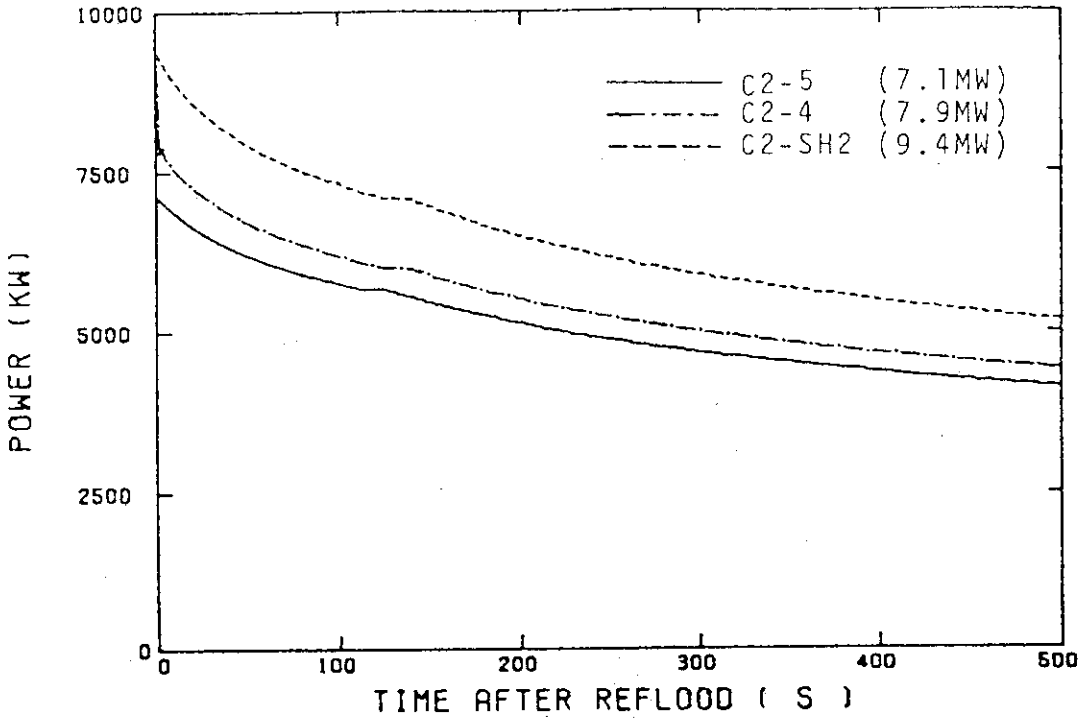

Fig. 3.3 Comparison of the power supplied to the core

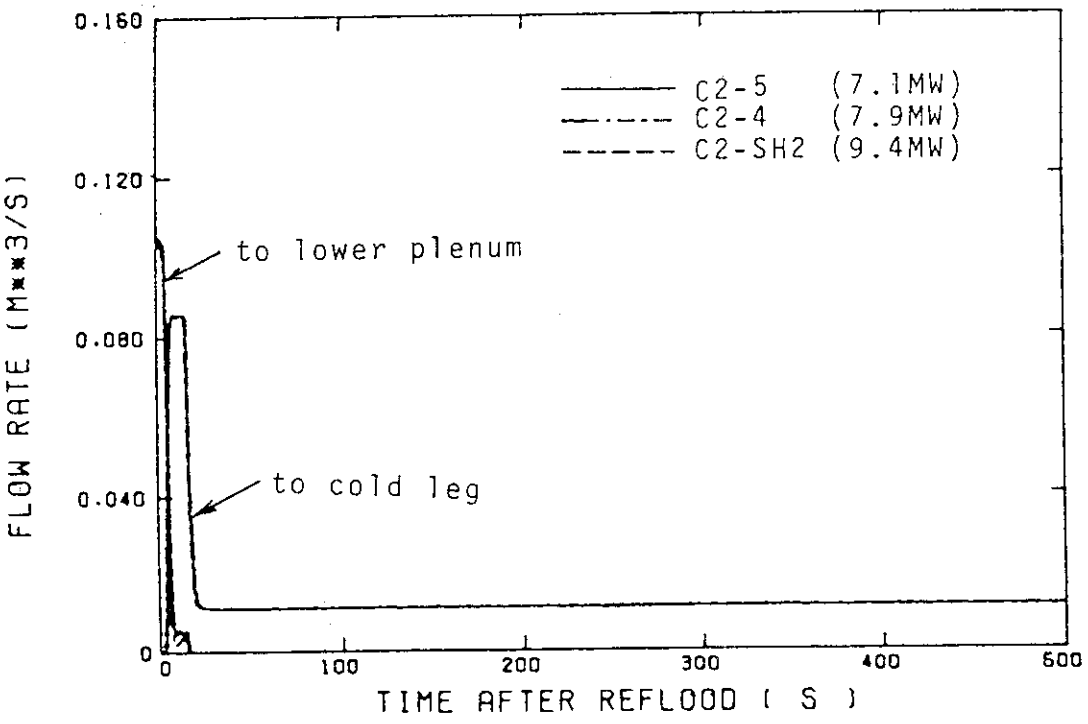

Fig. 3.4 Comparison of the ECC injection flow rate

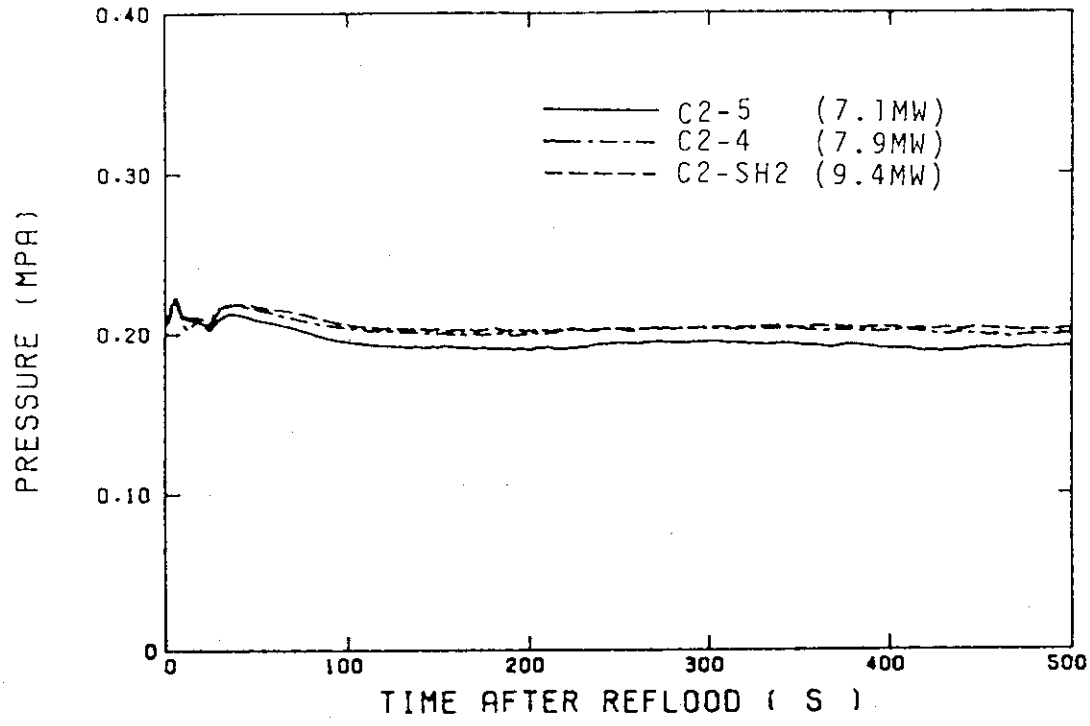

Fig. 3.5 Comparison of the pressure in the Containment tank 2

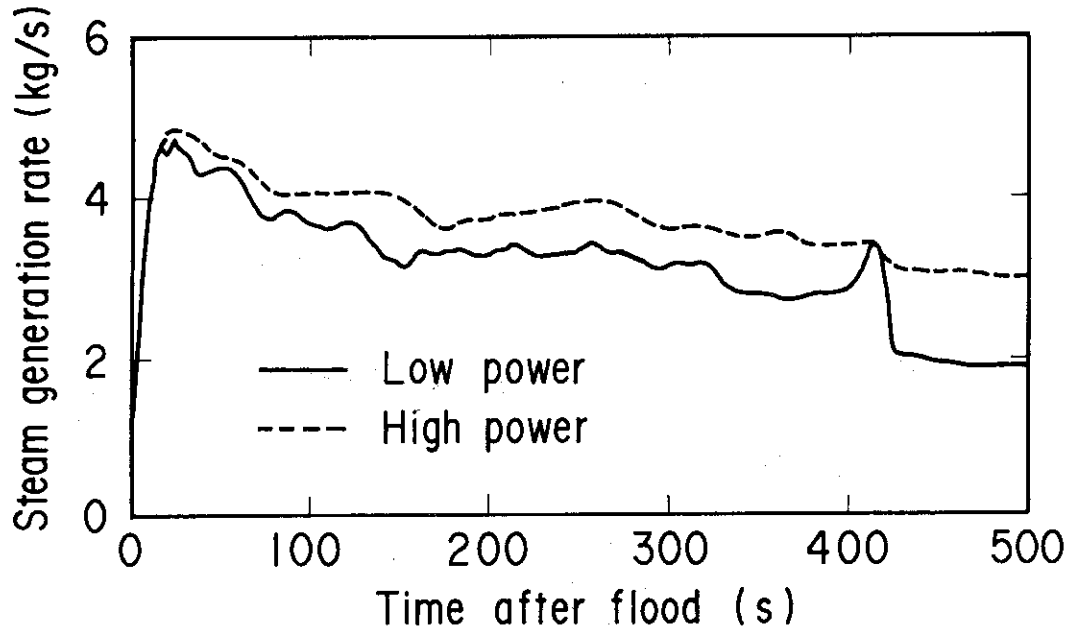

Fig. 4.1 Comparsion of steam generation rate in the core

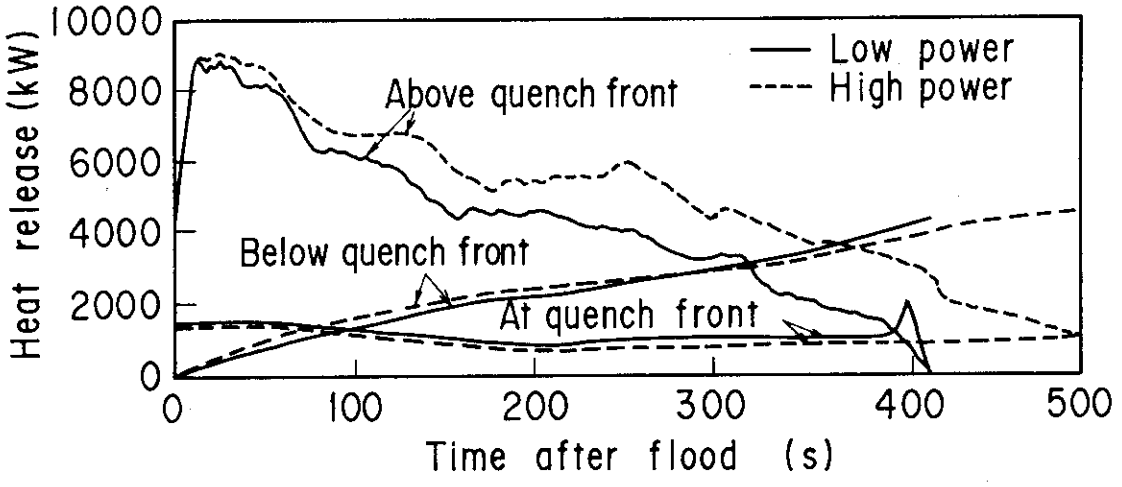

Fig. 4.2 Comparison of heat release in the core

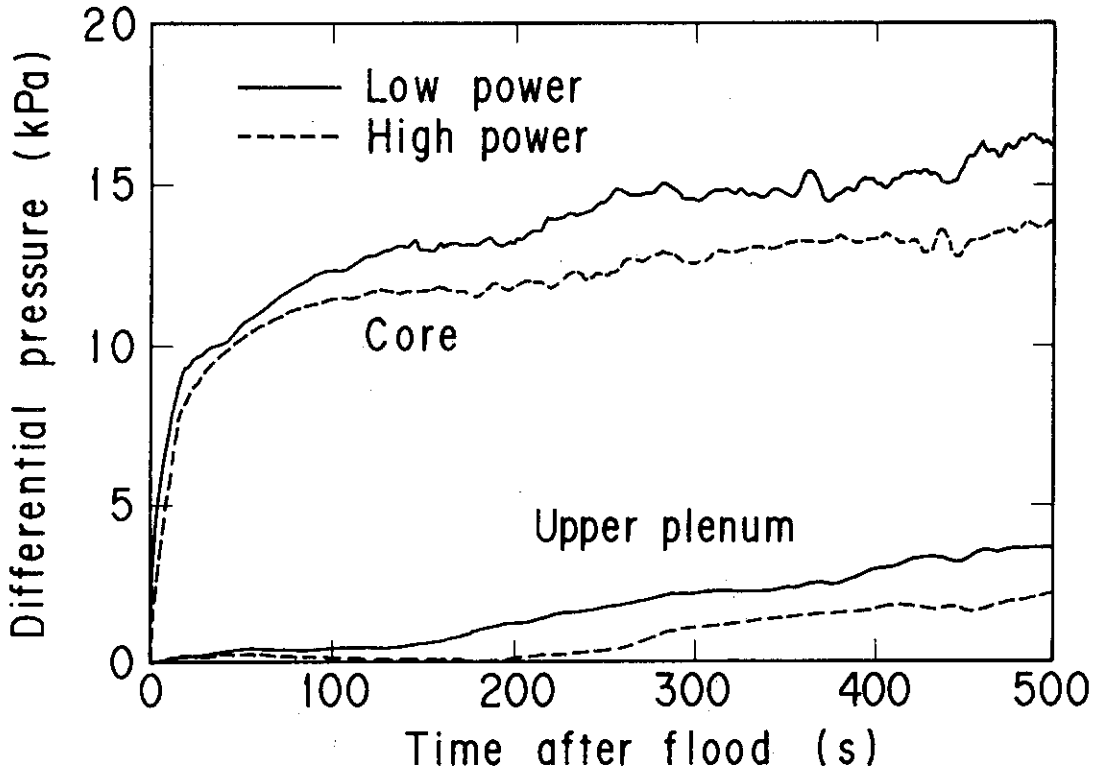

Fig. 4.3 Differential pressure in core

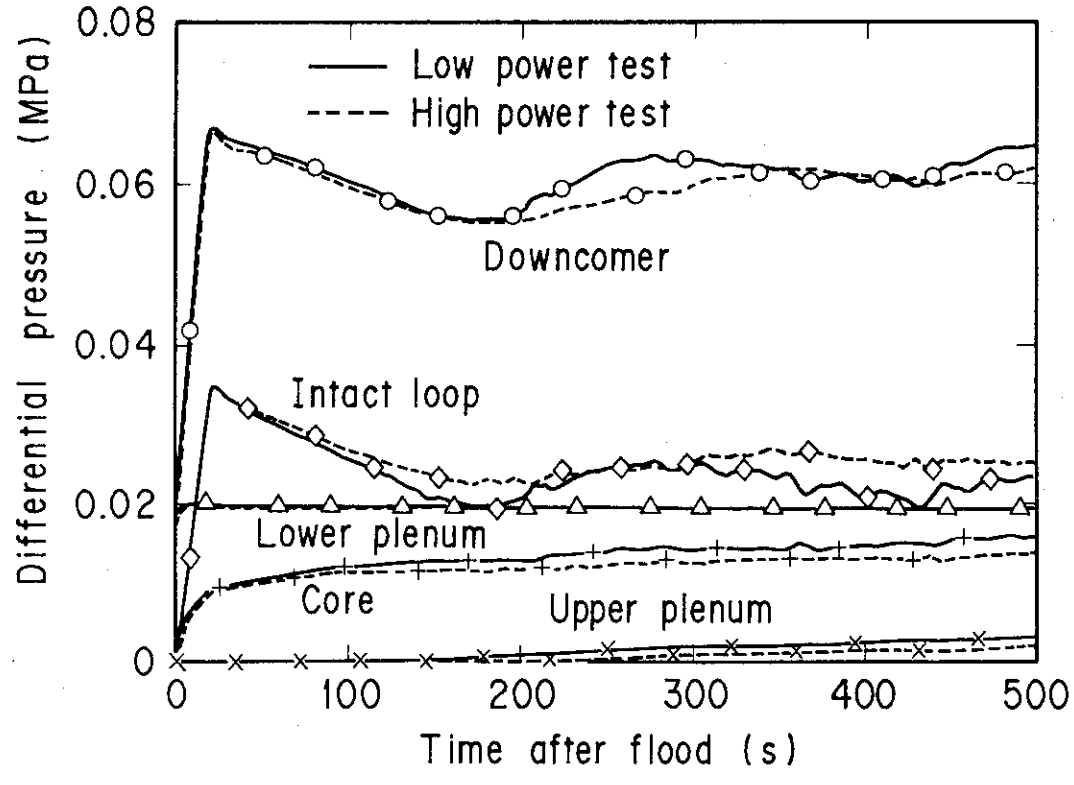

Fig. 4.4 Comparison of differential pressures at various locations

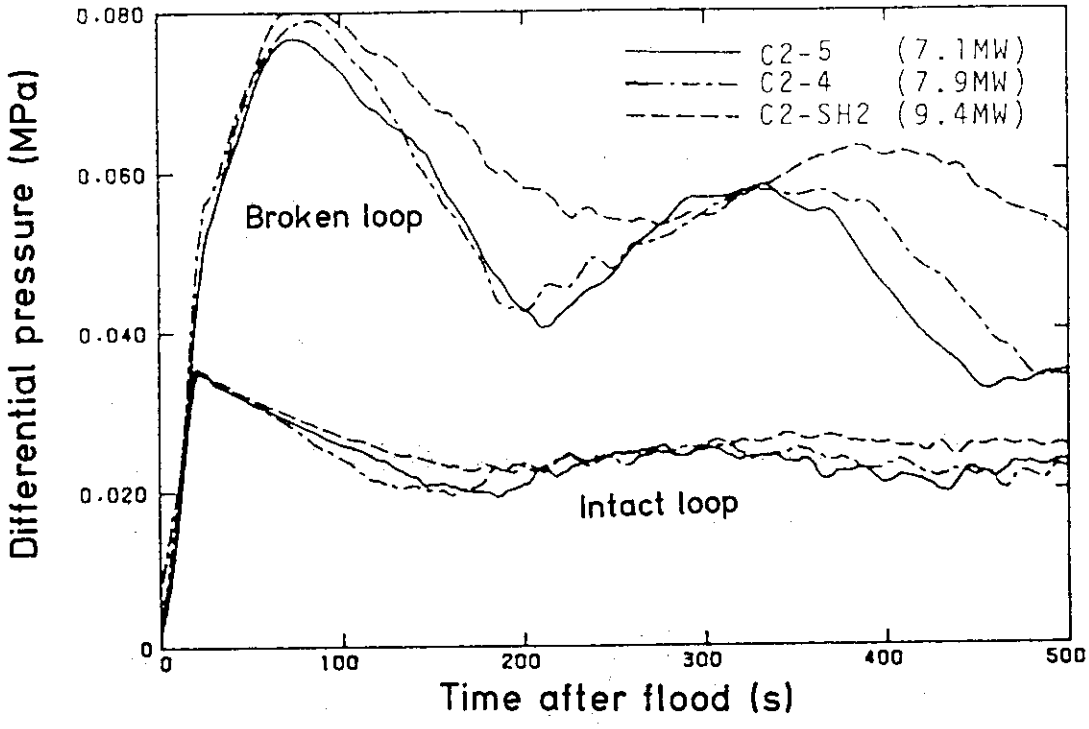

Fig. 4.5 Differential pressure across loops

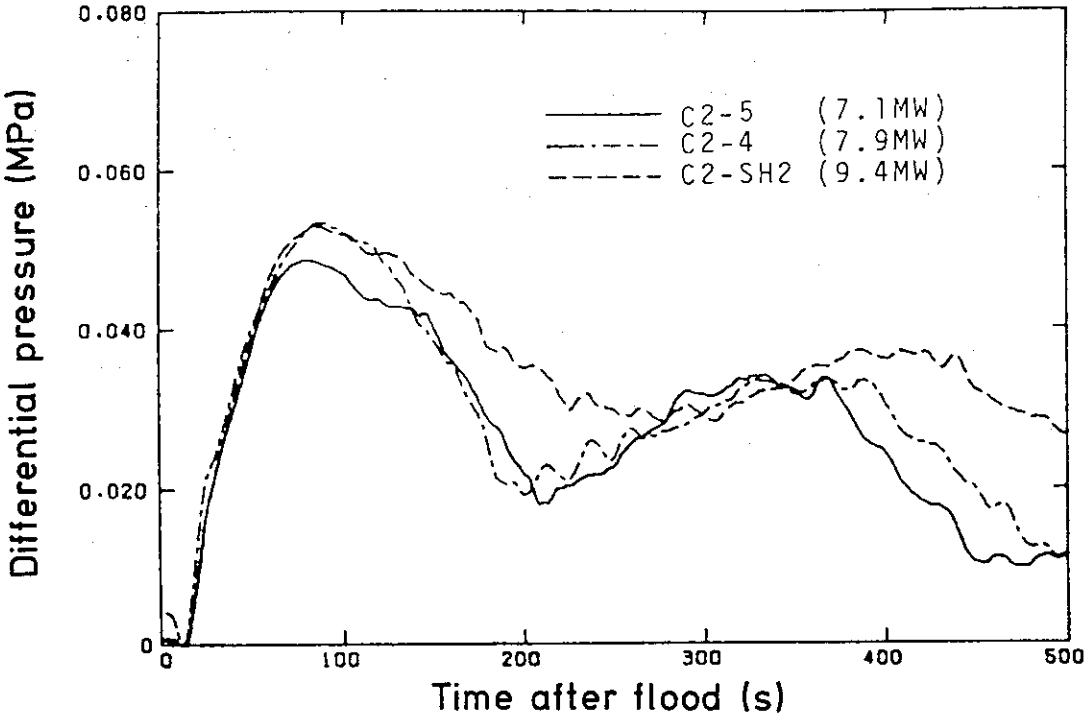

Fig. 4.6 Differential pressure across broken cold leg nozzle

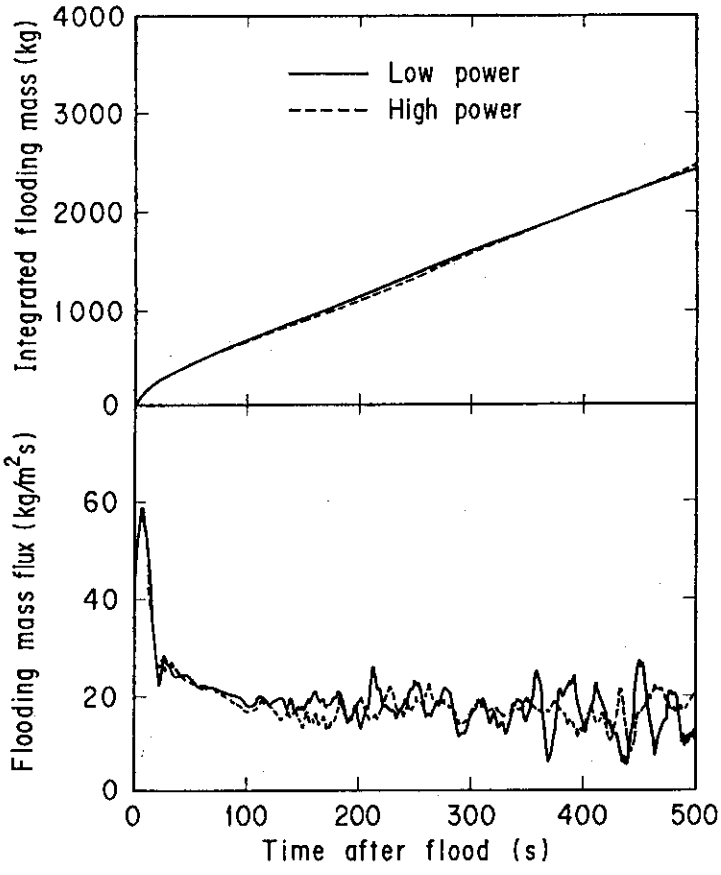

Fig. 4.7 Comparison of flooding mass flux and integrated mass flux into core

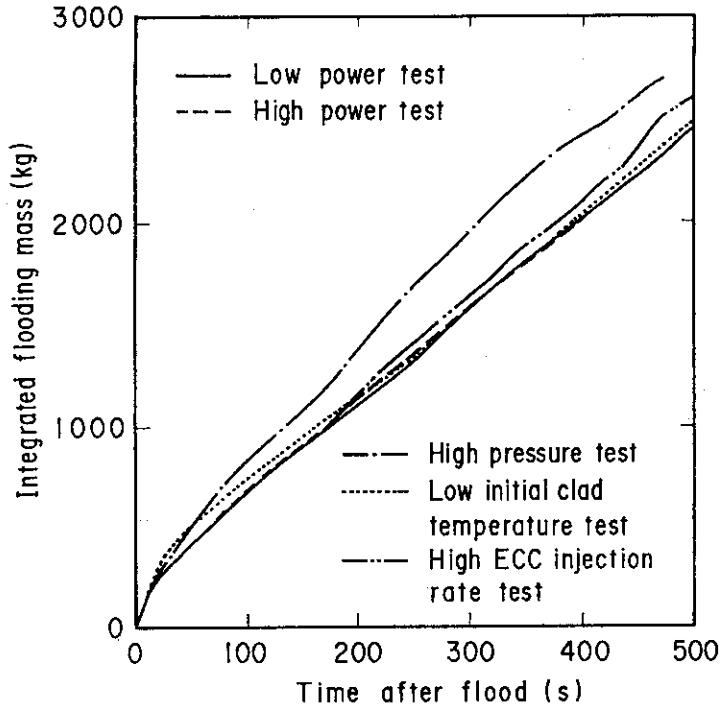

Fig. 4.8 Sensitivity of parameters on integrated flooding mass flux into core

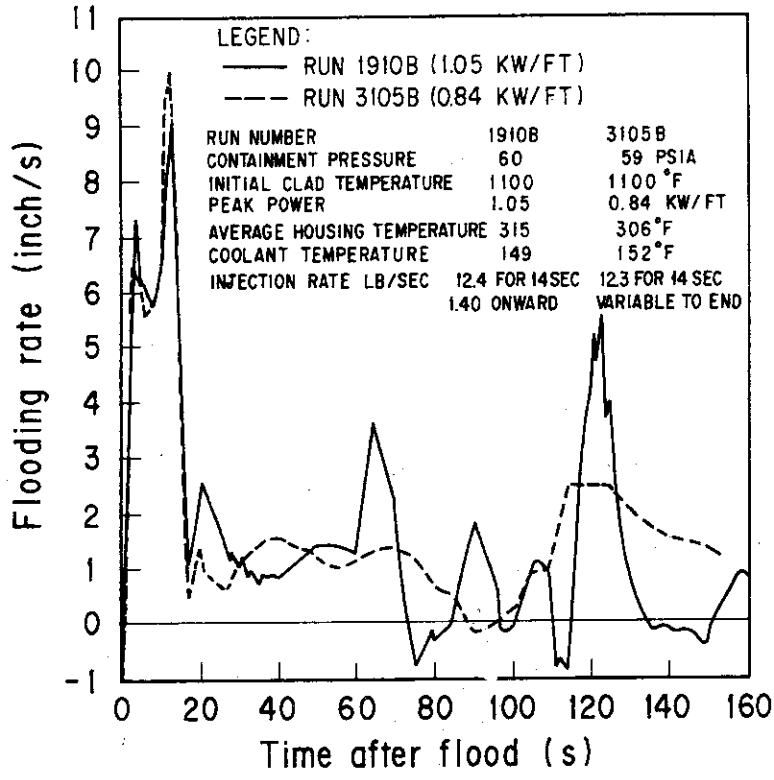

Fig. 4.9 Flooding rate in FLECHT-SET (Cited from Ref. (12))

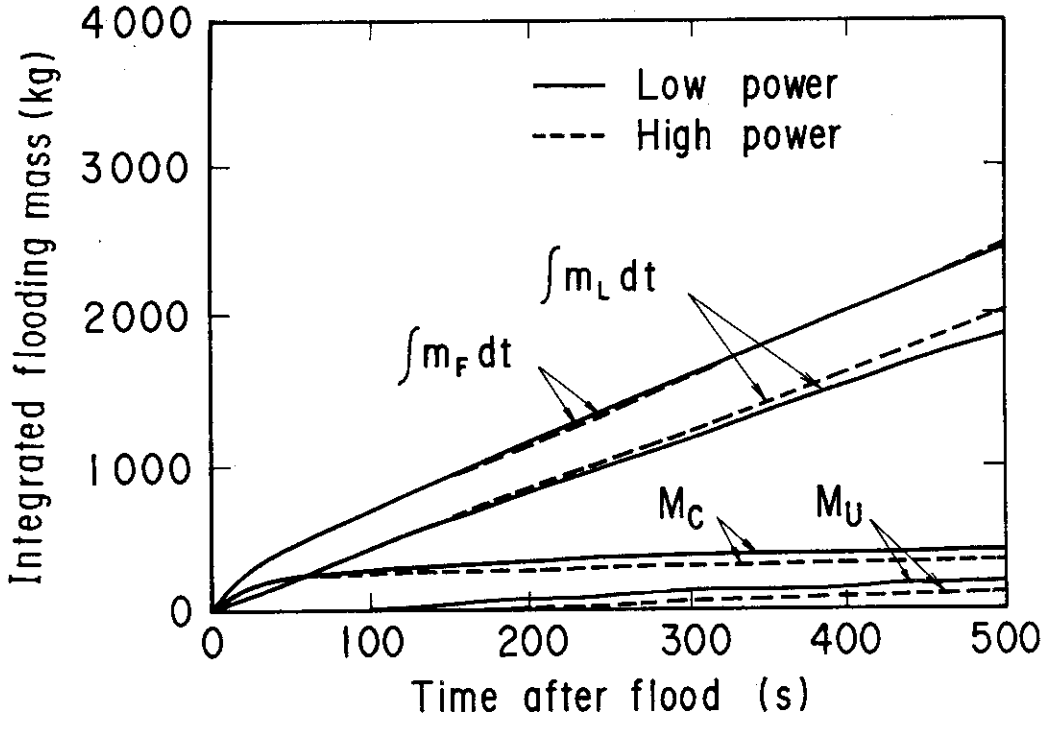

Fig. 4.10 Contribution of each term to integrated flooding mass flux into core

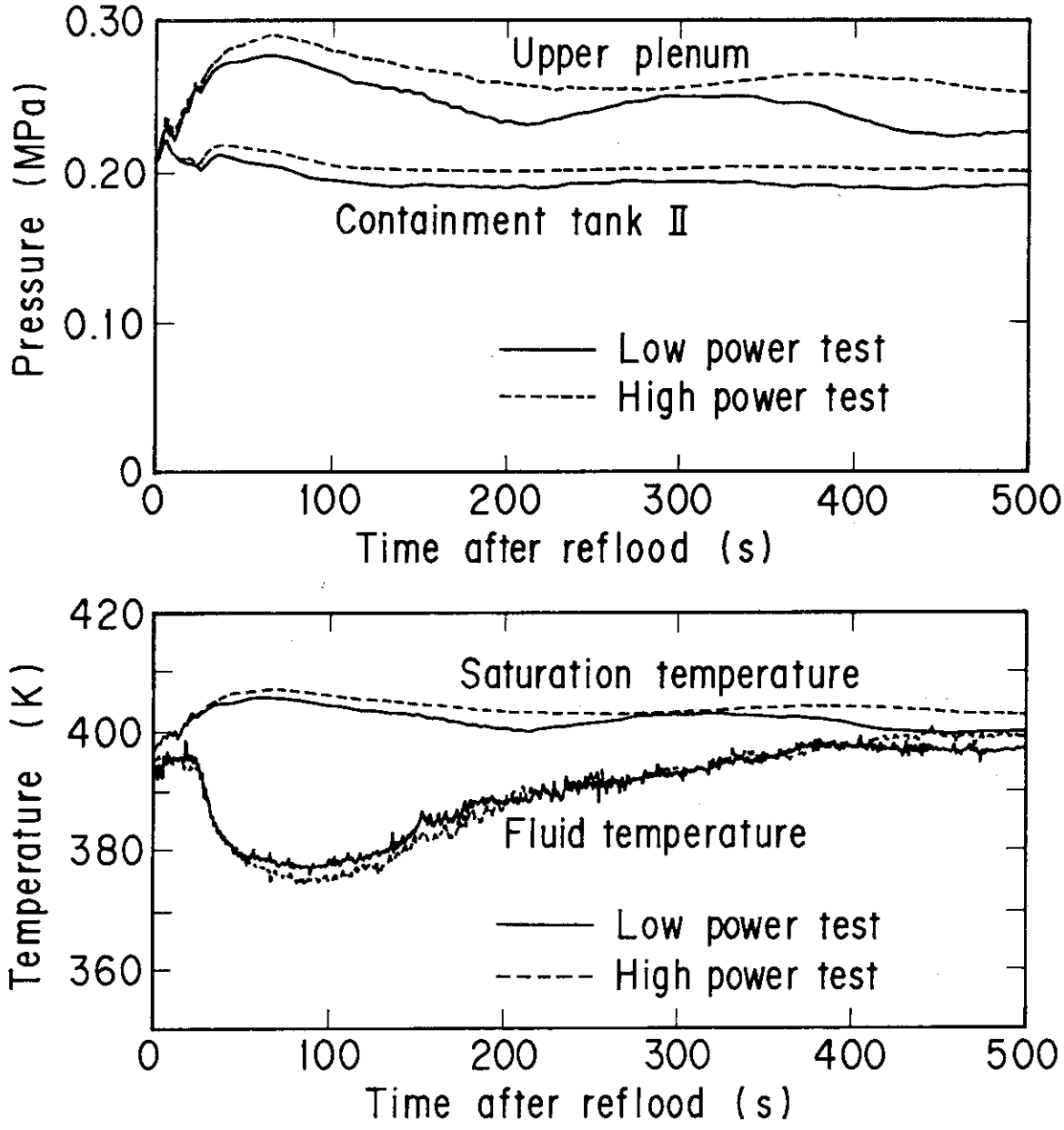

Fig. 4.11 Comparison of boundary conditions of core

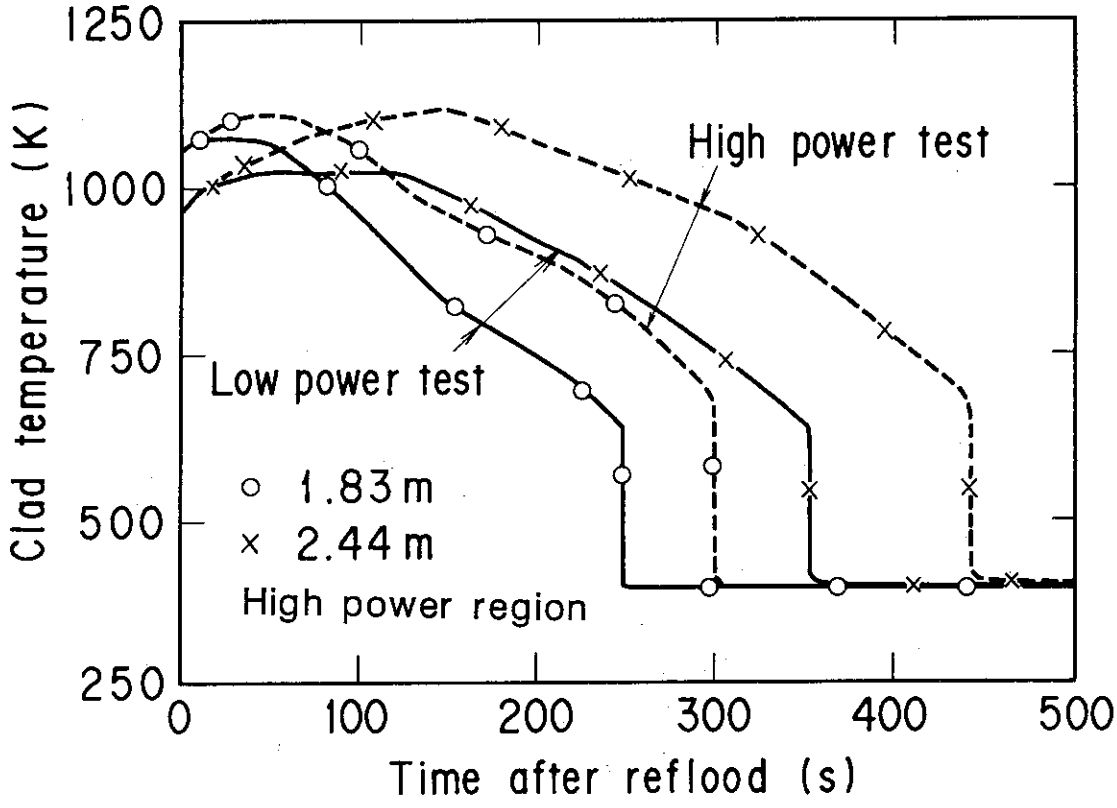

Fig. 4.12 Comparison of clad temperature

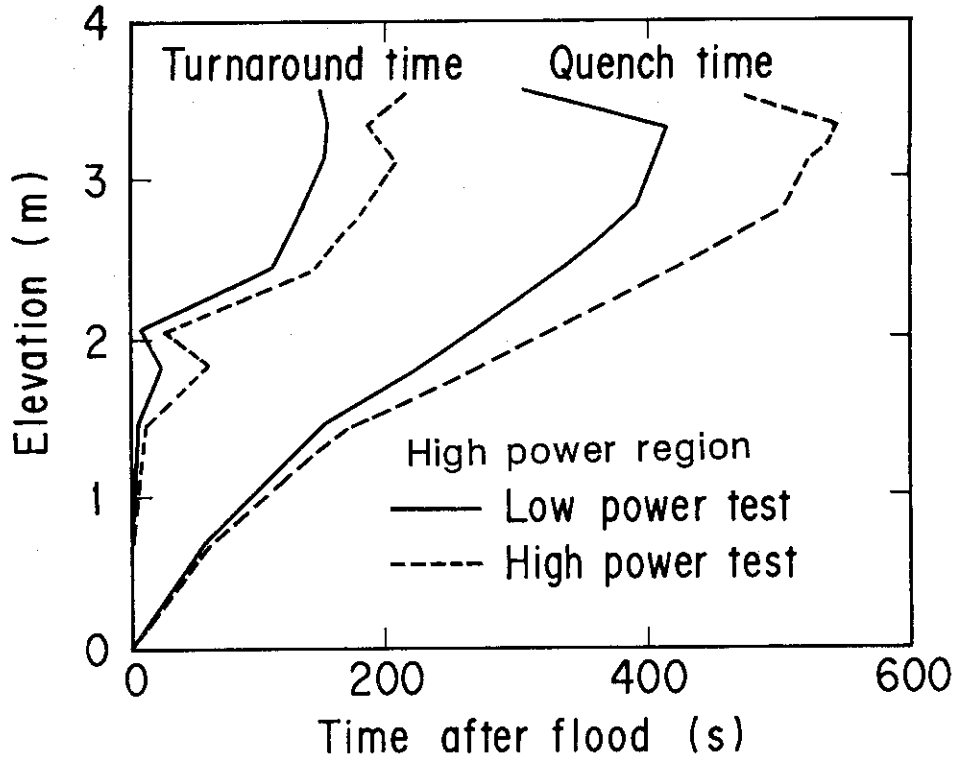

Fig. 4.13 Comparison of turnaround time and quench time

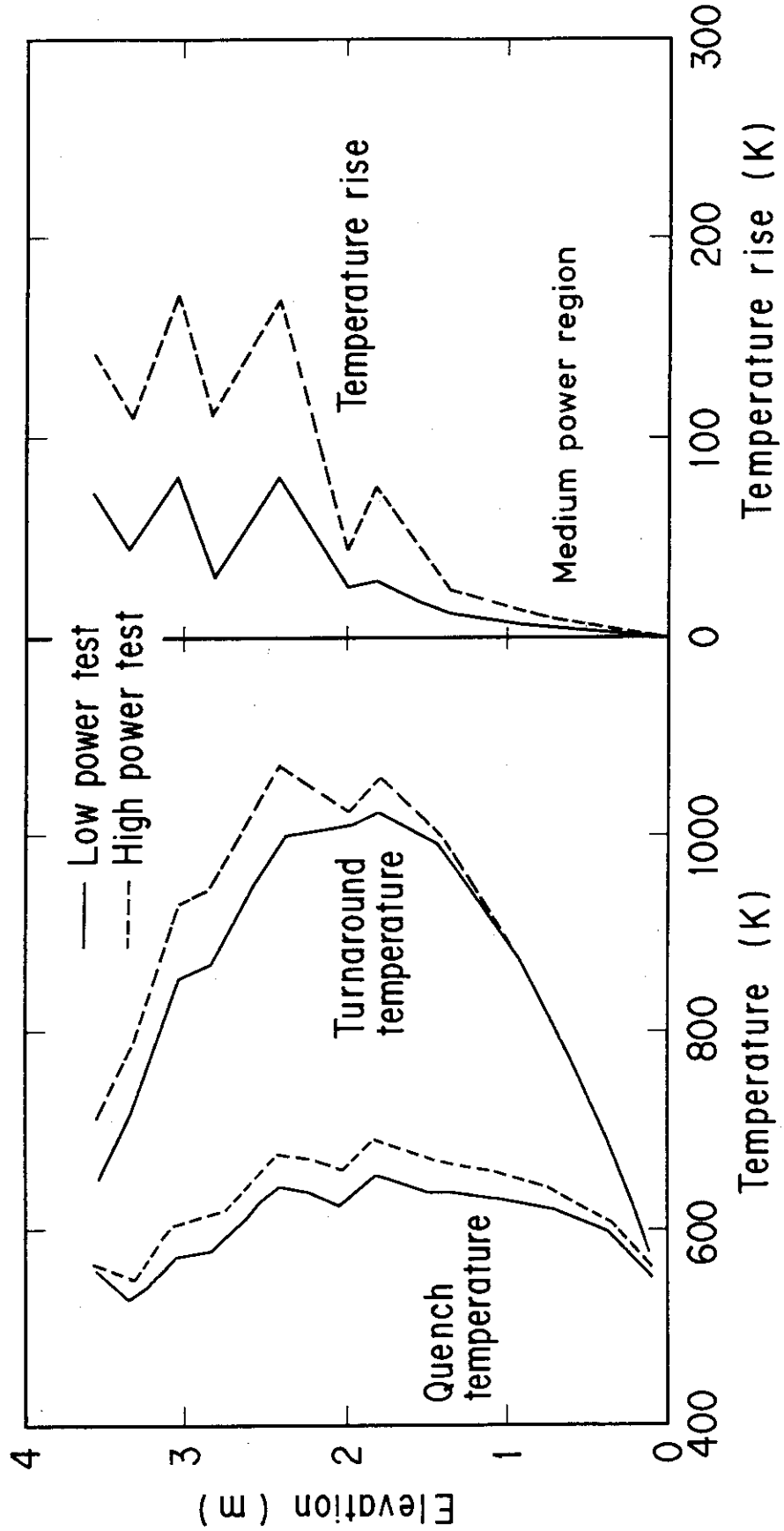

Fig. 4.14 Comparison of turnaround temperature, temperature rise and quench temperature

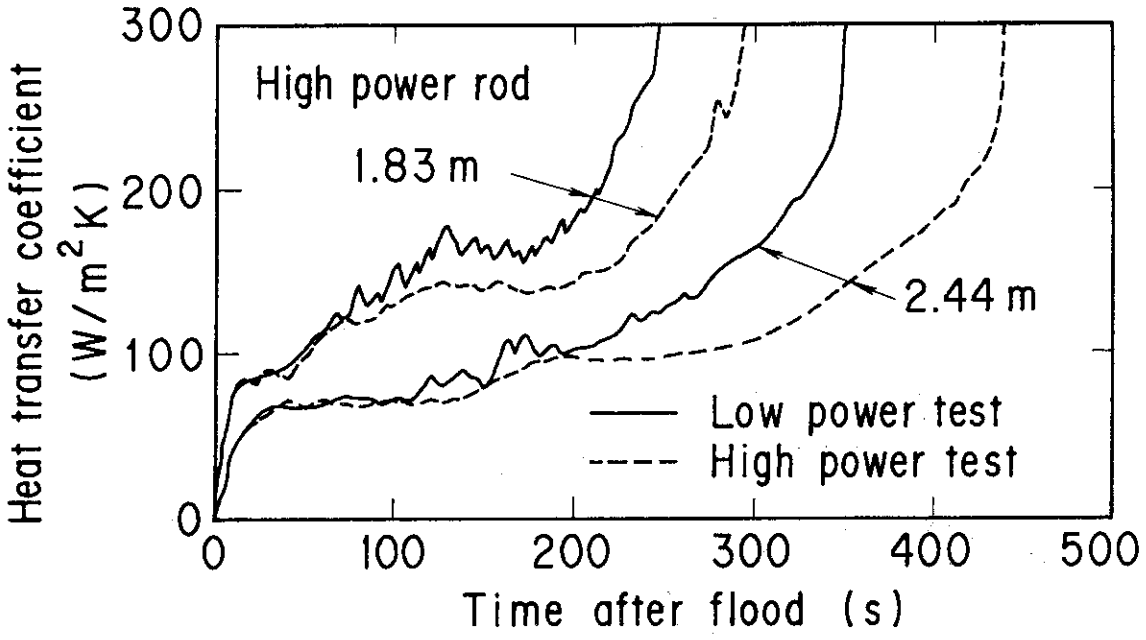

Fig. 4.15 Comparison of heat transfer coefficient

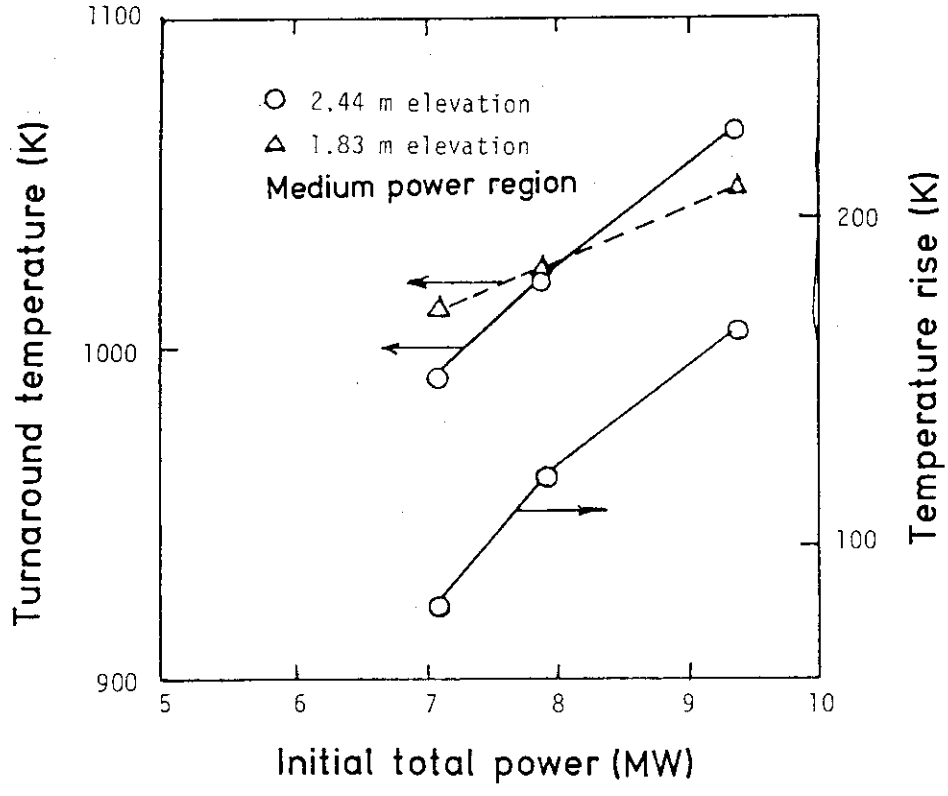

Fig. 4.16 Effect of power on turnaround temperature and temperature rise in medium power region

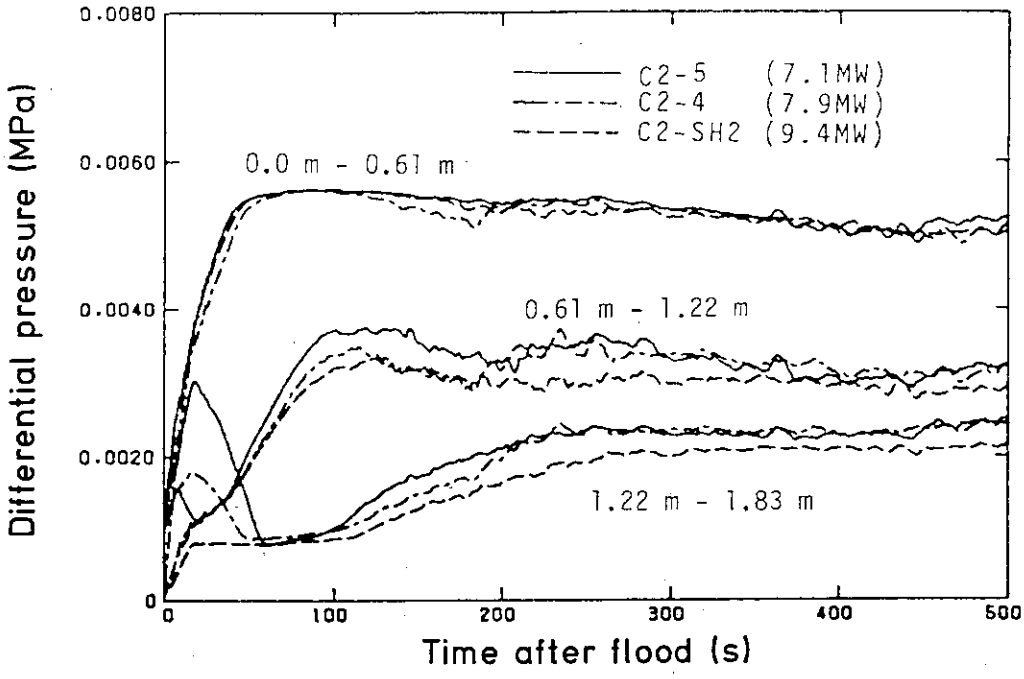

Fig. 4.18 Sectional differential pressure in upper core

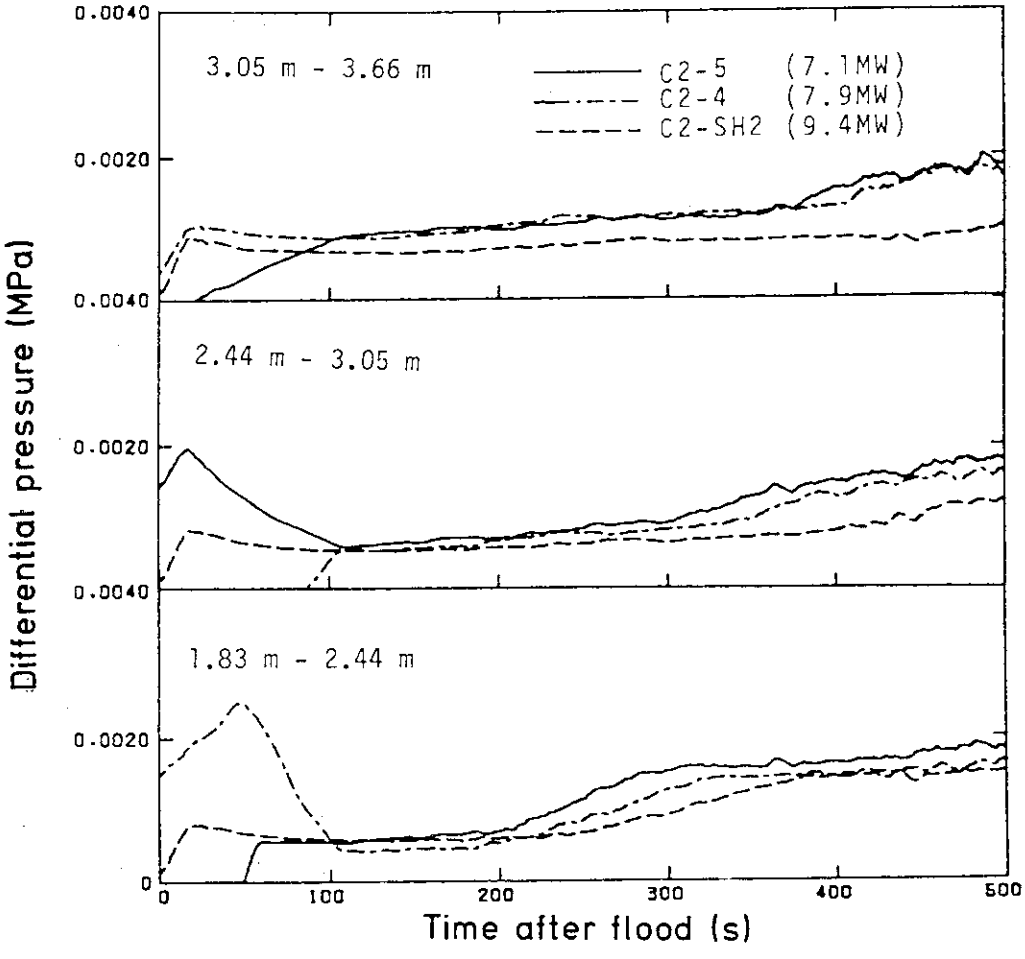

Fig. 4.17 Sectional differential pressure in lower core

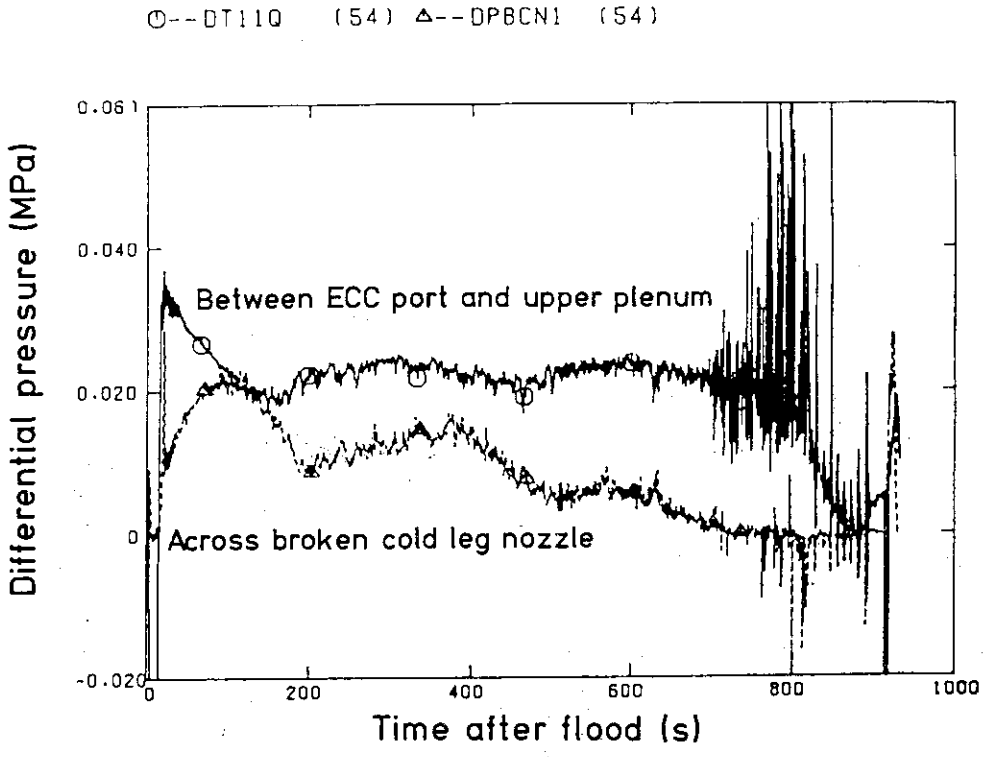

Fig. 4.19 Observed oscillation

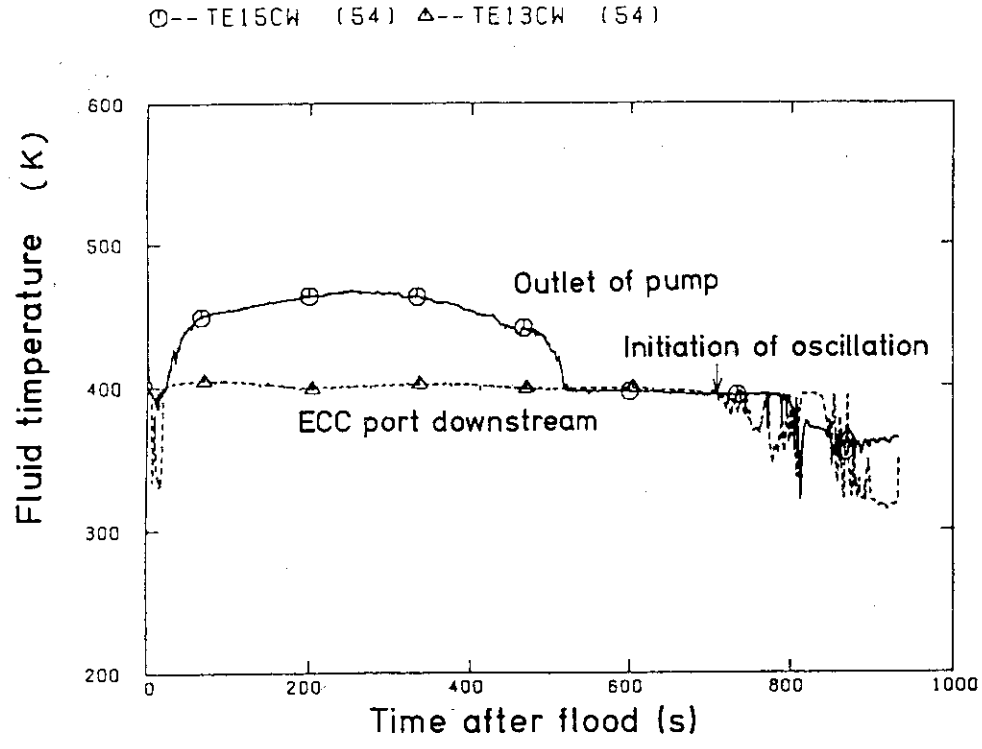

Fig. 4.20 Fluid temperature around ECC port

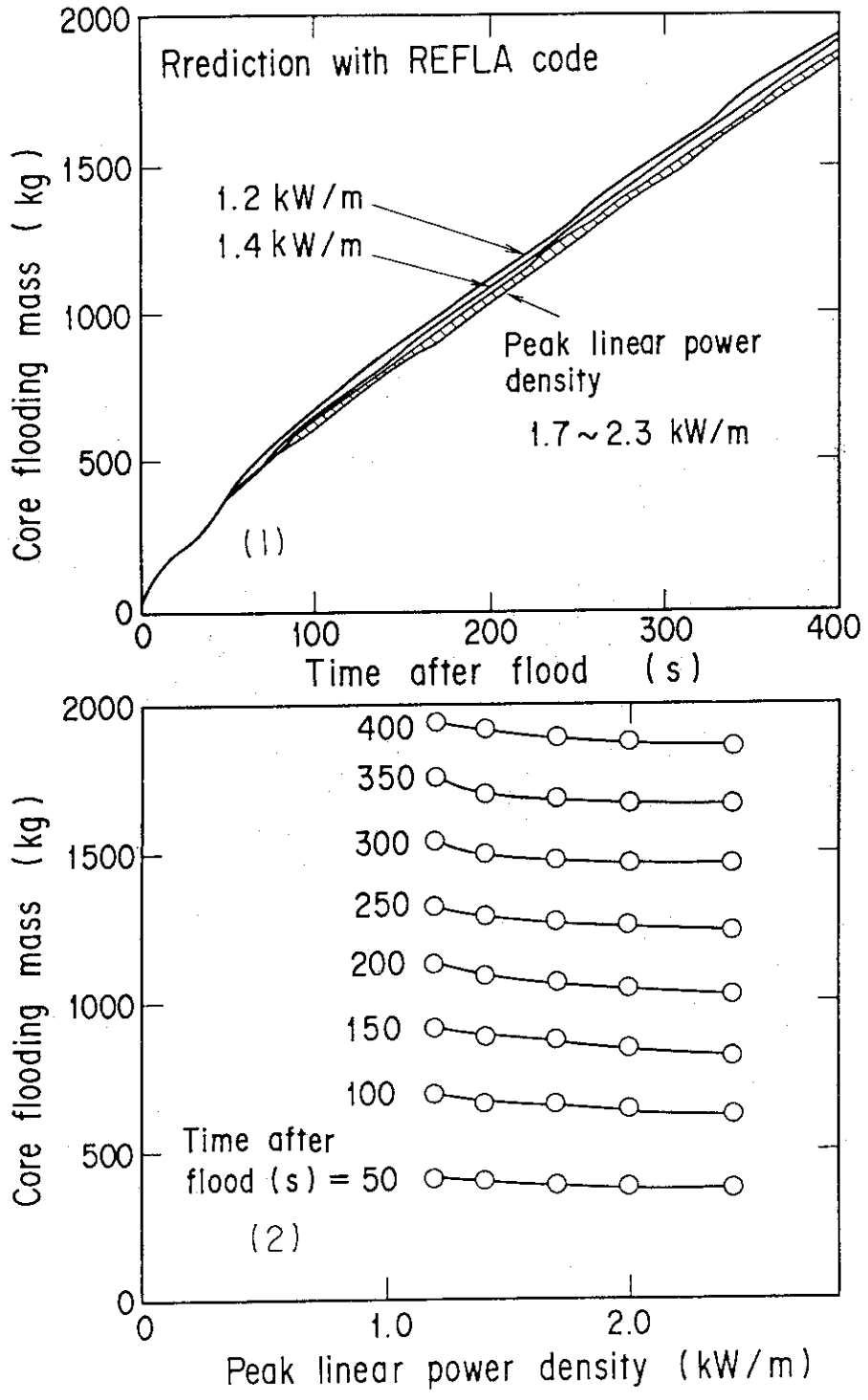

Fig. 4.21 Predicted linear power density effect on core flooding mass flow rate

Appendix A Definitions of Tag IDs

Figure List

1. Definition of Tag. ID for clad surface temperatures and heat fransfer coefficients

Notation : TEnnYlm (temperature)

HTEmmYlm (heat transfer coefficient)

nn : Bundle number (see Fig. A-1)

m : Elevation number

	Elevation (m)	Axial power factor
3	0.38	0.651
5	1.015	1.147
7	1.83	1.40
9	2.44	1.256
A	3.05	0.854

2. Definition of power zone and boundle number

See Fig. A-1

3. Definition of Tag. ID for void fraction

See Fig. A-2

4. Definition of Tag. ID for average linear power of heater rod in each power unit zone

See Fig. A-3

5. Definition of Tag. ID for differential pressure through downcomer, upper plenum, core and lower plenum

See Fig. A-4

6. Definition of Tag. ID for differential pressure through intact and broken loop and broken cold leg nozzle

See Fig. A-5

7. Definition of Tag. ID for fluid temperature in inlet and outlet plenum and secondary side of steam generator

See Fig. A-6

8. Definition of Tag. ID for ECC water injection rate, ECC water temperature and vented steam flow rate

See Fig. A-7

9. Definition of initial temperature, turnaround temperature quench temperature, temperature rise, turnaround time and quench time. (See Fig. A-8)

T_i : Initial temperature (Clad surface temperature at reflood initiation)

T_t : Turnaround temperature (Maximum clad surface temperature in each temperature history)

ΔT_r : Temperature rise ($= T_t - T_i$)

T_q : Quench temperature (Clad surface temperature at quenching)

10. Definition of quenching

See Fig. A-8

Quench time t_t is determined as

$$t_t = i \times \Delta t - \text{(reflood initiation time)}$$

In above equation, i is determined by the following criteria.

(1) Clad surface temperature is high, compared with the saturation temperature.

$$T_i > T_{sat} + \Delta T_1$$

(2) Decreasing rate of clad surface temperature is large.

$$\frac{T_{i+1} - T_i}{\Delta t} < - C_{st}$$

(3) Clad surface temperature falls around the saturation temperature.

$$T_{i + k_1} \leq T_{sat} + \Delta T_1$$

(4) If the determined i is inadequate, the value i is manually re-determined.

Δt : Data sampling period (s)

T_i : Clad surface temperature (K)

T_{sat}: Saturation temperature at the pressure in upper plenum (K)

ΔT_1 : Temperature discrepancy (K)
Default value = 50.0

C_{st} : Decreasing rate of clad surface temperature (K/S)
Default value = 25.0

k_1 : Number of referred data (-)
Default value = 6

11. Definition of Tag. ID for core inlet mass flow rate, time-integral core inlet mass flow rate and carry-over rate fraction

(1) Core inlet mass flow rate : $\dot{m}_F$
Notation : MLCRI□ (□ = N, 1 or 11)

(2) Time-intefral core inlet mass flow rate : $\int \dot{m}_F dt$
Notation : IMLCRI□ (□ = N, 1 or 11)

(3) Carry-over rate fraction : $(\dot{m}_F - \dot{m}_{CR})/\dot{m}_F$
Natation : CRF□ (□ = N, 1 or 11)

where $\dot{m}_F$: Core inlet mass flow rate (See item 12)

$\dot{m}_{CR}$: Water accumulation rate in core

Suffix	$\dot{m}_F$ base on
N	Eq.(A.2)
1	Eq.(A.1) with K=15
11	Eq.(A.1) with K=20

12. Evaluation of core inlet mass flow rate

The reflood phenomena is a relatively slow transient and a steady state condition can be applied. In a steady state condition, based on the mass balance relations of the system, the core flooding mass flow rates $\dot{m}_F$s can be written as follows:

By using the data measured at the downstream of the core inlet, $\dot{m}_F$ is derived as,

$$\dot{m}_F = \dot{m}_C + \dot{m}_U + \dot{m}_B + \Sigma \dot{m}_I \quad , \qquad (A.1)$$

where $\dot{m}_C$ and $\dot{m}_U$ are the mass accumulation rates in the core and the upper plenum respectively. The $\dot{m}_B$ and $\dot{m}_I$ are the mass flow rates in the broken loop and the intact loop, respectively.

By using the data measured at the upstream of the core inlet, $\dot{m}_F$ is derived as,

$$\dot{m}_F = \Sigma \dot{m}_{DL} - \dot{m}_D - \dot{m}_O + \dot{m}_{ECC/LP} \quad , \tag{A.2}$$

where $\dot{m}_{DL}$ and $\dot{m}_O$ are the mass flow rates of the water flowing into and overflowing from the downcomer, $\dot{m}_{ECC/LP}$ and $\dot{m}_D$ are the mass flow rate of the ECC water injected into the lower plenum and the water accumulation rate in the dowmcomer respectively.

The $\dot{m}_I$s and $\dot{m}_B$ can be obtained from the pressure drops at the pump simulators with orifices by assuming the K-factor of the orifice is constant. The values of $\dot{m}_C$, $\dot{m}_D$ and $\dot{m}_U$ can be evaluated with the differential pressure ΔP_C, ΔP_D and ΔP_U, respectively, as follows:

$$\dot{m}_n = d(\Delta P_n S_n/g)/dt \quad (n : C, D, U) \quad , \tag{A.3}$$

where g is the gravitational acceleration and S_n is the cross sectional area. The value of $\dot{m}_O$ can be obtained from the liquid level X in the Containment tank 1 as,

$$\dot{m}_O = d(X\rho_\ell S_o)/dt \quad , \tag{A.4}$$

where ρ_ℓ is the liquid density and S_o is the cross sectional area of the containment tank 1.

The value of $\dot{m}_{DL}$, $\dot{m}_{DV}$ and h, which are liquid flow rate, steam flow rate and enthalpy of two phase mixture downstream each ECC port respectively, are obtained from the following mass and energy balance relations at each ECC port under the assumption of thermal equilibrium:

$$\dot{m}_{DV} + \dot{m}_{DL} = \dot{m}_{ECC} + \dot{m}_I \quad , \tag{A.5}$$

$$(\dot{m}_{DV} + \dot{m}_{DL})i = \dot{m}_{ECC}h_{ECC} + \dot{m}_I h_I \quad , \tag{A.6}$$

$$\text{if} \quad h_g \geq h \geq h_\ell \ , \ (\dot{m}_{DV} + \dot{m}_{DL})h = \dot{m}_{DV}h_g + \dot{m}_{DL}h_\ell$$

$$\text{if} \quad h \geq h_g \quad , \ \dot{m}_{DL} = 0 \quad , \tag{A.7}$$

$$\text{if} \quad h \geq h_\ell \quad , \ \dot{m}_{DV} = 0$$

where h is enthalpy of fluid and h_ℓ and h_g are enthalpies of liquid and steam at the saturation temperature, respectively.

The fluid temperatures can be measured with thermocouples immersed in the fluid and the enthalpies h_I and h_{ECC} can be estimated.

Mass balance calculations were performed with Eqs. (A.1) and (A.2). The K-factor of the orifice in the pump simulator was evaluated in the following two ways.

The K-factor of 20 was obtained with the steam and water single phase calibration tests using the flow meter and spool piece data. The K-factor of 15 was obtained with the Pitot tube measurement in a typical reflood condition assuming the flat velocity profile in the pipings. In the differentiation, higher frequency components of the data tends to be amplified more. Therefore, in the differentiation of the differential pressure data, the smoothing procedure was used to suppress the high frequency components of the data.

In the Acc injection period, the calculated $\dot{m}_F$s with Eqs. (A.1) and (A.2) are significantly different from each other. This discrepancy may be caused by inaccuracy of the mass flow rate injected into the system and by the unaccounting of the storage of water in the cold leg pipe. The former might be introduced from the slow time response of the flow meter (time constant 1 second) and the change of the gas volume in the injection line. In this period, especially before the steam generation from the core becomes noticeable, the mass flow rate, $\dot{m}_F$, calculated with Eq. (A.1) is probably reasonable, since the calculation uses the increasing rates of the masses in the core and the upper plenum and their accuracy is good enough for our estimation.

In the LPCI injection period, the calculated $\dot{m}_F$s are slightly different from each other. Judging from the time-integral values of both $\dot{m}_F$s, their average values are nearly proportional. The discrepancy was inferred to be caused by the disregard of the bypass of steam and liquid from the upper plenum without going through the hot legs in the calculation with Eq. (A.1). And additionally the discrepancy was caused by the disregard of the steam generation in the downcomer due to the hot wall of the pressure vessel in the calculation with Eq. (A.2). It was estimated that the disregard of the downcomer steam generation causes the error of 0.25 kg/s on predicted $\dot{m}_F$. The estimation was made by comparing the results of the tests with hot and cold downcomer conditions.

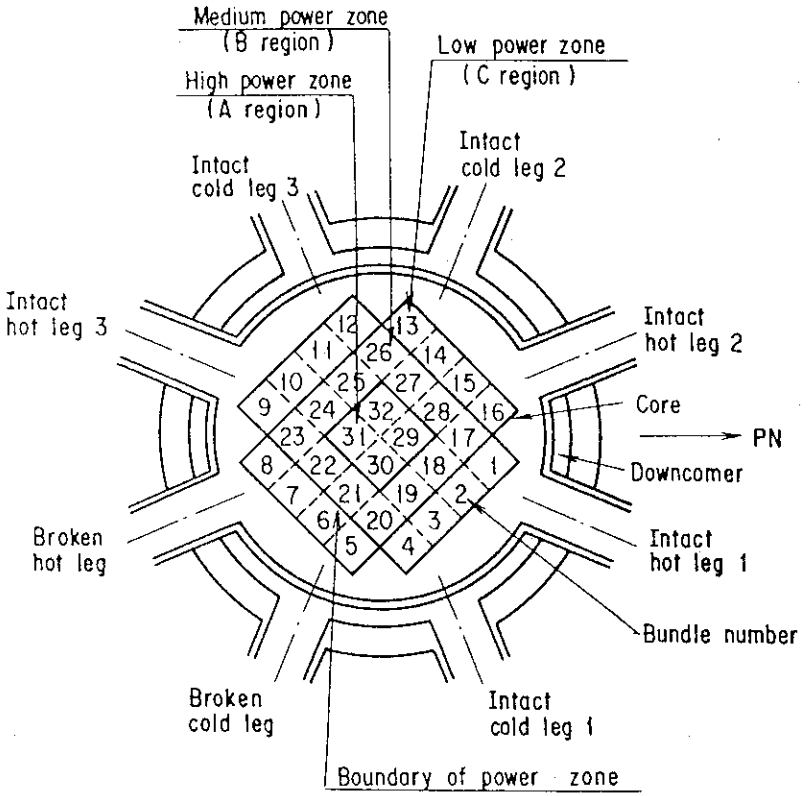

Fig. A-1 Definition of power zones and bundle numbers

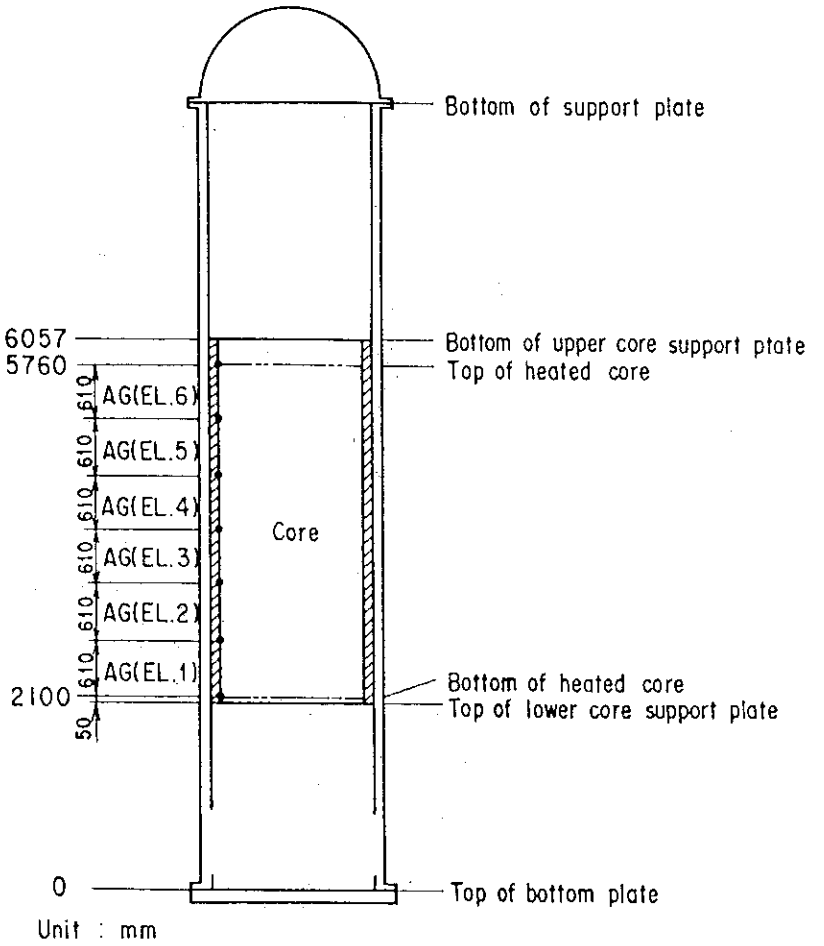

Fig. A-2 Definition of Tag. ID for void fraction (AG(EL.1) ∿ AG(EL.6))

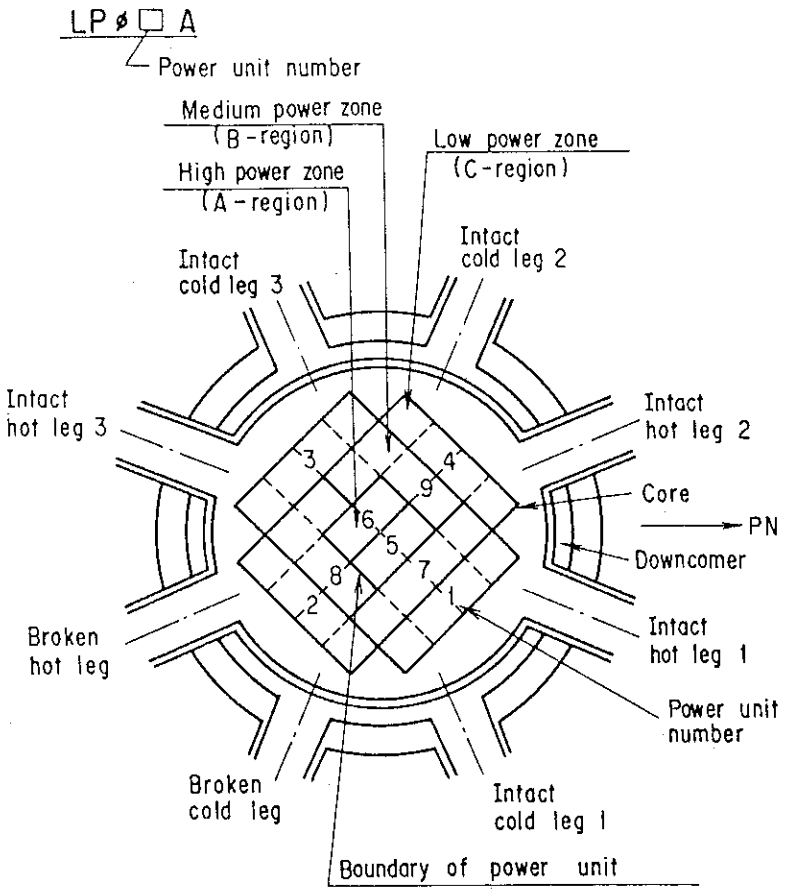

Fig. A-3 Definition of Tag. ID for average linear power of heater rod in each power unit zone (LP01A ∿ LP09A)

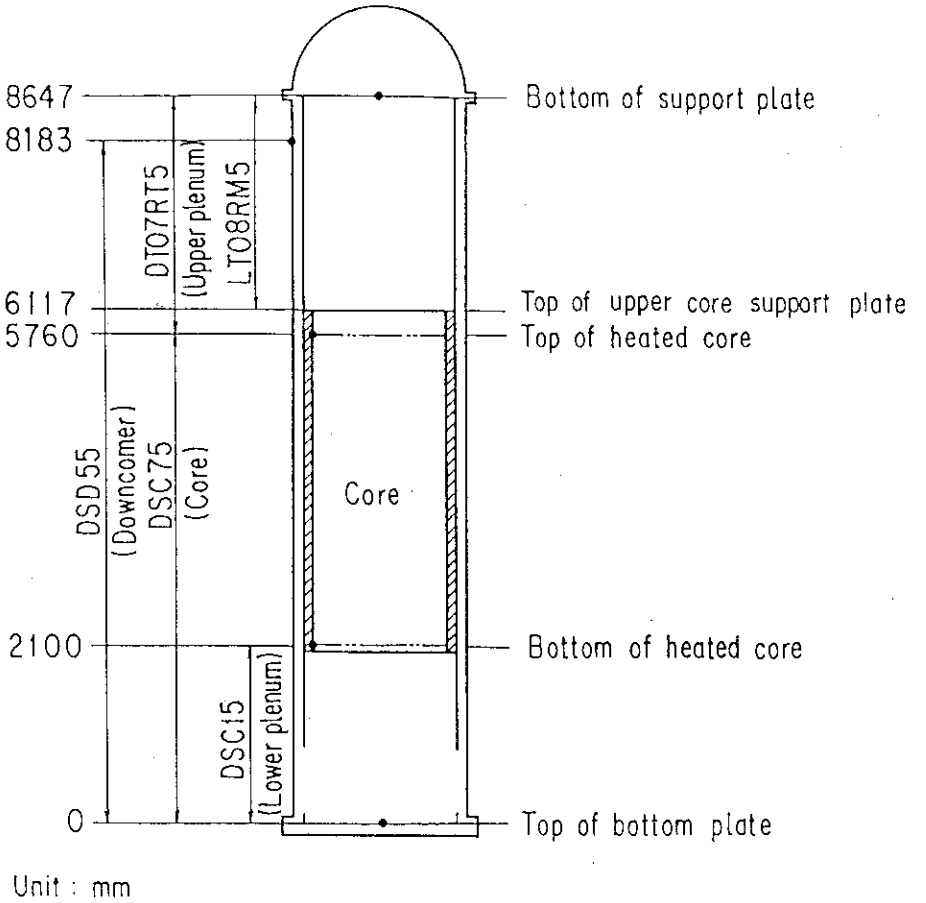

Fig. A-4 Definition of Tag. ID for differential pressure through downcomer, upper plenum, core, and lower plenum (DSD55, DT07RT5, LT08RM5, DSC75, DSC15)

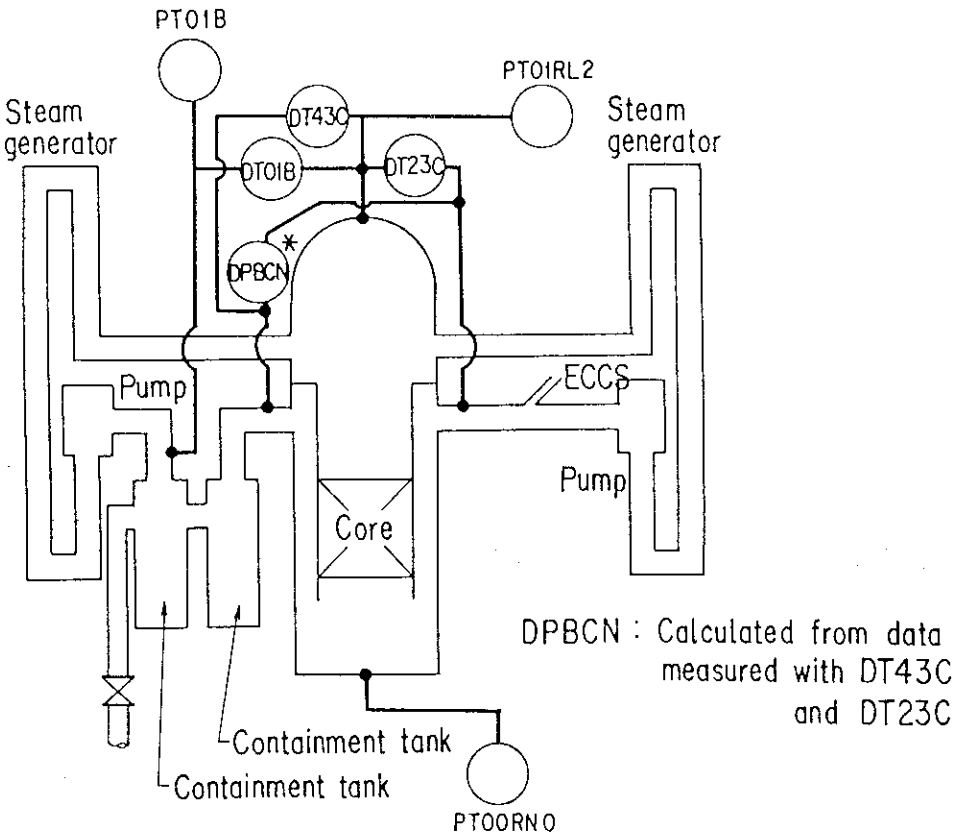

Fig. A-5 Definition of Tag. ID for pressures in upper and lower plena and containment tank 2 (PT01RL2, PT00RN0, PT01B) and for differential pressure through intact and broken loop and broken cold leg nozzle (DT23C, DT01B, DPBCN)

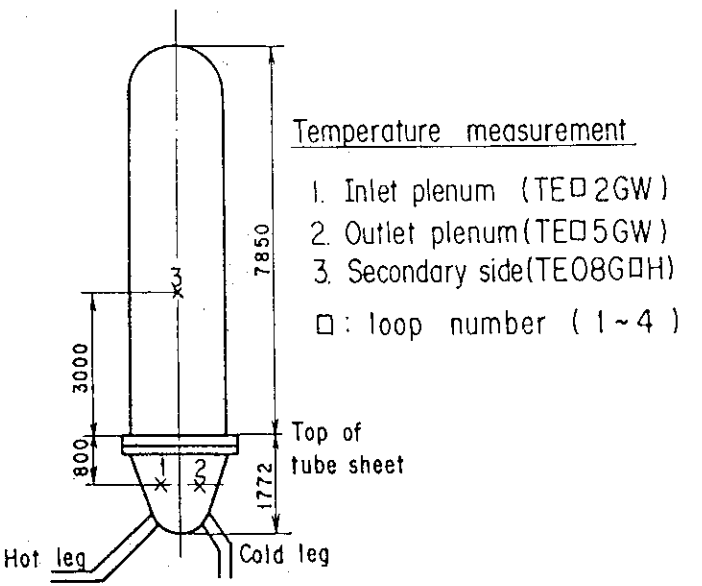

Fig. A-6 Definition of Tag. ID for fluid temperature in inlet and outlet plenum and secondary of steam generator (TE□2GW, TE□5GW, TE08G□H)

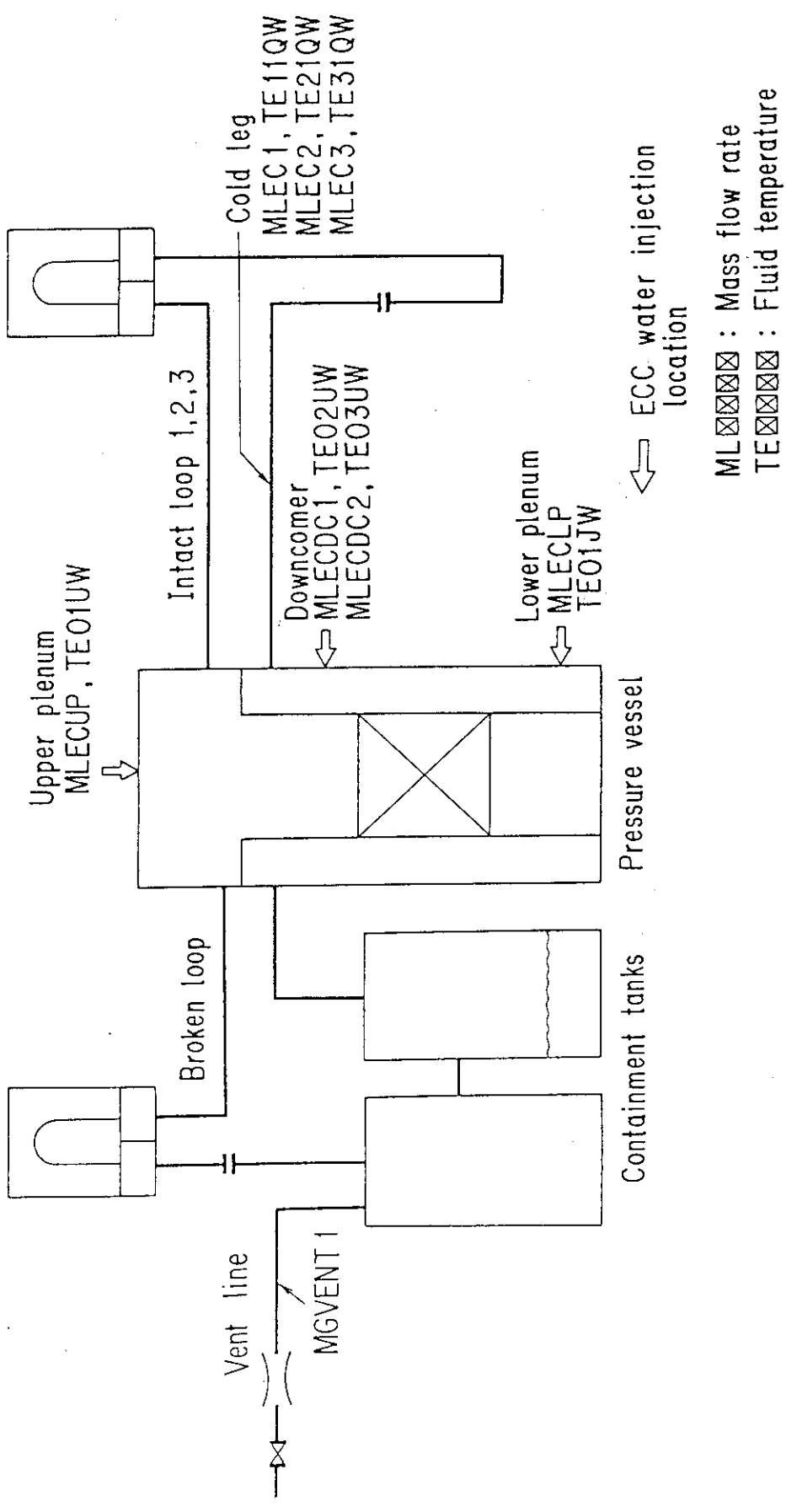

Fig. A-7 Definition of Tag. ID for ECC water injection rate, ECC water temperature and vented steam flow rate
(MLEC1, MLEC2, MLEC3, MLECLP, MLECUP, MLECDC1, MLECDC2, TE11QW, TE21QW, TE31QW, TE01JW, TE01UW, TE02UW, TE03UW, MGVENT1)

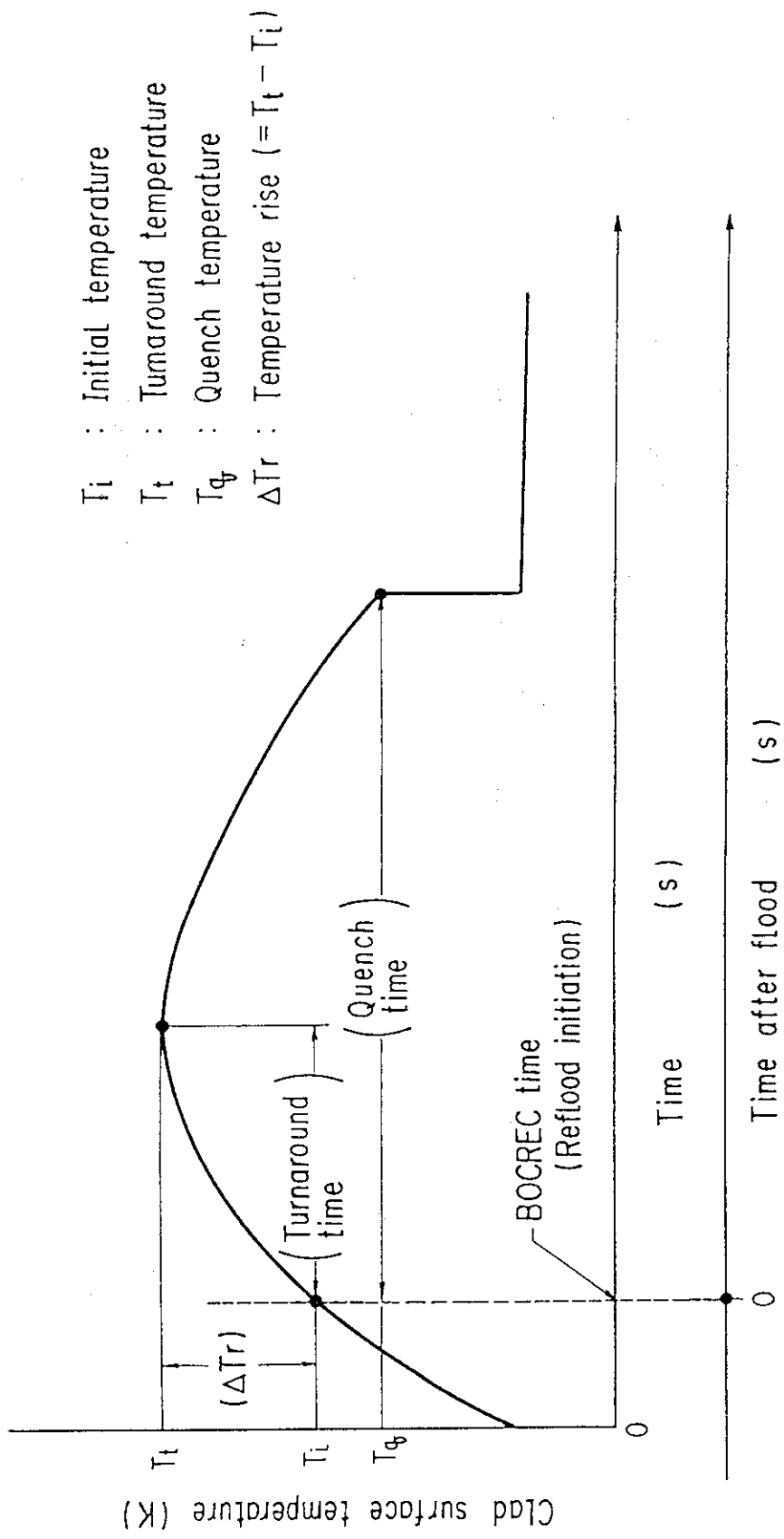

Fig. A-8 Definition of initial temperature, turnaround temperature, quench temperature, temperature rise, turnaround time and quench time

Appendix B Selected Data of CCTF Test C2-5 (Run 63)

Figure List

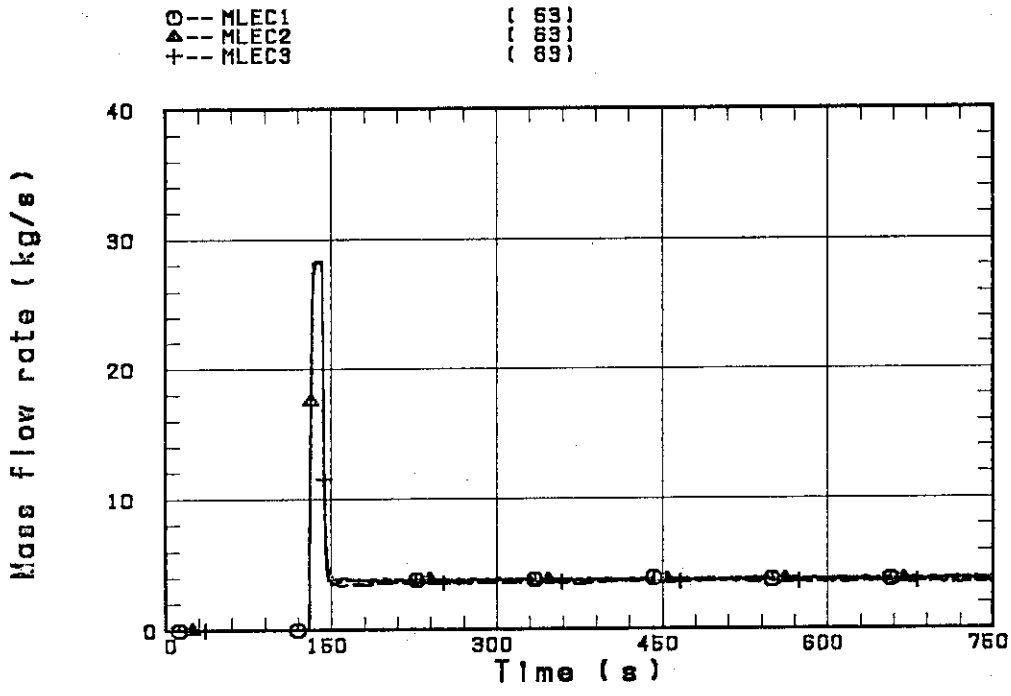

Fig. B-1 ECC water injection rates into the primary system

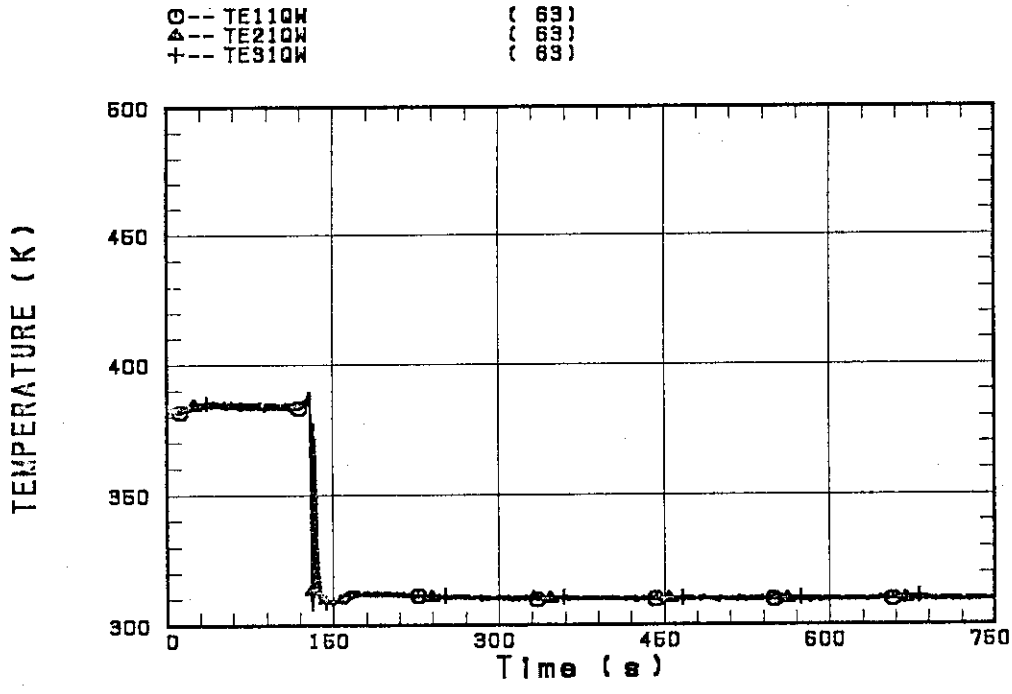

Fig. B-2 ECC water temperature

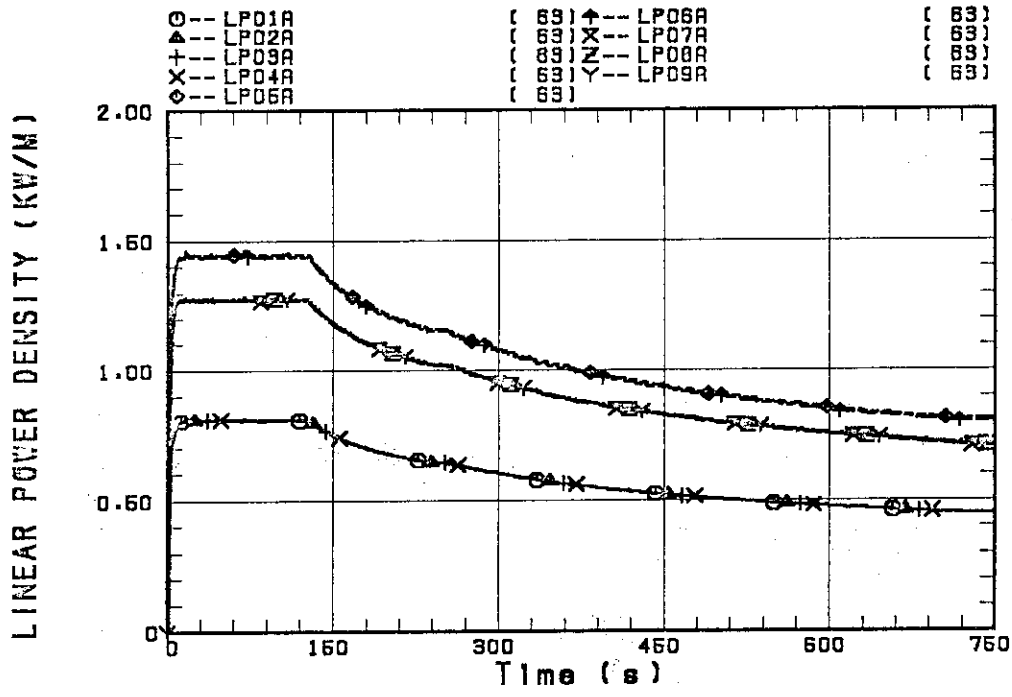

Fig. B-3 Average linear power of heater rod in each power unit zone

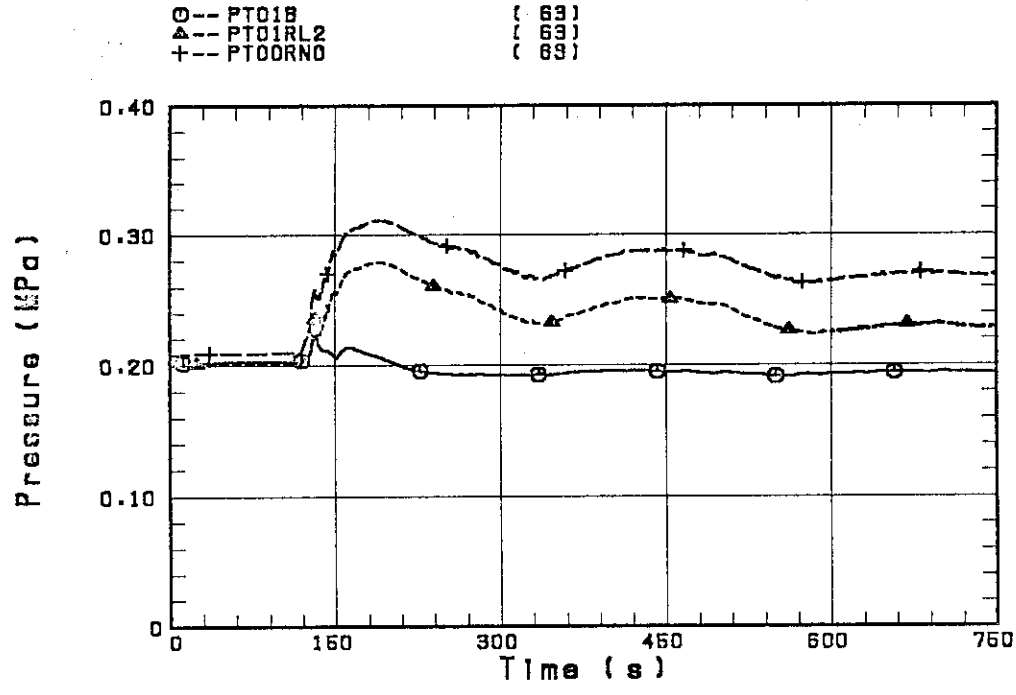

Fig. B-4 Pressure history in containment tank 2, upper plenum and lower plenum

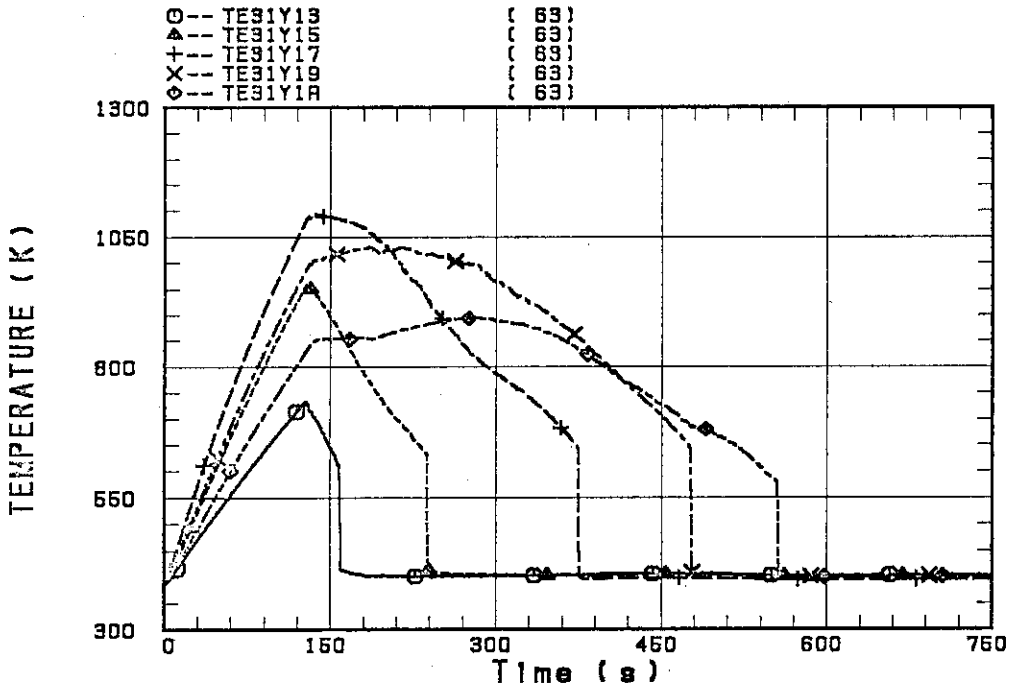

Fig. B-5 Clad surface temperature at various elevations along a heater rod in high power region (A region)

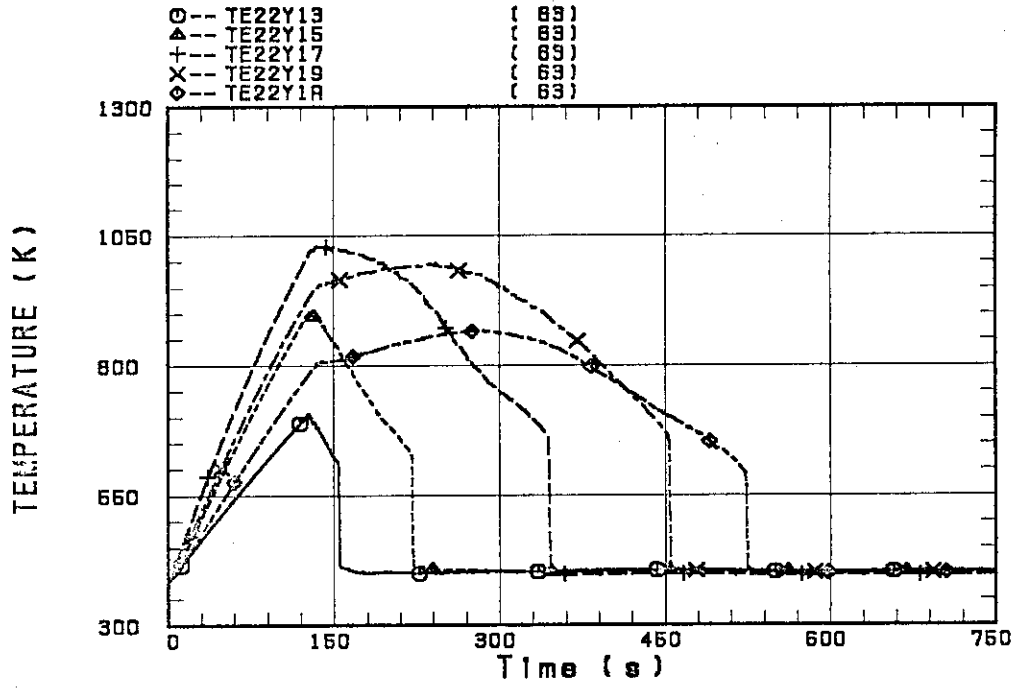

Fig. B-6 Clad surface temperature at various elevations along a heater rod in medium power region (B region)

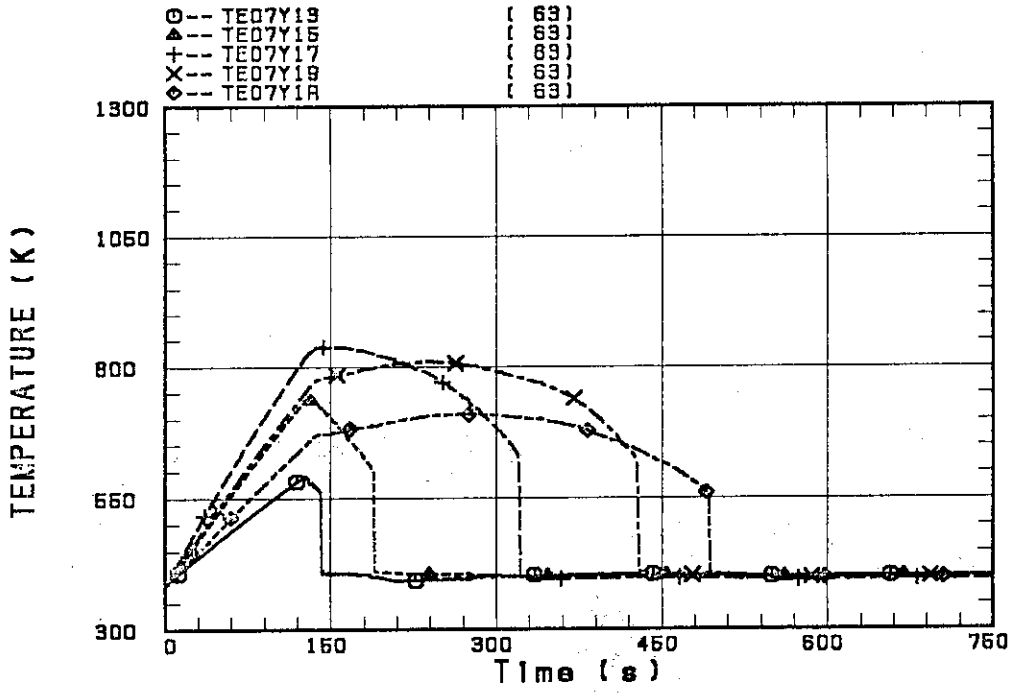

Fig. B-7 Clad surface temperature at various elevations along a heater rod in low power region (C region)

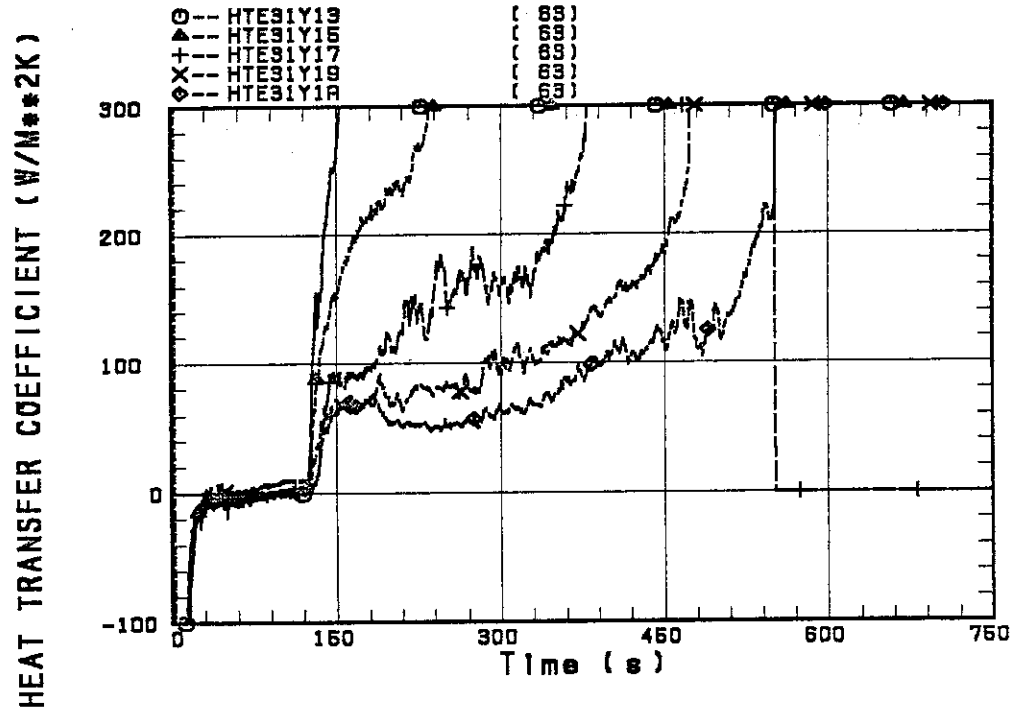

Fig. B-8 Heat transfer coefficient at various elevations along a heater rod in high power region (A region)

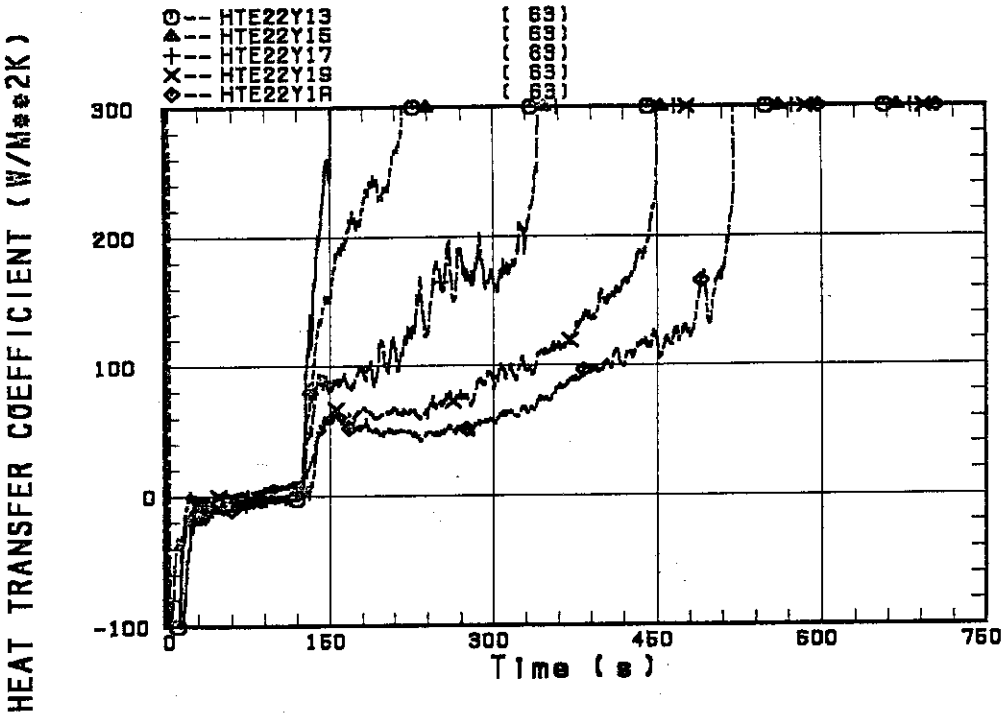

Fig. B-9 Heat transfer coefficient at various elevations along a heater rod in medium power region (B region)

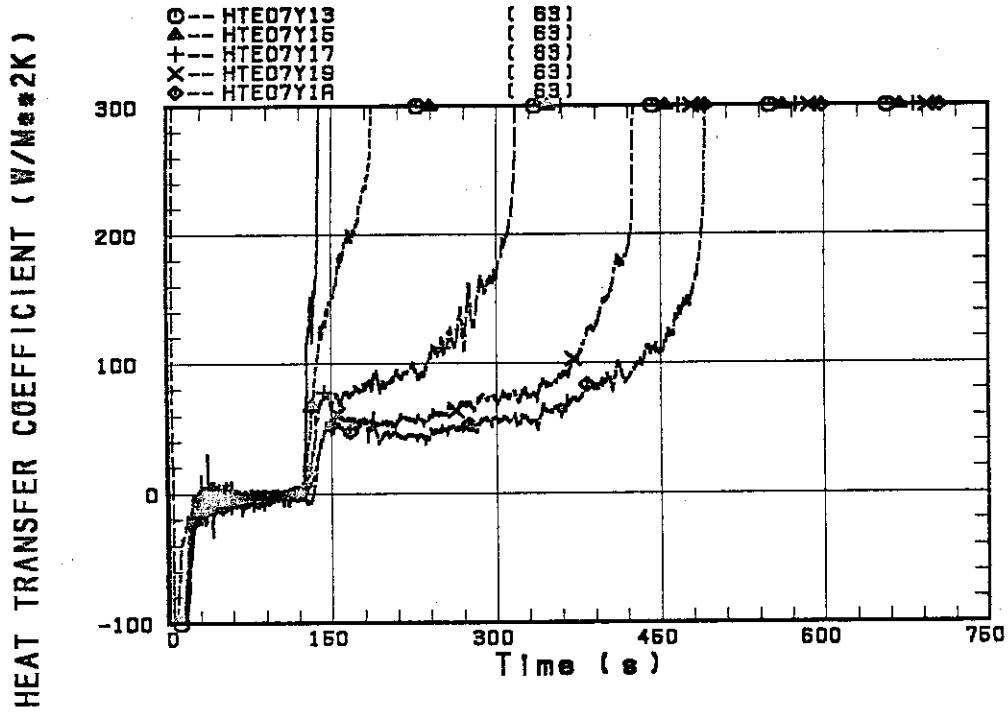

Fig. B-10 Heat transfer coefficient at various elevations along a heater rod in low power region (C region)

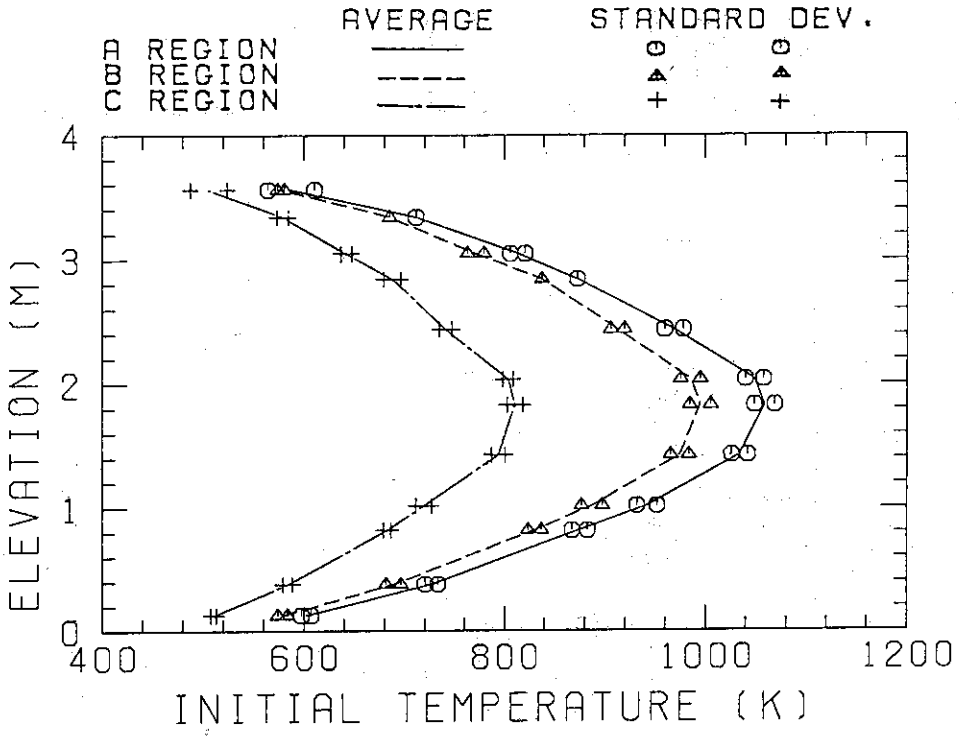

Fig. B-11 Initial clad surface temperature

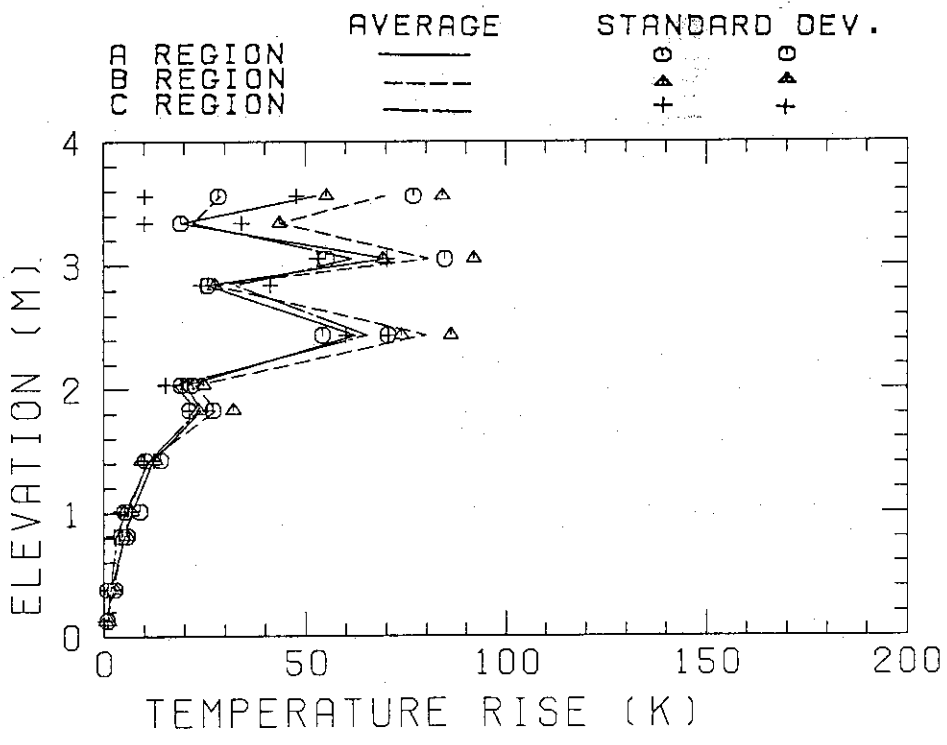

Fig. B-12 Temperature rise

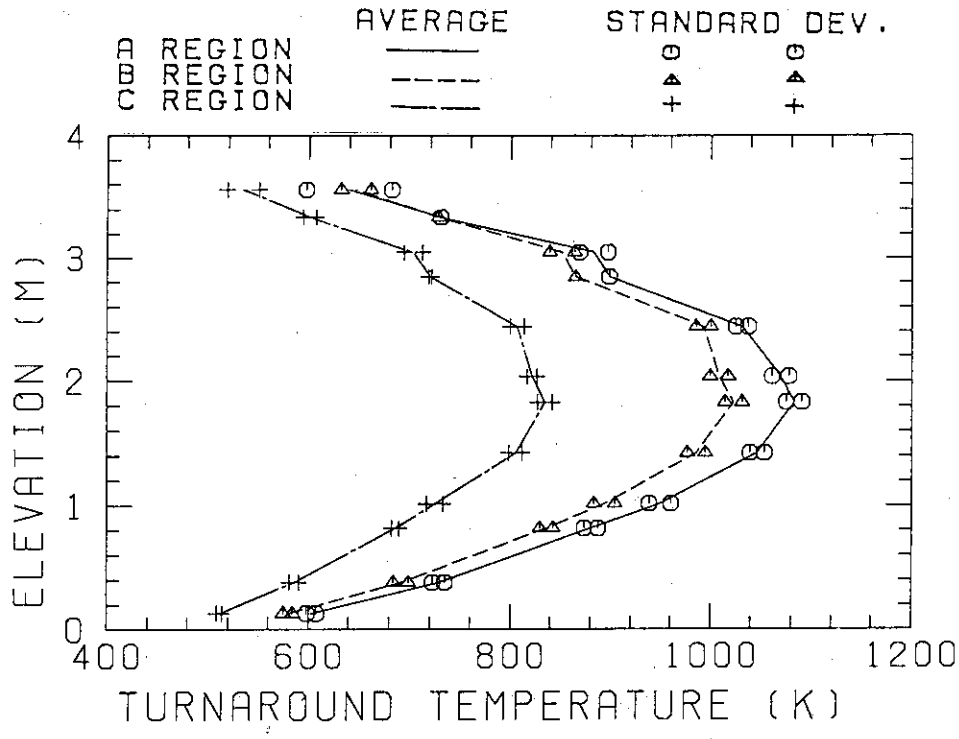

Fig. B-13 Turnaround temperature

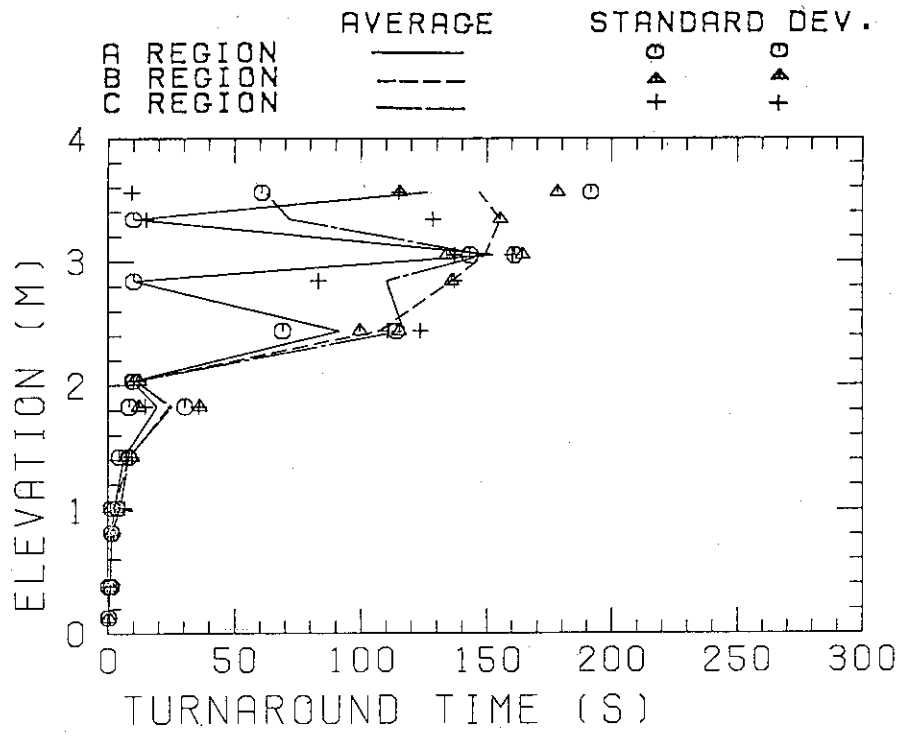

Fig. B-14 Turnaround time

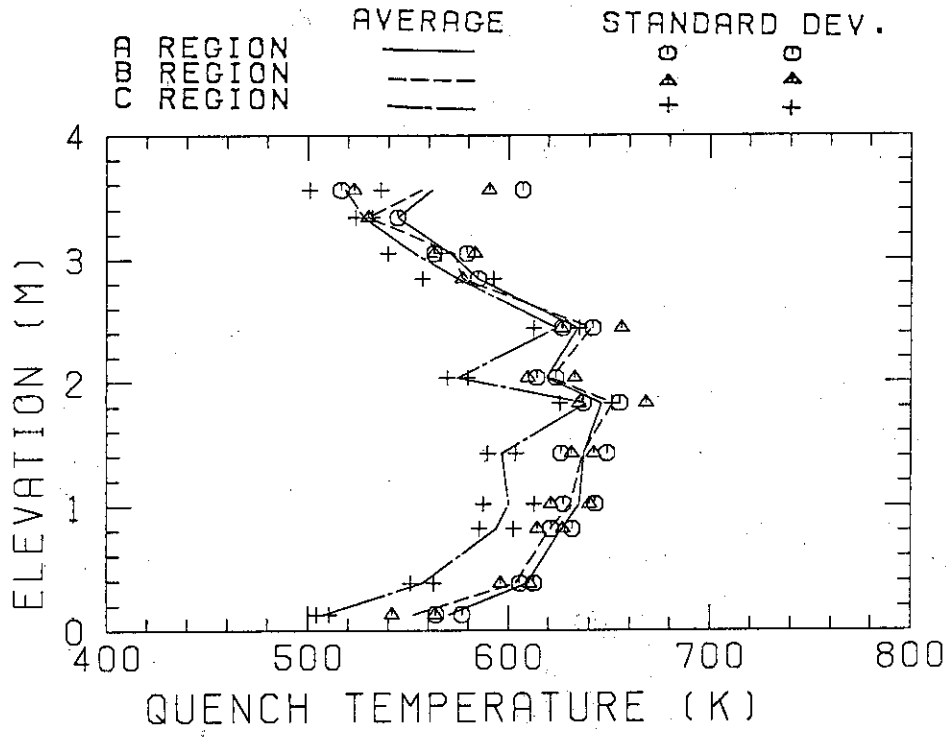

Fig. B-15 Quench temperature

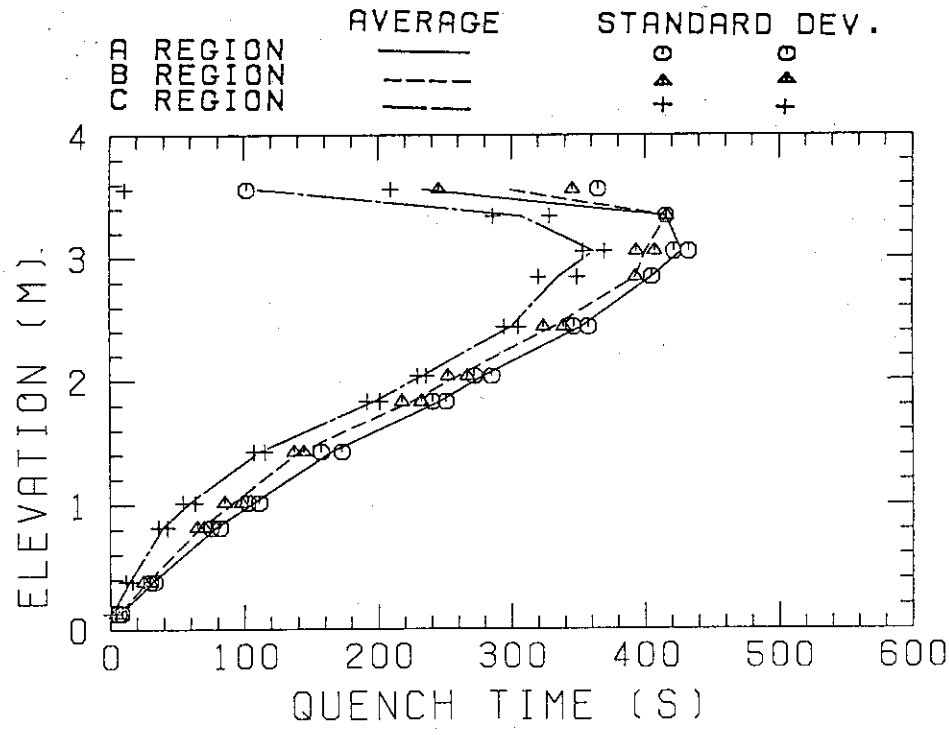

Fig. B-16 Quench time

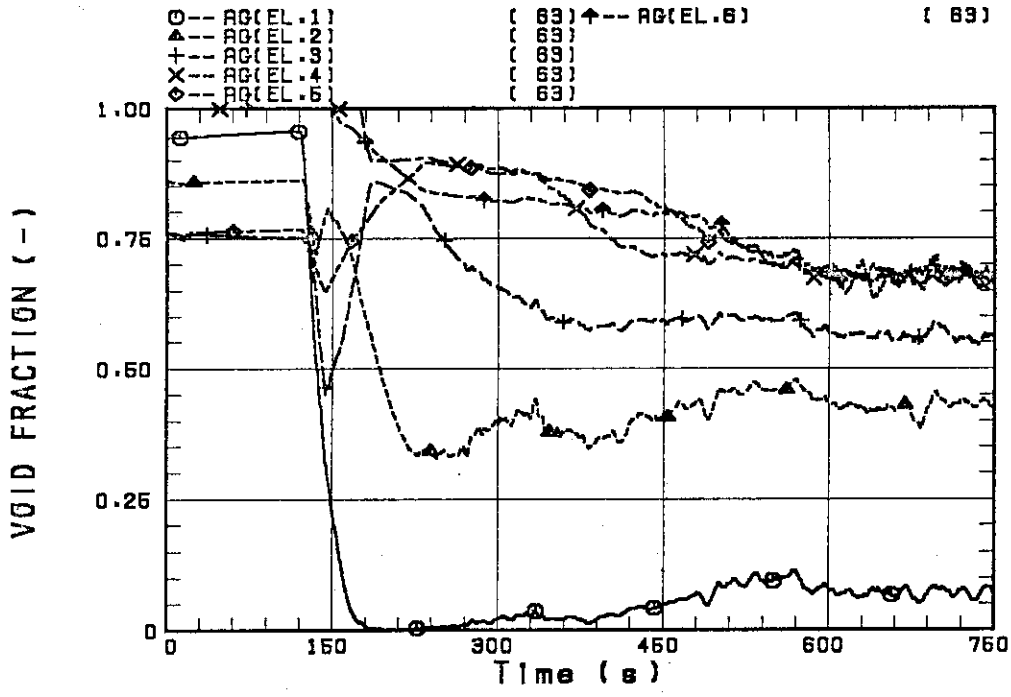

Fig. B-17 Void fraction in core

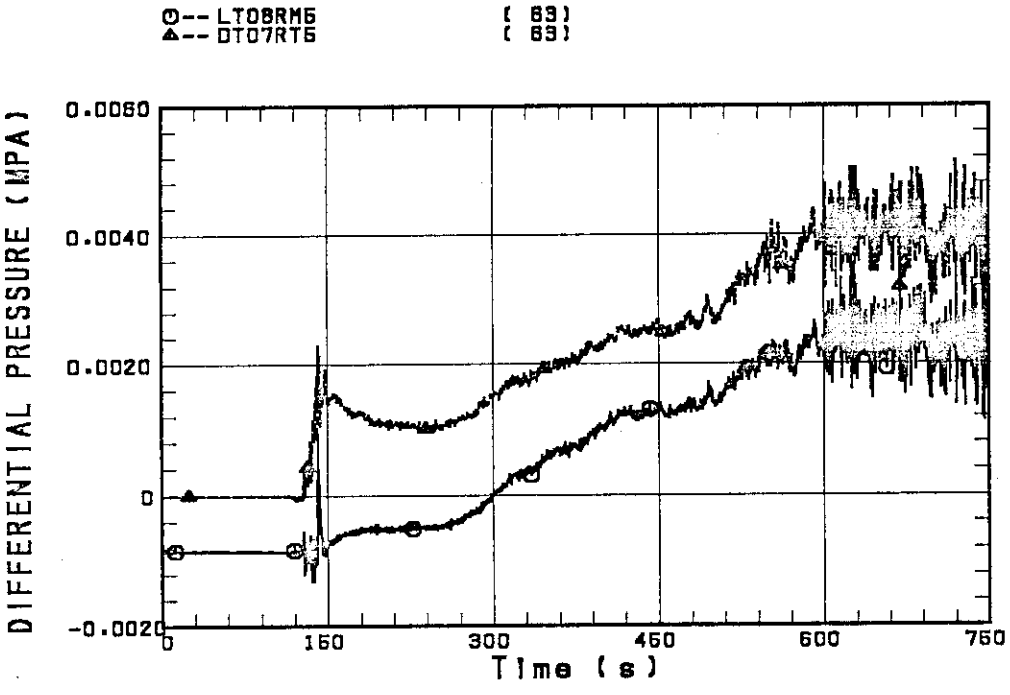

Fig. B-18 Differential pressure through upper plenum

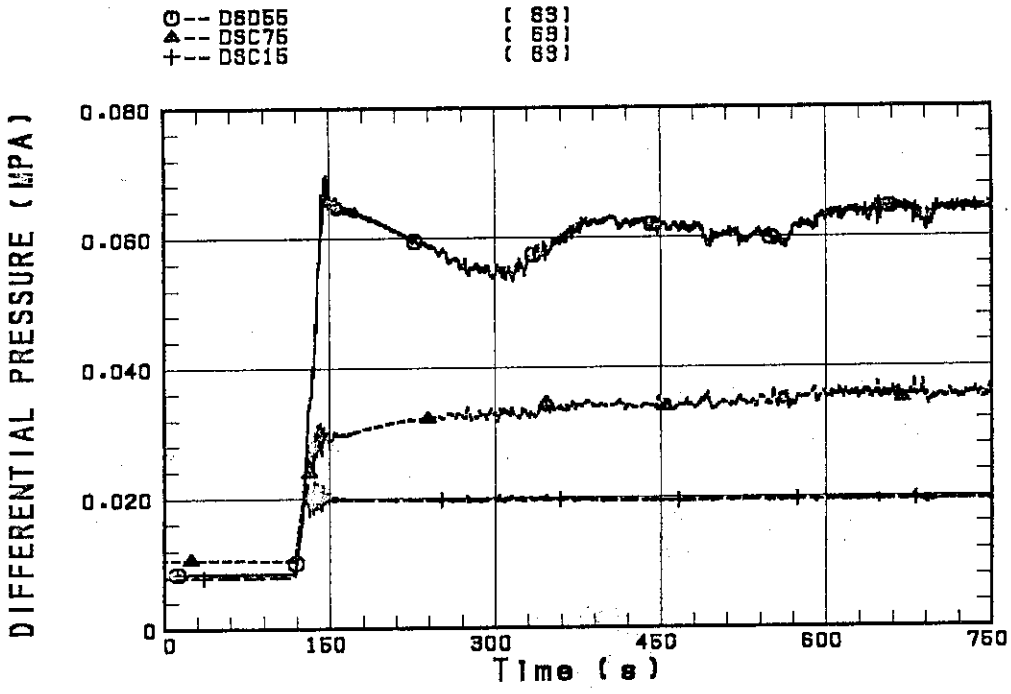

Fig. B-19 Differential pressure through downcomer, core, and lower plenum

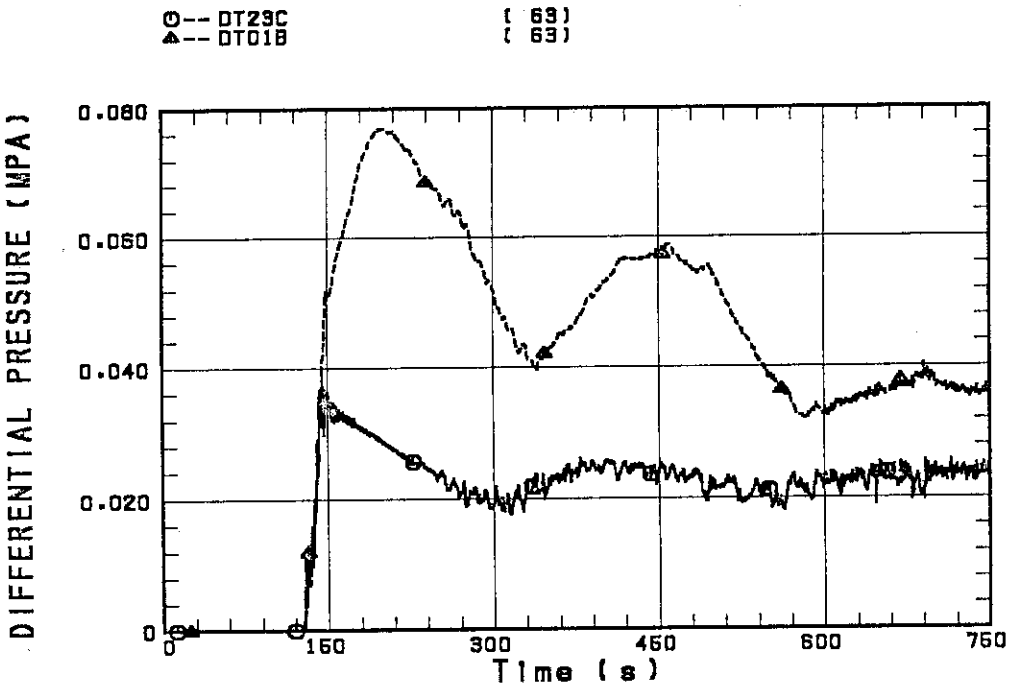

Fig. B-20 Differential pressure through intact and broken loops

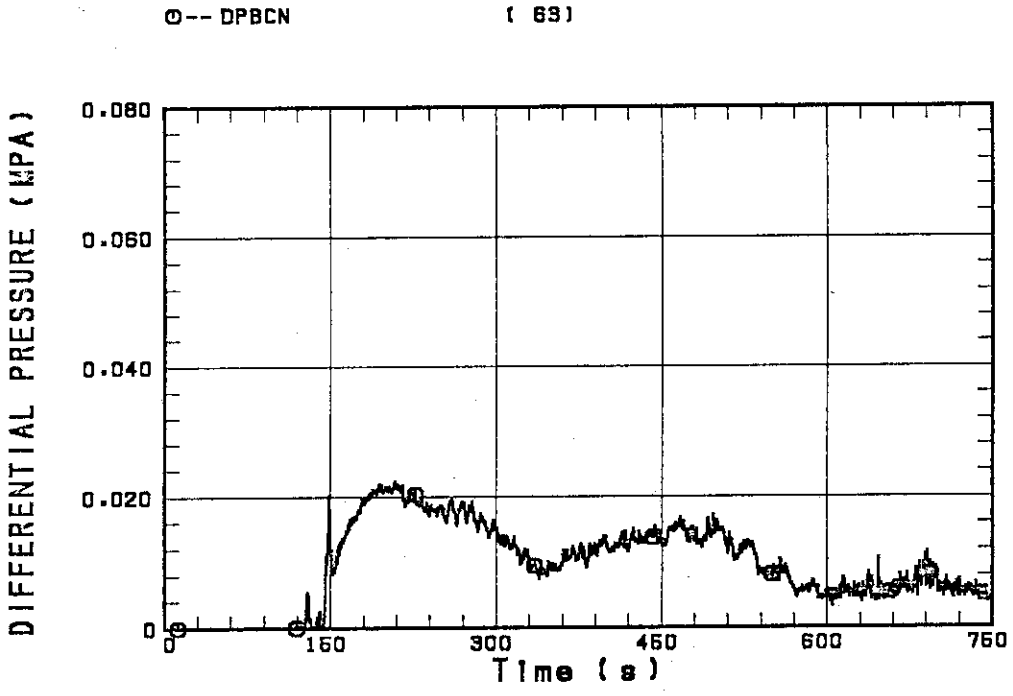

Fig. B-21 Differential pressure through broken cold leg nozzle

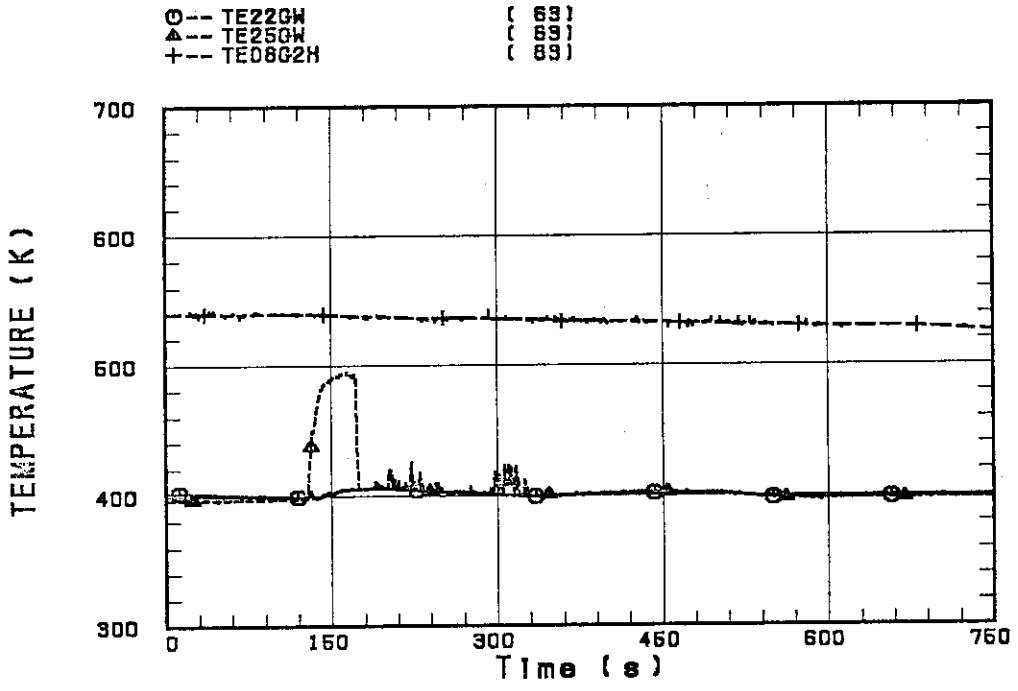

Fig. B-22 Fluid temperature in inlet plenum, outlet plenum, and secondary of steam generator 1

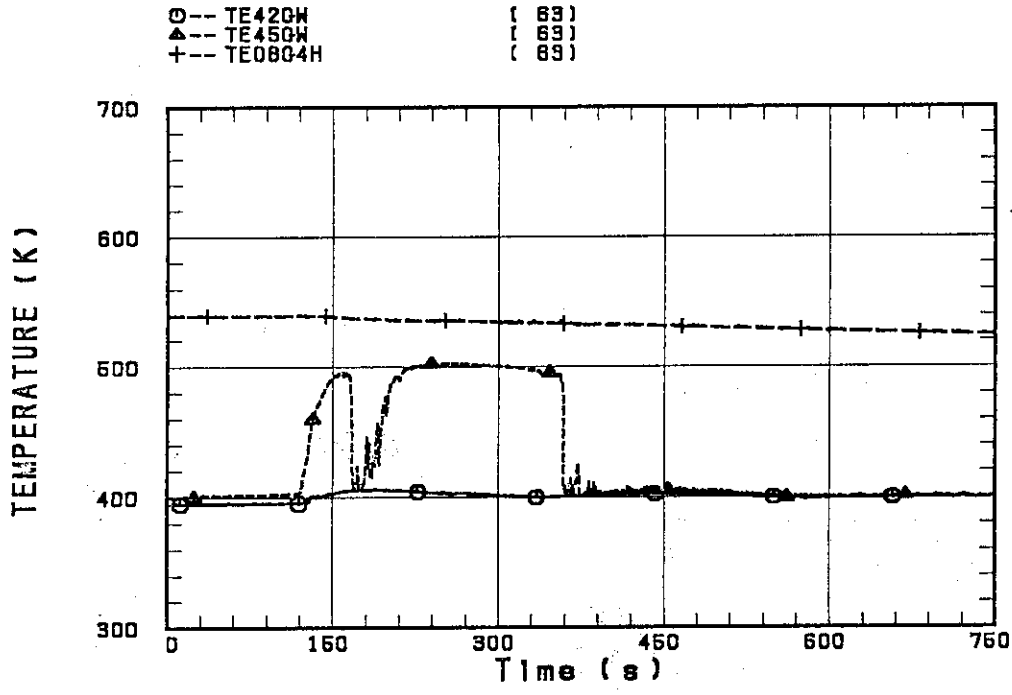

Fig. B-23 Fluid temperature in inlet plenum, outlet plenum, and secondary of steam generator 2

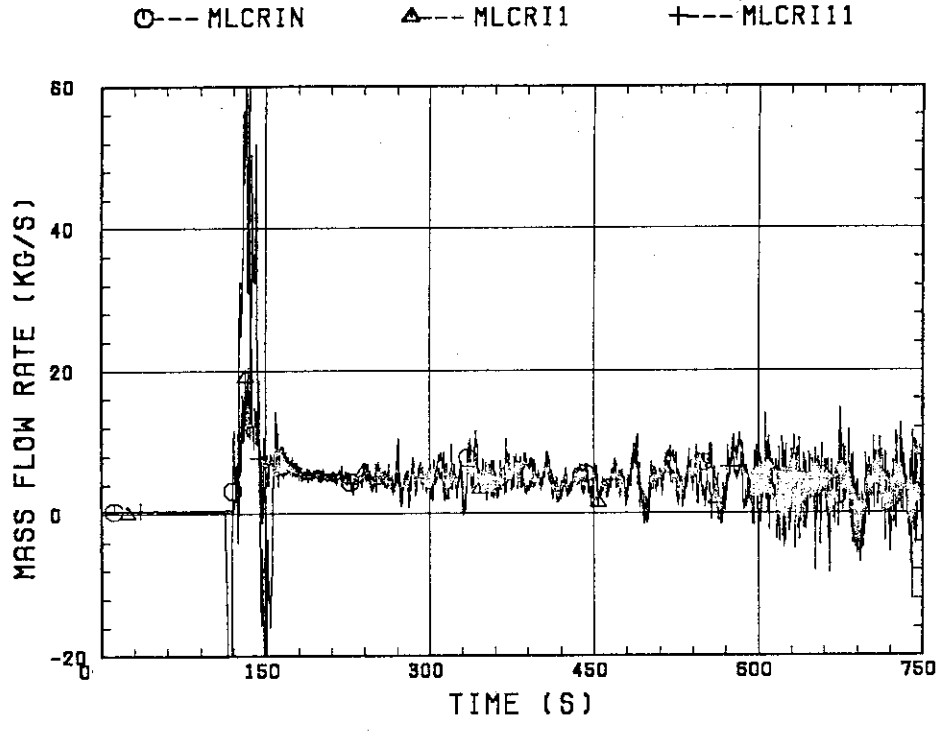

Fig. B-24 Core flooding mass flow rates evaluated with Eqs. (A.1) and (A.2)

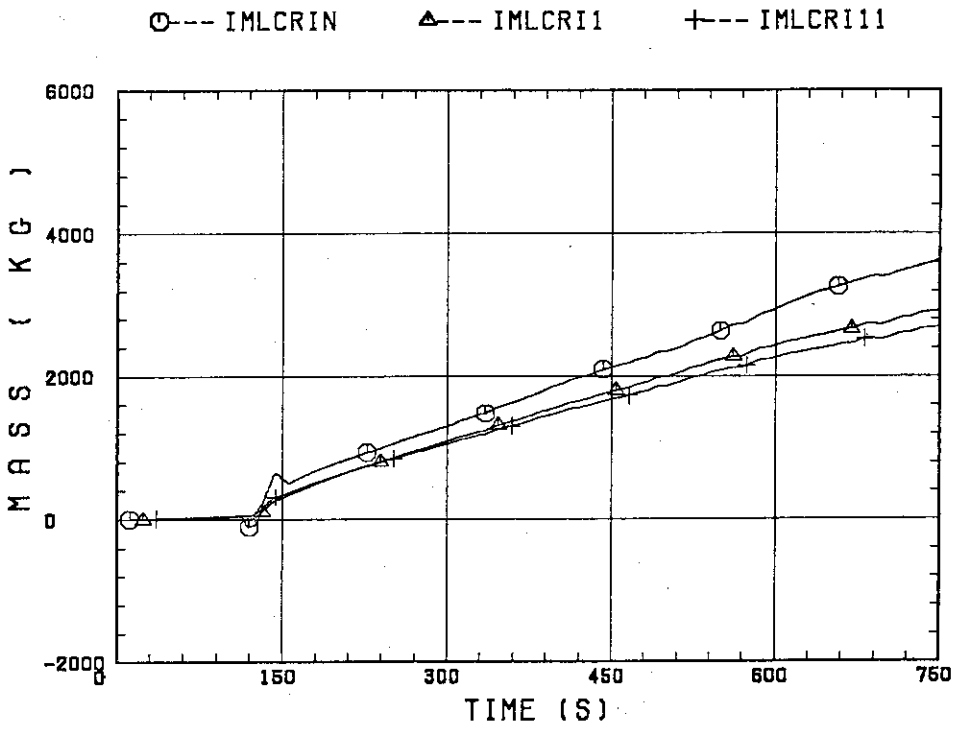

Fig. B-25 Time-integral mass flooded into core evaluated with Eqs. (A.1) and (A.2)

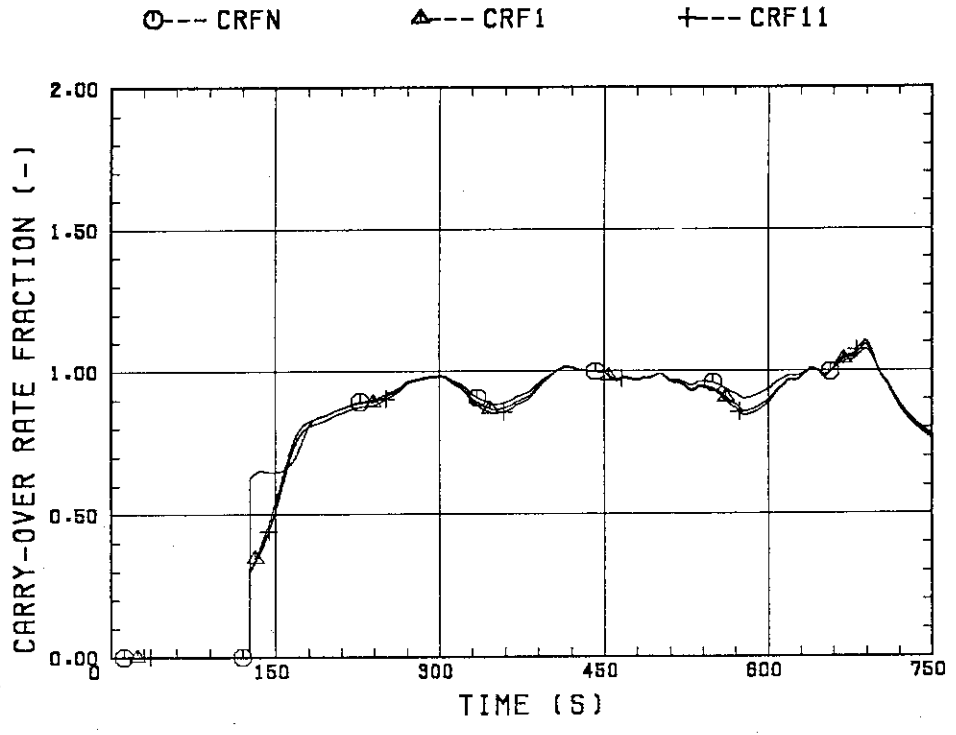

Fig. B-26 Carry-over rate fraction

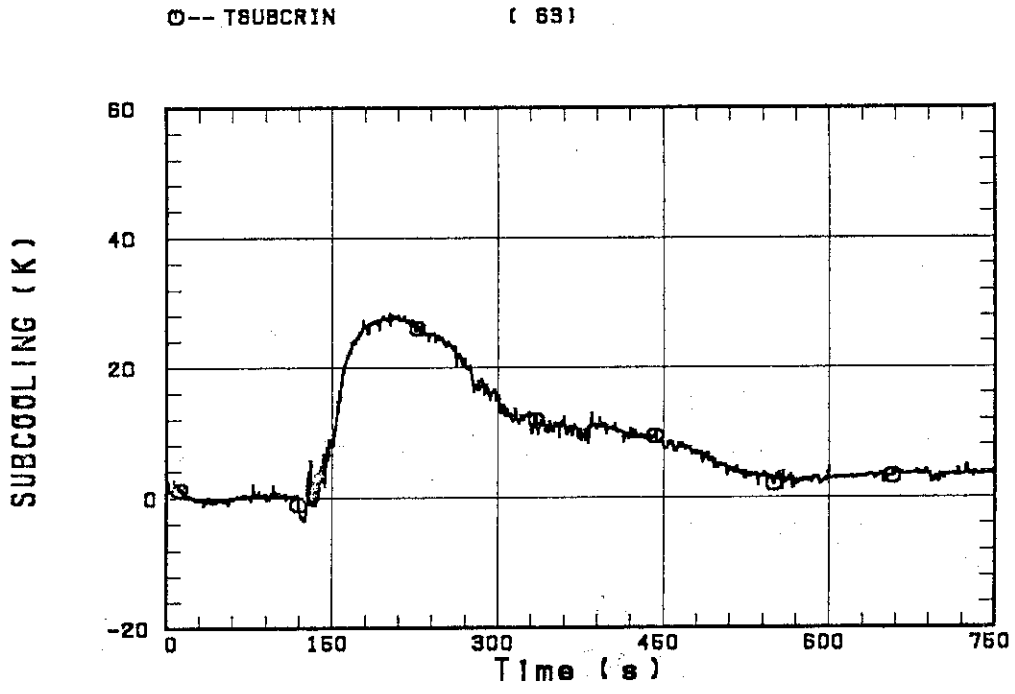

Fig. B-27 Core inlet subcooling

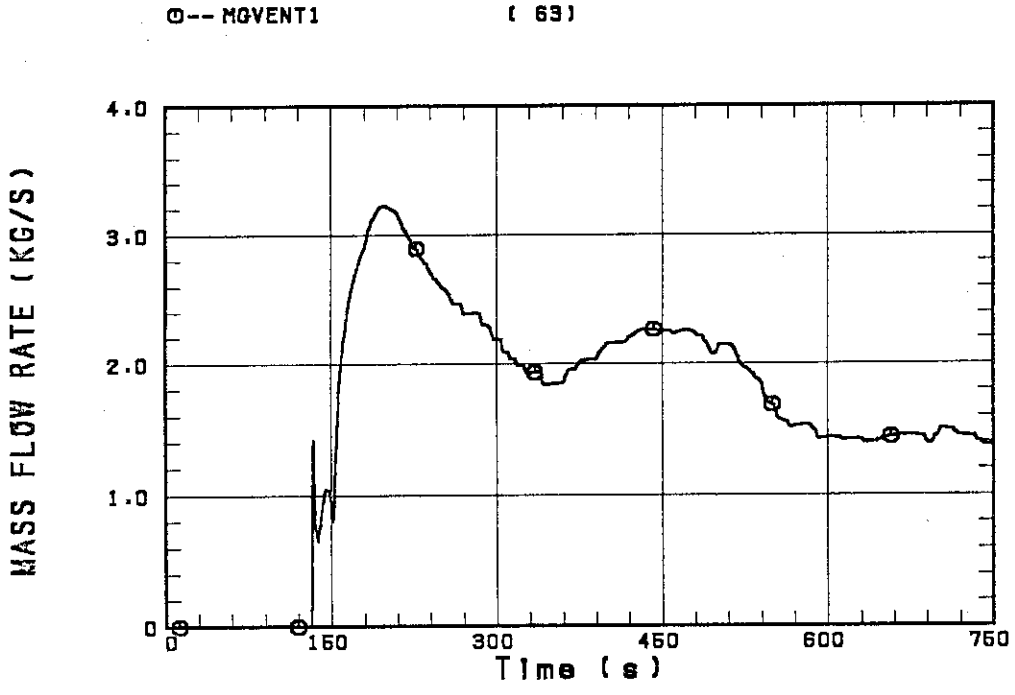

Fig. B-28 Exhausted mass flow rate from containment tank 2